Ab initio Studies of the Origin of Spectral Tuning Mechanisms in Rhodopsin, Bathorhodopsin and Isorhodopsin

To the Department of Chemistry at the University of Duisburg-Essen for securing the academical degree of

Doctor rer. nat.

A dissertation submitted in fulfilment of the requirements

by

M.Sc. Sivakumar Sekharan

born in

Chennai - INDIA

Tag der mündlichen Prüfung: 19.03.2007

Gutachter: Prof. Volker Buß

Prof. Wolfgang Gärtner

This research work was carried out from 04/2003 till 12/2006 in the Department of Chemistry at the University of Duisburg-Essen under the supervision of Prof. Dr. Volker Buß.

List of Publications

Parts of the work described in this thesis have been published:

[1] **S. Sekharan**, M. Sugihara, O. Weingart, T. Okada, and V. Buss, "Protein Assistance in the Photoisomerization of Rhodopsin and 9-*cis*-Rhodopsin – Insights from Experiment and Theory", ***J. Am. Chem. Soc.*** *129*, 1052-1054 (**2007**).

[2] **S. Sekharan**, M. Sugihara, and V. Buss, "Origin of Spectral Tuning in Rhodopsin – It is Not the Binding Pocket", ***Angew. Chem. Int. Ed.*** *46,* 269-271 (**2007**); ***Angew. Chem.*** *119,* 273-275 (**2007**).

[3] **S. Sekharan**, O. Weingart, and V. Buss, "Ground and Excited States of Retinal Schiff Base Chromophores by Multiconfigurational Perturbation Theory", ***Biophys. J.*** *91,* L7-L9 (**2006**).

Acknowledgements

This is perhaps the easiest and hardest chapter that I have to write. It will be simple to name all the people that helped to get this done, but it will be tough to thank them enough. I will nonetheless try…

How does the 498 nm absorption maximum come about in the visual protein rhodopsin? This question has concerned the lives of many scientists since George Wald first posed it in the early 1950s, and indeed since 2004 it has occupied mine.

Thanks are therefore in order to my supervisor, Prof. Dr. Volker Buß. His forbearance has been remarkable, given my organisation all'Indiana and obscene tendency to overlook good advice. It was so very rewarding to work with a supervisor who keenly encouraged me to follow new ideas, and whose door was always open for vigorous, free-form discussions. It became a lighter and more concise thesis after his suggested improvements (however not even he could remove all the verboseness I have put in this thesis, so the entire ramble you encounter here is due to the great amount of work I have put him to do). He could not even realize how much I have learned from him. Besides being an excellent supervisor, Prof. Buß was as close as a relative and a good friend to me. I am really glad that I have come to know him and his family in my life. Thank you Sir, for dedicating so much of your time to introduce me to rhodopsin, I ardently hope that you have been able to impart to me but a small part of your discipline.

Indeed, I believe there is a strong case to be made for canonizing all members of the Buss group, for I have witnessed many miracles, the most astonishing being that, despite sharing close quarters with me for the past three years, no-one has been overcome with the urge to strangle me. It was a privilege for me to be involved so closely with Dr. Klaus Kolster, Dr. Marko Schreiber, Dr. Minoru Sugihara, and Daniel Richter, whose experience, talent and patience made the learning curve a whole lot less steep for me. I owe Dr. Oliver Weingart a hearty round of thanks for setting up the number crunching monster "Xenon", and for patiently answering all my silly questions and being able to fix, almost in an instant, whatever was wrong with my jobs. As for Igor Schapiro, I have been prolifically impressed this year by your extensive knowledge of all things computational, cynical and nihilistic. Throughout my thesis-writing period, you provided encouragement, good company,

and lots of good ideas. I would also like to thank Robert and Karin for their love and care in making my environment a better place to live and work with.

Thanks must also be extended to Dr. Lars Packschies from the computational center of the University of Köln. The calculations of Chapter-3 would have been all the more dastardly were it not for his generosity in providing me with ample scratch space.

I would like to thank the many people who have taught me chemistry: my high school teachers (especially Hanah Ranjini) and my undergraduate teachers (especially Dr. R. Gopalan, Dr. Sulochana Nagarajan and Dr. L. Cindrella).

Many thanks go to Kalpana (graduate student, Tulane University-USA) for continually providing encouragement and helpful advice, especially during the frenzied final stages of my thesis. With all the 'cells' passing in this world it is a fortune that ours 'collided'. I also thank my close friends, Ram, Chandru, Hari and Sangeetha who have always stood by my side asking over and over again "When will you get it done? Next week? Next Month? When?"

Turning now to the world beyond the Chemistry building, even though Heisenberg would confidently assert that it does not exist when we are not looking, I feel a deep sense of gratitude to my brother and sister and their respective spouses for rendering me the sense and the value of brotherhood. They bore me, supported me, taught me, and loved me. I am glad to be one of them.

Lastly, and most importantly, I wish to thank my parents, V. Sekharan and Latha Sekharan for their spiritual support. I thank them for putting up with my frustrations, my spoiled weekends, my bad temper, but also always found a way of encouraging and pet me. But that is what parents are for, right? (I don't suppose my mother knew what she was getting herself into nonetheless she managed to pull through and do what she could do best, given the son in question). They liberally encourage whatever interests –sensible or otherwise – I wish to pursue, and have unquestioningly provided me with so many educational opportunities. To them I dedicate this thesis.

Mind Without Fear

Where the mind is without fear and the head is held high;
Where knowledge is free;
Where the world has not been broken up
into fragments by narrow domestic walls;
Where words come out from the depth of truth;
Where tireless striving stretches its arms towards perfection;
Where the clear stream of reason
has not lost its way into the dreary desert sand of dead habit;
Where the mind is led forward by thee into ever-widening thought and action-
Into that heaven of freedom, my Father, let my country awake.

GITANJALI – Rabindranath Tagore

Abstract

One of the most basic and unresolved puzzle in the chemistry of vision is the mechanism regulating the absorbance of the visual photoreceptors. Rhodopsin, the rod pigment that mediates black/white vision in the human eye, absorbs at 498 nm; while the artificial retinal analogue isorhodopsin containing the isomeric 9-cis form peaks at 485 nm and the early photo intermediate bathorhodopsin encompassing a distorted all-trans-retinal absorbs at 543 nm. The spectra of these pigments are clearly a function of the protein environment the chromophore "sees"; in other words, the spectra are tuned by the protein.

Three mechanisms are generally agreed to be involved in spectral tuning: 1) distortion of the chromophore as a result of steric interactions with the protein binding pocket; 2) interaction of the chromophore with the counterion balancing its positive charge; and 3) interaction of the chromophore with the remaining polar and/or non- polar amino acids lining the binding pocket. Employing the best available structural data we show that the three contributions discussed above add up quantitatively to the experimentally observed spectral shift of the chromophore on going from the vacuum to the rhodopsin molecule.

We have studied the wavelength dependence of 11-cis-, 9-cis- and all-trans-retinal absorbencies of the chromophore at the multiconfigurational level of theory using second order perturbation theory (CASPT2) within an atomic natural orbital (ANO) basis set on MP2 and SCC-DFTB optimized geometries in vacuo and in protein environments. In addition to the quantum-mechanical description for the chromophore and its counterion we have used three types of atomic charges obtained from a natural population analysis (NPA), Mulliken population analysis (MPA) and from the environment insensitive CHARMM charges, to account for the electrostatic interaction between the chromophore and the polar amino acids.

We demonstrate that in vacuo, the sensitivity of the retinal chromophore to its protonation state covers a wavelength range of 610 to 353 nm. In protein, by far the largest effect is exerted by the counterion (Glu-113) on the absorption maximum. Since the protein environment provides and stabilizes the chromophore distortion necessary for the selective and ultrafast transformation to bathorhodopsin, we conclude that this is its primary role and that spectral tuning by the binding pocket is not the goal pursued by evolution.

1 PREAMBLE 11

1.1 The Rhodopsin Puzzle 12

1.2 Photoreceptors 13

1.3 Nomenclature 15

1.3.1 M/LWS family 15

1.3.2 SWS1 family 16

1.3.3 SWS2 family 17

1.3.4 RH1 family 17

1.3.5 RH2 family 17

1.4 Structure of Rhodopsin 18

1.4.1 Chromophore Conformation 19

1.4.2 Protonation State 24

1.4.3 The Counterion 25

1.5 Rhodopsin Photocycle 26

1.6 Wavelength Regulation Mechanism 28

1.6.1 Effect of Protonation 28

1.6.2 π-Electron Delocalization 29

1.6.3 External Point Charge Model 30

1.6.4 Accumulated Evidence 31

2 THEORETICAL FRAMEWORK 33

2.1 *Ab Initio* Quantum Chemistry 35

2.1.1 The Many-Electron Wavefunction 36

2.1.1.1 Configuration Interaction Wavefunctions 37

2.1.1.2 Variational Principle 38

2.2 Single-Determinant Methods 39

2.2.1 Hartree-Fock (HF) Theory 40
2.2.1.1 Self-Consistent Field (SCF) method 43
2.2.2 Correlation Energy 44
2.2.2.1 Multiconfigurational SCF Theory (MCSCF) 47
2.2.2.2 Configuration Interaction (CI) 47
2.2.2.3 Møller-Plesset Perturbation Theory (MPPT) 50

2.3 Multi-Reference Methods 52
2.3.1 CASSCF 53
2.3.1.1 Practical Aspects 53
2.3.2 CASPT2 56
2.3.2.1 Intruder States 58

2.4 Technical Details 62

3 THEME 63

3.1 Spectral Tuning in Rhodopsin 64
3.1.1 Chromophore – Protein Interplay 65
3.1.2 Vacuo 68
3.1.2.1 Reference Point 68
3.1.2.2 Stern Test for Theory 70
3.1.2.3 Absorption Maximum in *Vacuo* 73
3.1.3 Binding Pocket 78
3.1.3.1 Effect of Geometric Distortion 79
3.1.3.2 Effect of the Counterion 84
3.1.3.3 Residual Effect Vs Counterion Effect 87
3.1.3.4 Effect of the Polar and/or Non-Polar Amino Acids 93
3.1.4 Retinal “Sees” the Water 95
3.1.5 Mechanism of Energy Storage & Origin of Bathochromic Shift 100
3.1.6 How to Annul the Counterion 106

4 CONCLUSION.....108

5 REFERENCES 111

1 Preamble

Molecules such as the chlorophylls for photosynthesis, the heme pigments for cellular respiration and the carotenoids and vitamin A for photoreception, have been chosen by nature to perform basic cellular functions. These molecules possess certain properties that enable to react with *"light"* to perform their functions in organisms, and there is no doubt that the better we come in each case to understand the nature of the problem, the clearer it will be why those molecules and not others were selected by nature at first place.

For an example, three animal phyla on the Earth, having developed three very different kinds of eyes completely independent from one another, have all arrived at the same molecule, the protonated Schiff base of 11-*cis*-retinal, as the chromophore of their visual pigments. Yet the 11-*cis*- isomer is an improbable, intrinsically unstable isomer of the retinal family. Why then is it chosen repeatedly for this function?

It has turned out that the only action of light in vision is to change the shape of a molecule; and 11-*cis*-retinal fills that role in an exemplary way, light isomerising it from the bent 11-*cis*- to the twisted all-*trans*- configuration with high efficiency. The same forces that guided the selection of this improbable molecule three times independently on this planet might well arrive at the same or similar solutions elsewhere.

We have been told so often and on such tremendous authority as to seem to put it beyond question, that the essence of things must remain forever hidden from us; that we must stand forever outside nature, like children with their noses pressed against the glass, able to look in, but unable to enter. This concept of our origins encourages another view of the matter. We are not looking into the universe from

outside. We are looking at it from inside. Its history is our history; its stuff, our stuff. *From that realization we can take some assurance that what we are going to see in my thesis is real.*

1.1 The Rhodopsin Puzzle

One of the most basic and unresolved puzzle in the chemistry of vision is the mechanism which regulates the absorbance of the visual photoreceptors.[1] The focus of my thesis is studying this long standing puzzle in visual protein chemistry that concerns the origin, nature and course of the spectroscopic property of the protonated Schiff base of 11-*cis*-retinal chromophore.[2] Retinal chromophores not only serve as effective reporter groups for studying the chromophore-protein interplay, but also for understanding the structure–function relationship of rhodopsins in general.[3,4]

For example, rhodopsin, the rod pigment that mediates dim/light vision in the human eye absorbs at 498 nm[5,6] while the three cone pigments contained in human cone cells responsible for trichromatic (colour) vision peak at 425 (blue), 530 (green), and 560 nm (red), and thus constitute the basis for the color vision (*Figure 1).*[7]

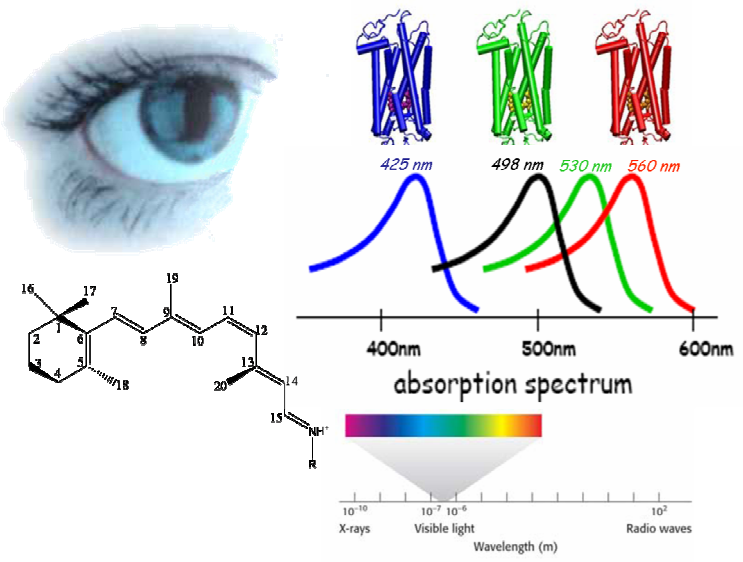

Figure 1 *Color sensed by blue, green and red visual photoreceptors.*

Since the chromophore in these receptors is the same protonated Schiff base of 11-*cis*-retinal (PSB11), the spectra of these pigments are clearly a function of the protein environment which the chromophore "sees", in other words they are tuned by the protein.[8] The spectral sensitivity of rhodopsin clearly appears to be a product of chromophore-protein interplay and thus continues to remain a classic workshop for developing and applying wide ranging experimental and theoretical techniques.

The reader is introduced to templates of several steps starting with a short commentary on photoreceptors and their physiological properties, and gradually moves on to the vertebrate visual pigment rhodopsin, its structure, function, and applications. In order to help the reader put the methodology in the correct perspective an overview on theoretical studies of rhodopsin is also presented.

1.2 Photoreceptors

Retinal binding proteins, consisting of a retinal molecule covalently linked to an instrinsic membrane embedded apoprotein, are ubiquitously found as photosensory receptors in visual systems throughout the animal kingdom.[9] In archae, some retinal pigments function as energy transducters, by executing light-driven transport of ions.

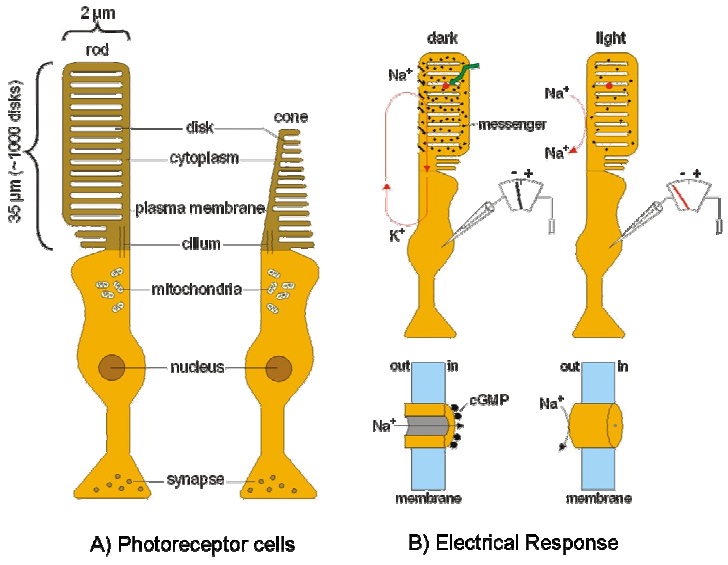

Figure 2 *A) Schematic drawing of rod and cone photoreceptor cells modified from Purves et al. (Ed.), "Neuroscience", 1997, Sinauer Associates Inc. Publishers). The primary events of*

photoreception take place in the outer segment of the cell, shown in brown. B) Electrical response of photoreceptors to illumination. In darkness, CNG channels in the plasma membrane of photoreceptor outer segments are kept open by cGMP and the cell depolarizes (left). Upon illumination, CNG channels close and the photoreceptor hyperpolarizes (right).

In the vertebrate eye, the visual pigments are located in the photoreceptor cells.[10] There are two types of photoreceptors, the rod/cone cells of vertebrates and the rhabdomeric cells of invertebrates.[11] Both consist of inner and outer segments and it is the latter which contain the photoreceptors (*figure 2).* The rod outer segment (ROS) contains ~1,500 stacked disks; the rhodopsin molecules which are responsible for black and white sensation in dim-light are embedded in these disks.[12,13] Light streaming into the eye is detected by specialized neurons (photoreceptors) in the retina (*Figure 3*). Rod cells on the retina respond to the light and send a message through the optic nerve fibre to the brain**.**

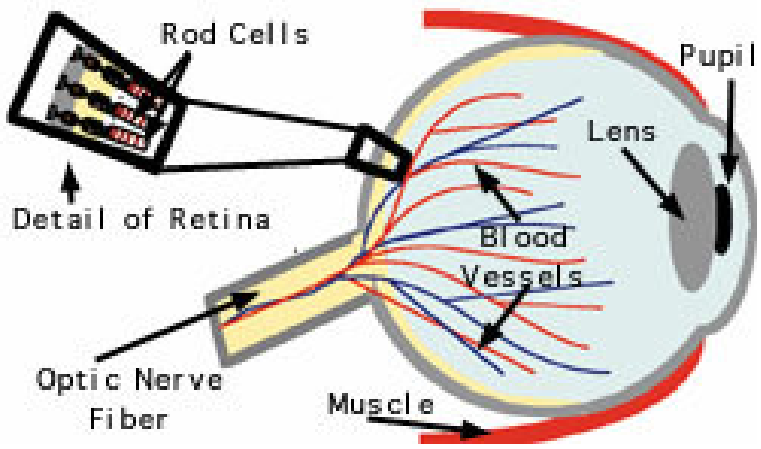

Figure 3 *This is a schematic drawing of the human eye adapted from a tutorial on "vision and light induced molecular changes" by Dr. Casiday and Dr. Frey at the Department of Chemistry Washington University. St. Louis.*

In response to light, a coordinated chain of molecular events – known as the phototransduction cascade[14-18] – is triggered in the cell *(Figure 4).* Photons excite pigment containing the rhodopsin proteins, which then switch on the protein transducin by loading it with guanosine triphosphate (GTP). When bound to GTP, transducin turns on a phosphodiesterase, an enzyme that breaks down cyclic

guanosine monophosphate (cGMP). High concentrations of cGMP open specialized ion channels in the outer cell membrane.

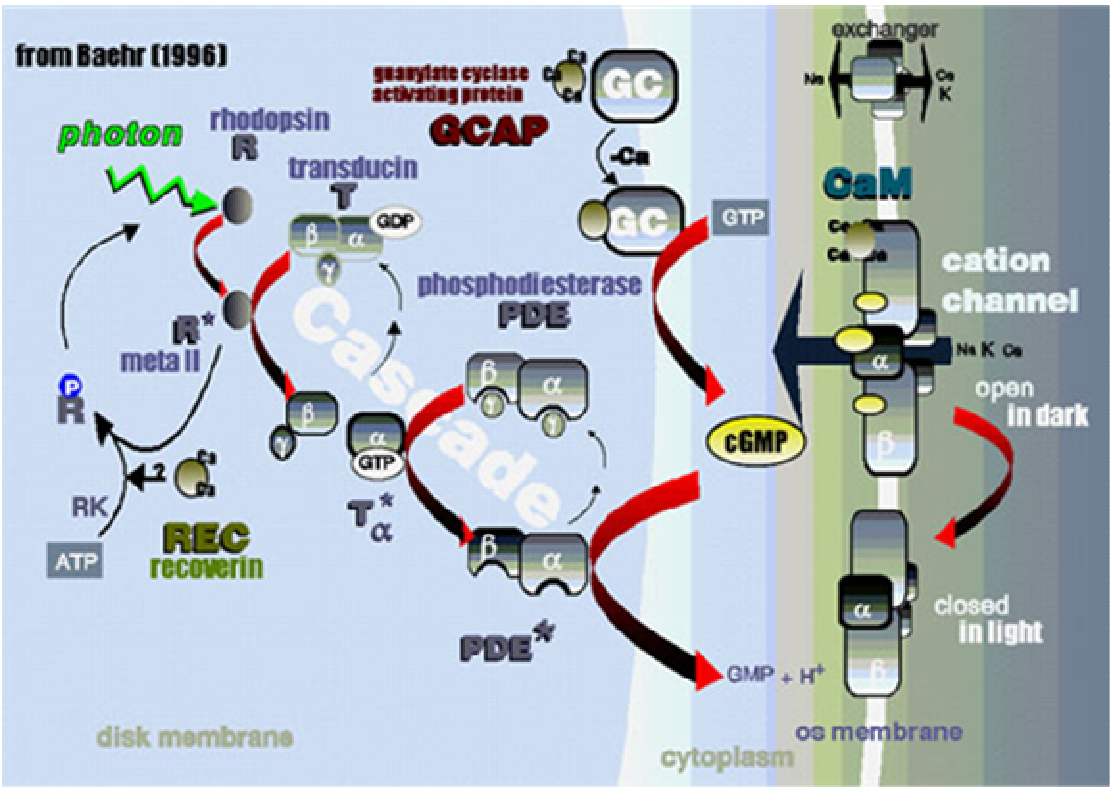

Figure 4 *Schematic diagram of the phototransduction cascade in rhodopsin.*

Thus, by reducing the concentration of cGMP, light changes the flow of ions across the membrane of photoreceptive neurons, producing an electric signal that is communicated via the optic nerve to the brain.[19-21]

1.3 Nomenclature

So far about 100 vertebrate visual pigments are known to have been sequenced. All of them seem to fall into one of the five classes of vertebrate visual pigments namely: M/LWS (Mid and Long Wavelength Sensitive), SWS1 (Short Wavelength Sensitive1), SWS2, RH1, and RH2.

1.3.1 M/LWS family

The M/LWS visual pigment family contains both the human "red" and "green" cone pigments. Their amino acid sequences are quite similar to each other, as

well as to the long wavelength cone pigments of most other species which have been investigated. This family also contains pigments whose absorption maxima overlap with some members of two of the other families (RH1 and RH2), so there is no clear division of pigment families based on each family encompassing a distinct range of absorption maxima. The spread of the known absorption maxima is from 521 to 575 nm (for retinal pigments with a Cl-binding site).

Green-mouse (508 nm), rat (509 nm), human (531 nm), rabbit (509 nm), cave fish (521 nm), gecko (521 nm), red-human (558 nm), goat (533 nm), cave fish (563 nm), goldfish (524 nm), chameleon (560 nm), iodopsin-chicken (571 nm), xenopus (575 nm), lw dolphin (524 nm) are species with pigments belonging to this M/LWS class.

Most M/LWS visual pigment's absorption spectra are chloride sensitive; their absorption maximum shifts being 20±50 nm to longer wavelengths in the presence of physiological concentrations of chloride. The pigments from the other four classes of visual pigments are missing the chloride binding site.

In addition at least some members of one mammalian subclass, the rodents, seem to have lost the chloride-binding site and so the absorption maxima of their M/LWS pigments are at much shorter wavelengths than the other members of this family.[22,23] Some mammalian and fish retinas contain two members of the M/LWS family. Most, but not all, members of the M/LWS family are found in morphological cones.[24]

1.3.2 SWS1 family

This group contains mostly pigments whose absorption maxima are in the ultraviolet, but it also has the human "blue" cone pigment, shifted further to the red than most other members of this family. The known absorption maxima of SWS1

pigments range from 358 to 425 nm. Pigeon (393 nm), UV-budgerigar (370 nm), violet-chicken (415 nm), blue-anolis (358 nm), squirrel, monkey (430 nm), human (420 nm), monkey (430 nm), rat (358 nm), mouse (359 nm), salamander (367 nm), xenopus (425 nm), goldfish (359 nm) belong to this category.

1.3.3 SWS2 family

So far members of this pigment category have not been found in mammals, but are present in many bird, fish, reptile, and amphibian retinas. Pigments in this class absorb around 440 nm. Their known absorption maxima range from 437 to 455 nm. Blue chicken (455 nm), anolis (437 nm), goldfish (441 nm) and green rod frog (440 nm) constitute this class.

1.3.4 RH1 family

This class contains most if not all of the standard "rod" pigments, the rhodopsins. Terrestrial species have their absorption maxima clustered around 500 nm, while deep sea fish tend to have their absorption maxima at ~470±20nm.[25] Blue conger eels (487 nm), goldfish (492 nm), bovine (498 nm), human (497 nm), alligator (500 nm), chicken (503 nm), frog (500 nm), xenopus (500 nm), salamander (506 nm), lamprey (503 nm) and skate (497 nm) are some of the rhodopsin species that fall into this category.

1.3.5 RH2 family

Related to the rhodopsins is the last group of retinal visual pigments that mostly absorb around 500 nm. They range from 466 to 511 nm. Members of the RH2 family are found in both morphological rods and cones. The green-1 (511 nm), green-2 (504 nm) goldfish, blue chameleon (495 nm), green chicken (508 nm), blue gecko (466 nm) belong to this group.

1.4 Structure of Rhodopsin

Primary sequence alignments split retinal proteins into two clearly distinct families. One family (type-1) consists of the archaeal-type rhodopsins first observed in the archae on *Halobacterium salinarum*, a halophilic prokaryote, and now also found in eukaryotic microbes. Type-1 rhodopsins function as light-driven ion transporters (*bacterio*rhodopsin[26-32] and *halo*rhodopsin[33]), phototaxis receptors (sensory rhodopsins I and II), or have as yet undiscovered functions (e.g. fungal rhodopsins). Type-2 rhodopsins consist of the photosensitive receptor proteins in animal eyes, including human rod and cone visual pigments, receptor proteins in the pineal gland, hypothalamus, and other tissues of lower vertebrates.[9,10]

Rhodopsin is the vertebrate dim-light photoreceptor, belonging to the super family of guanine nucleotide-binding proteins generally referred to as G-protein-coupled signal-transducing membrane proteins. GPCRs are the first large family of cell-surface receptors to be sequenced, cloned, and crystallized.[34-38] The crystal structure of rhodopsin provides significant insights concerning structure/activity relationships in visual pigments and related GPCRs. It is composed of the protein opsin (~40 kD in size). The specific arrangement of seven transmembrane (TM) helices is stabilized by a series of intermolecular interactions that appear to be conserved among several opsin families of photoreceptors.[39-41]

Opsin encompasses a 348 amino acid polypeptide chain. In addition to the shared seven-helix architecture, spectroscopic and chemical analyses show that retinal is attached in a protonated Schiff base linkage to a lysine residue at position 296 in R, 216 in bR, 306 in hR, 242 in sRI and 205 in sRII in the centre of the seventh TM.[42-46]

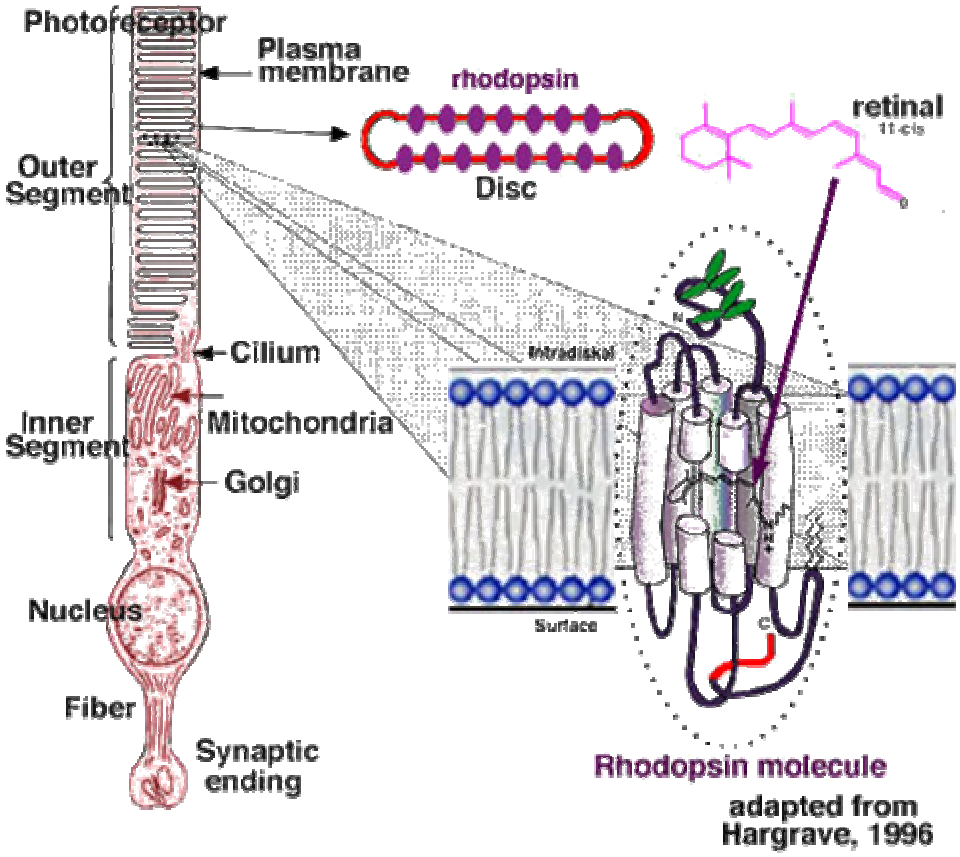

Figure 5 *Schematic diagram of Rhodopsin in the Rod Outer Segment (ROS) disks.*

There have been an enormous number of visual pigment amino acid sequences determined in the past 15 years, starting with bovine rhodopsin, first reported by Ovchinnikov[47] and Hargrave et al.[48] followed by Nathans and co-workers, who confirmed the bovine rhodopsin sequence[49] and reported the three human cone pigment sequences, all by sequencing the DNA.[50] After the bovine sequences, all of the other visual pigment sequences have been determined by this method.

1.4.1 Chromophore Conformation

Like all polyene chains, retinal can exist in a number of different configurations, corresponding to the possible *cis-trans* isomerizations around the different double bonds of the molecule.[51,52] In the case of retinal (*Figure 6*), these

possible isomerizations may occur essentially around the bonds 9-10, 11-12, and 13-14. The names of the principal isomers are given below.[53]

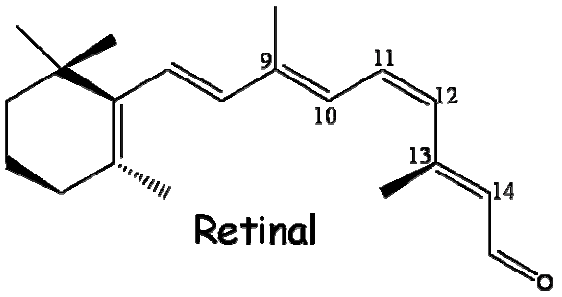

Figure 6 *The aldehyde of vitamin A.*

Stereochemistry about bonds	Nomenclature
9-10	9-*cis*-retinal
11-12	11-*cis*-retinal
13-14	13-*cis*-retinal
9-10, 13-14	9,13-di-*cis*-retinal
11-12, 13-14	11,13-di-*cis*-retinal

The existence of the 11-*cis* isomer was considered to be very improbable because steric interference of the methyl group at position 13 with the hydrogen atom at position 10 would prevent the molecule from being entirely planar, thus causing a loss of resonance energy. It was consequently surprising, at least at first sight, to observe that the very isomer of retinal which is involved in the process of vision has in fact the 11-*cis* configuration. Moreover, it was also shown that when the all-*trans* retinal is irradiated with white light, the 11-*cis* isomer is formed about 8 times as fast as the 9-*cis*-isomer. However, at the same time, a comparison of the all-*trans*-, 9-*cis*-, 11-*cis*-, 13-*cis*- and 9,13-di-*cis*-retinal shows that the 11-*cis*- compound is the most thermolabile of these molecules. This isomer is also the most labile upon irradiation by light.[54,55]

In visual pigments with absorption maxima larger than 440 nm, this Schiff base is protonated and therefore positively charged. What is the conformation of the chromophore chain? There are indications that the chromophore is strongly twisted in the central region, from C10 to C13.[56-59] Evidence for the 6-s-*cis*- assignment of the *β*-ionone ring in rhodopsin[60] was gathered from solid-state NMR-spectral data of 11-*cis*-retinal labelled with ^{13}C at the C5 position. From a comparison of the principal tensor elements with $^{13}C5$ labelled 6-s-*cis*- and 6-s-*trans*- retinoic acid, a nonplanar 6-s-*cis*-conformation has been experimentally deduced for rhodopsin[61] and supported by theoretical studies.[62,63] Resonance Raman spectra and that the spectrum of 11-*cis*-retinal is quite similar but not identical with that of rhodopsin. Due to the fact that the Raman spectra of 11-*cis*-retinal in rhodopsin show bands near 998 and 1018 cm^{-1}, a spectral region assigned to C-Me stretching motions, it is suggested that the steric interaction between C10-H and C13-CH_3 groups in the 12-s-*trans* conformer gives rise to this effect. However, in the case of 11-*cis*-retinal crystal, the 12-s-*cis* conformer with less steric interaction is preferred and the methyl rocks have similar frequencies.[64]

Determination of the absolute sense of twist around the 12-s-bond adjacent to the *cis-trans* isomerization site of the chromophore is critical, since the helicity direction should determine the chromophore movement after the photoisomerization. However, elucidating the nature of the twist around this 12-s-*cis* bond proved to be controversial. Namely, a negative helicity of the retinal chromophore around the 12-s-bond, that is, with 13-Me in the rear of the plane, was proposed by theoretical calculations,[65] solid-state NMR studies,[60,66] the CD of rhodopsin with 11,12-dihydro chromophores,[67] and studies with 11,12-cyclopropyl-Rh.[68] On the other hand, semi empirical and non empirical calculations of the chiroptical data of the retinal

chromophore have led to a positive helicity around the C12─C13 bond,[69,70] that is, 13-Me in front of the plane.

An analysis of chiroptical data by Buss[70] using the best available theoretical analysis at that time as well as more approximate methods has led to a correlation between a positive rhodopsin CD α-band and a positive twist of the 12-s-bond.[70] Based on the 2.8-Å resolution X-ray structure[34] and *ab initio* data,[70] the 12-s-bond helicity is most likely positive. The conclusion that the torsion is positive was also observed in a study of 11-*cis*-locked cyclopropyl retinals.[71] Thus experimental and theoretical studies reached a common ground that the twist is negative about the C11═C12 bond and positive about the C12─C13 bond.

The first highly resolved structure of rhodopsin, at 2.8-Å resolution (PDB:1F88),[34] showed the major structural features as predicted from biochemical, biophysical, and bioinformatics studies on wild type and mutated proteins. Crystallographic refinement of the two molecules in the asymmetric unit generated another model of rhodopsin (PDB:1HZX).[35] The extracellular and intracellular regions of rhodopsin each consist of three interhelical loops (given the prefix E or I, for extracellular and intracellular, respectively) as well as of two tails (i.e) (N-term and C-term, respectively).

Differences between 1F88 and the refined 1HZX structures concern the intracellular region (I3), which was rebuilt in 1HZX, lacking residues 236-240. In contrast, the extracellular loops and the chromophore were changed minimally. Furthermore, in 1HZX additional amino acids in the C-tail (i.e. residues 328-330) are missing as compared to 1F88, whereas the amino acid stretch 334-348, which in 1F88 was filled with Ala residues, carries all the side chains in 1HZX. Improved resolution was obtained in later structural models, 1L9H (2.6-Å)[36] and 1U19 (2.2-Å).[38]

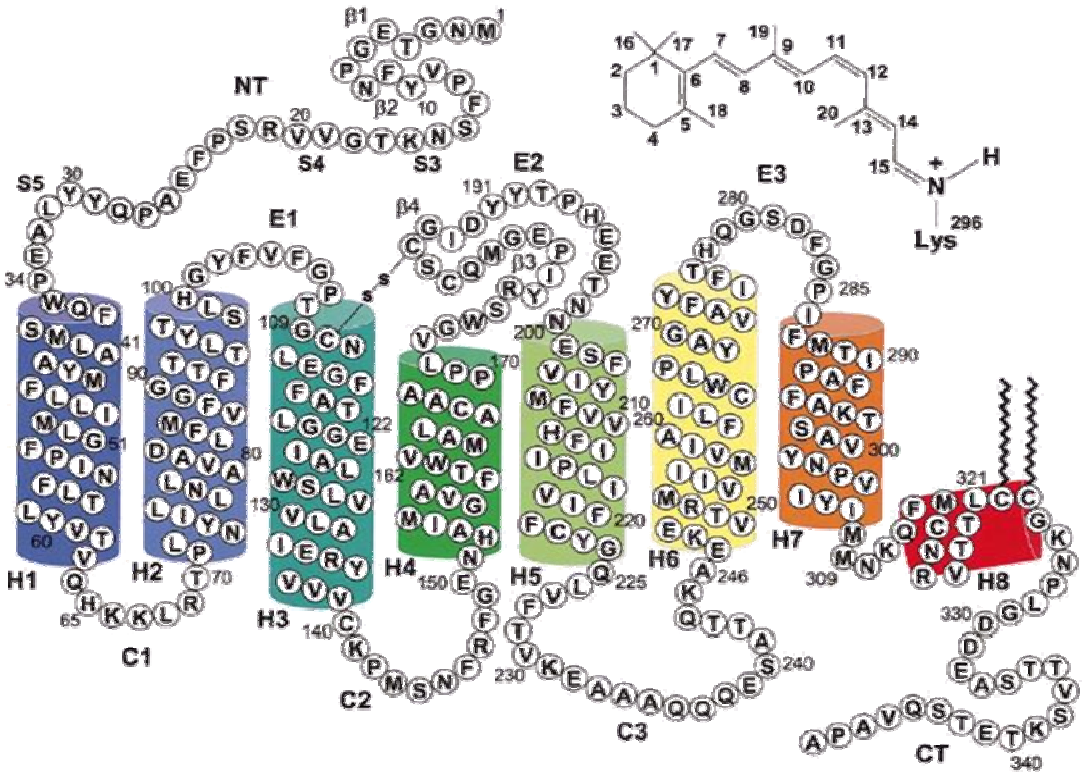

Figure 7 *A secondary structure diagram of bovine Rhodopsin. Amino acids are depicted with single letter code. The amino-terminal tail and extracellular domain is toward the top, and the carboxyl-terminal tail and cytoplasmic domain is toward the bottom. Transmembrane α-helical segments (H1 to H7) and the cationic amphipathic helix H8 are shown in cylinders. An essential disulphide bond links Cys-110 and Cys-187. Cys-322 and Cys-323 are palmitoylated. Inset: The structure of the 11-cis-retinylidine chromophore. Carbon atoms are numbered 1 through 20. This figure is adapted from Reference 10.*

The latest and most refined rhodopsin structure, 1U19, completes the description of the protein backbone and is in general agreement with earlier diffraction studies. The main differences between the 2.6 and 2.2-Å structural models essentially concern the completion of I3 and the C-term in the latter structure.

The structures of the 11-*cis*-retinal chromophore and its binding site have been defined with greater precision than ever before in the 2.2-Å resolution structure, demonstrating a significant pretwist of the C11═C12 double bond, which is suggested to be critical for the function of rhodopsin. The position of water molecules in 1L9H had already been defined with high precision. In this respect, some of the highly conserved residues within the family of GPCRs, including D83, N302, and Y306, are found to form binding sites for these water molecules. The latest structure by Okada

and co-workers confirms the water molecule topography found in 1L9H but also adds new molecules, without leaving any cavity in the protein.

1.4.2 Protonation State

One of the most promising tools for elucidating the conformational changes in retinal during the initial stages of the visual excitation is provided by resonance Raman (RR) spectroscopy.[72-75] In the RR process it is possible to use laser excitation of a given electronic level to achieve an enormous enhancement of the Raman transitions coupled to that electronic level. The RR vibrational spectra of certain substrates can be obtained even when they are inside the protein active site. The resulting spectra can provide direct information about the interactions between the substrate and its active site. In rhodopsin, this allows selective enhancement of the vibrations of the chromophore and probing of their local environment.

A direct investigation was performed by Mendelsohn[76] who observed the C-N stretching frequency at 1622 cm^{-1} in the purple membrane pigment of *Halobacterium halobium.* The similarity of the C-N frequency in the pigment to that of the unprotonated Schiff base in solution (~1620 cm^{-1}) led Mendelsohn to propose that the Schiff base of retinal in the purple membrane is unprotonated.

In such a case the shift in λ_{max} must result from a charge transfer complex rather than the protonation of the Schiff base. Apparently Mendelsohn misinterpreted the fact that his observation was made in D_2O suspension in which deuteration shifts the C-N frequency[77,78] from ~1645 cm^{-1} to ~1620 cm^{-1} Lewis et al.[79] examined the resonance Raman spectrum of bovine rhodopsin and observed the C-N stretching mode at 1645 cm^{-1} (that of protonated Schiff.base in solution is ~1650cm^{-1}). They concluded that the Schiff base nitrogen in rhodopsin is indeed protonated.

1.4.3 The Counterion

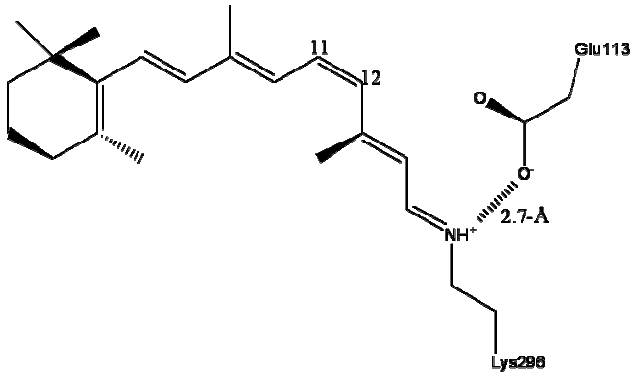

Figure 8 *11-cis-protonated Schiff base plus counterion from the theoretically refined 2.2-Å crystal structure.*

All vertebrate visual pigments carry a glutamate in the third transmembrane (TM3) segment corresponding to glutamate at position 113. By using site-directed mutagenesis, charged amino acids in bovine rhodopsin transmembrane helix C were systematically replaced. Substitution of glutamic acid-134 or arginine-135 did not affect spectral properties. However, substitution of glutamic acid-122 by glutamine or by aspartic acid formed pigments that were blue-shifted in light absorption (λ_{max} = 480 nm and 475 nm, respectively). While the substitution of glutamic acid-113 by aspartic acid gave a slightly red-shifted pigment (λ_{max} = 505 nm), replacement by glutamine formed a pigment that was strikingly blue-shifted in light absorption (λ_{max} = 380 nm). The 380 nm species existed in a pH-dependent equilibrium with a 490 nm species such that at acidic pH all of the pigment was converted to λ_{max} = 490 nm. It was concluded that glutamic acid-113 serves as the retinal Schiff base counterion in rhodopsin.[80-82]

The data support a model in which spectral tuning in bovine rhodopsin results from interactions between the polyene chain of 11-*cis*-retinal and uncharged amino acids in the binding pocket. However, the distance of the counterion to the Schiff base nitrogen atom is still a matter in debate. The most recent crystal structure at 2.2-Å

resolution places the counterion at 3.2-Å as against 2.7-Å from theoretical refinements.

Two of the Drosophila visual pigments also contain a glutamic acid adjacent to a conserved cysteine near the intradiskal surface of TM3. Interestingly, the Drosophila UV pigment does not. The absence of this potential Schiff base counterion may explain the absorption maximum of about 370 nm of this pigment, which is similar to that of mutant E113Q. The Drosophila photopigments reversibly interconvert between two spectrally distinct forms upon photon absorption.[83] The photoconversion of the Drosophila pigment between 370 nm and 470 nm species may involve protonation and deprotonation of the Schiff base. The octopus rhodopsin lacks a potential Schiff base counterion in TM3.[84] The Schiff base in this pigment remains unhydrolyzed after photolysis. Also, the octopus rhodopsin could be converted from an acid metarhodopsin ábsorbing at 510 nm to an alkaline form absorbing at 376 nm.[85] An aspartic acid (Asp-113) in helix C of a β_2-adrenergic receptor has also been indicated to be the counterion to cationic amine ligands.[86]

1.5 Rhodopsin Photocycle

Absorption of light transforms rhodopsin into the active state,[4] which interacts with a heterotrimeric G protein to initiate an enzyme cascade leading to visual transduction. To reach this active state, called Metarhodopsin (meta) II, rhodopsin must pass through a number of intermediates that have been characterised by UV-visible, Fourier-transform infrared (FTIR), Raman, and NMR spectroscopies, in addition to spin-labelling and biochemical studies.[87] One way to characterise intermediates of the photocycle is by trapping them at low temperatures. This approach has led to the classical “bleaching” scheme:

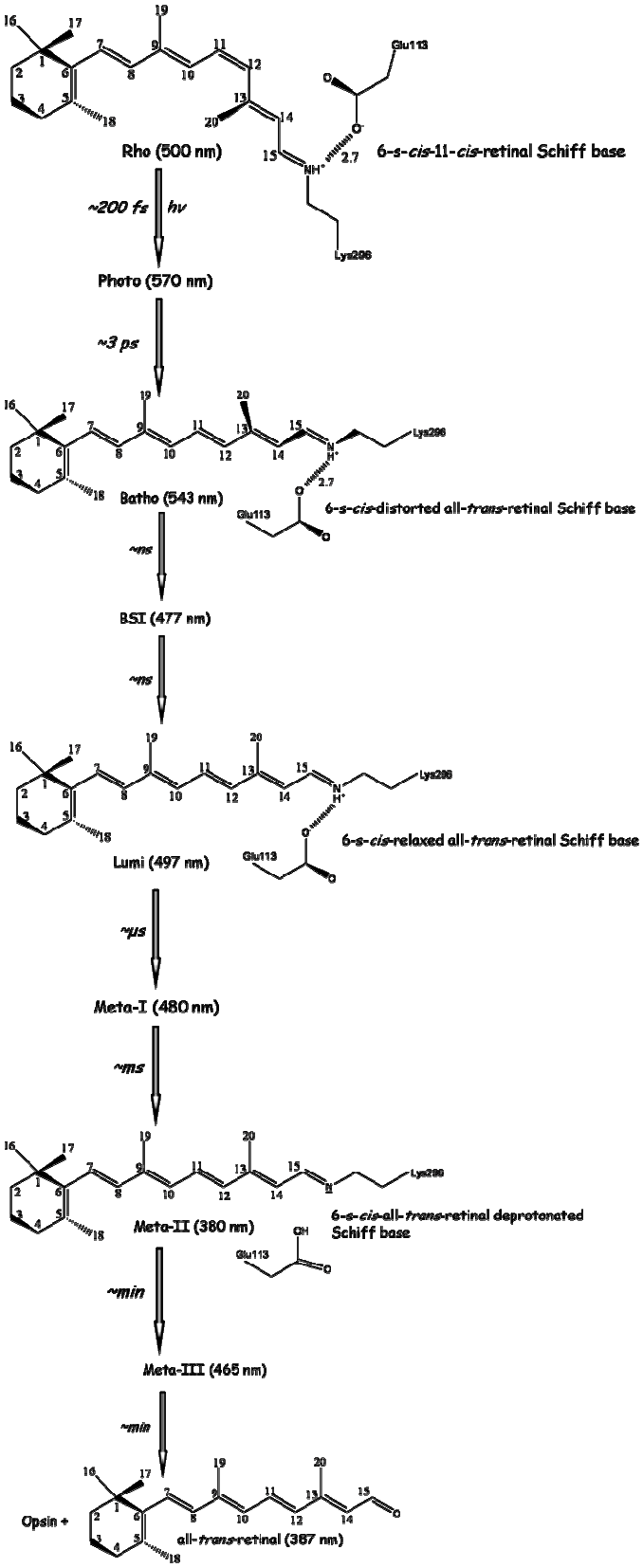

Figure 9 *Schematic representation of the rhodopsin intermediates, chromophore conformation and changes in absorption maximum accompanying the photocycle.*

Rhodopsin^{498} → Bathorhodopsin^{543} → Lumirhodopsin^{497} → Metarhodopsin I^{480} ↔ Metarhodopsin II^{380} ↔ Metarhodopsin III^{465} → opsin+all-*trans*-retinal (387 nm). However, at more physiologically relevant temperatures, time-resolved measurements up to 1 msec after photolysis reveal a new blue shifted intermediate (BSI) and a different kinetic scheme spanning a nanosecond-to-microsecond time scale:

Rhodopsin^{498} → Bathorhodopsin^{529} → Blue-Shifted Intermediate (BSI)^{477} → Lumirhodopsin^{492} → Metarhodopsin-I^{480} → Metarhodopsin-II^{380}. Formation of the BSI is entropically favoured and thus cannot be trapped at low temperatures. The 11-*cis*-retinal chromophore is converted to the 11-*trans*- structure in the first excited electronic state (S_1), which then decays to photorhodopsin. Photo changes within ~3 ps to batho, which is transformed via lumi and meta I to meta II. Metarhodopsin II (the phototransformed protein, RX) initiates processes that temporarily decrease the concentration of cyclic guanosine 3',5'-monophosphate (cGMP) within the cell. The initial step is the phototransformed rhodopsin promoted displacement of guanosine diphosphate (GDP) by guanosine triphosphate (GTP) from the transducin [T; G-protein] complex with GDP. The flow of information to the nervous system from a photon absorbed by a rod or cone cell may be expressed as

$$\text{photon} + R \rightarrow RX \rightarrow T\text{-}GTP \rightarrow (\text{-cGMP}) \rightarrow (\text{signal to visual nerve}).$$

1.6 Wavelength Regulation Mechanism

1.6.1 Effect of Protonation

Experiments with retinal and its derivatives in solution have led to a number of plausible mechanisms for wavelength regulation in visual pigments.[100-106] The two photochemical properties of retinal that are considered to be most relevant are the shift in absorption maximum from 357 nm to 440 nm upon formation of the protonated

Schiff base (*Figure 10*), and the increase in π-electron delocalization and the concomitant change in dipole moment that accompanies photoexcitation.

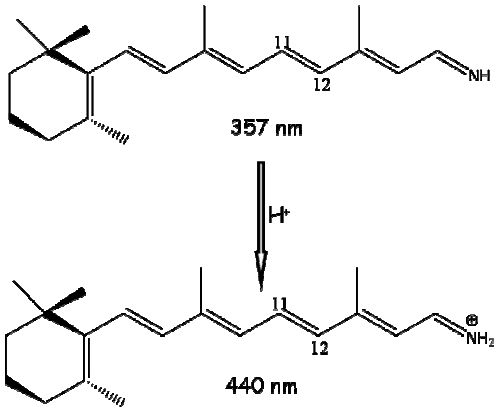

Figure 10 *Effect of protonation on the retinal Schiff base absorption maximum.*

1.6.2 π-Electron Delocalization

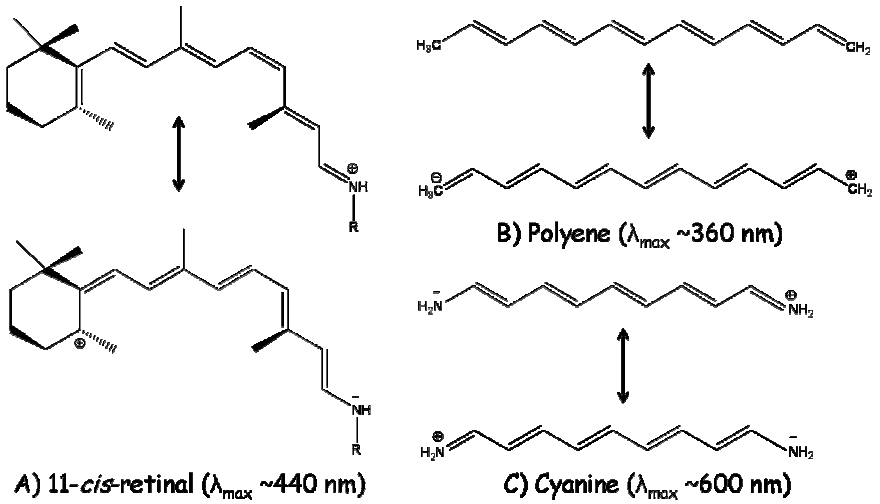

Figure 11 *Resonance structures of π-systems with 12 π-electrons and the respective absorption maxima: A) protonated 11-cis-retinal Schiff base, B) polyene, and C) cyanine.*

The positive charge on the protonated Schiff base is partially delocalized by alternate resonance structures (*Figure 11*). This delocalization is relevant to spectral tuning, because the spectral consequences of any perturbation can be understood by assessing its effect on π-electron delocalization within the 11-*cis*-retinal chromophore. Thus an increase in delocalization leads to a red shift and a decrease in delocalization induces a blue shift.[107-109]

This effect can be assessed in comparison with model compounds that represent the extremes of π-electron localization and delocalization. A polyene with six double bonds has strong bond length alternation, minimal π-electron delocalization, and absorbs at ~360 nm. In contrast, the corresponding cyanine has equivalent bond lengths, maximal π-electron delocalization, and peaks at ~600 nm.

1.6.3 External Point Charge Model

Common sense suggests that amino acids lining the apoprotein alter the polarity and polarizability, around the conjugated π-electron system of the protonated retinal Schiff base shifting the absorption spectrum of the pigment toward 500 nm. The protonated Schiff base (SBH^+) of retinal with n-$BuNH_2$ absorbs at 440 nm (22,700 cm^{-1}, in CH_3OH) while the SBH^+ in visual pigments absorbs at 440-650 nm (22,700-15,400 cm^{-1}). The red shift of 2,620 cm^{-1} in going from 11-*cis*-retinal SBH^+ in CH_3OH to the pigment e.g., bovine rhodopsin, 498 nm or 20,080 cm^{-1}, was defined as "***opsin shifts" (OS)***. The OS is the value which reflects the difference between the environment of SBH^+ in CH_3OH and within the binding site. In bacteriorhodopsin, a light induced proton-translocating pigment the SBH^+ now absorbs at 560 nm (17,860 cm^{-1}).

Nearly 20 years ago, based on experiments with dihydroretinals an external point charge model (*Figure 12*) was proposed by Nakanishi and co-workers.[110,111]

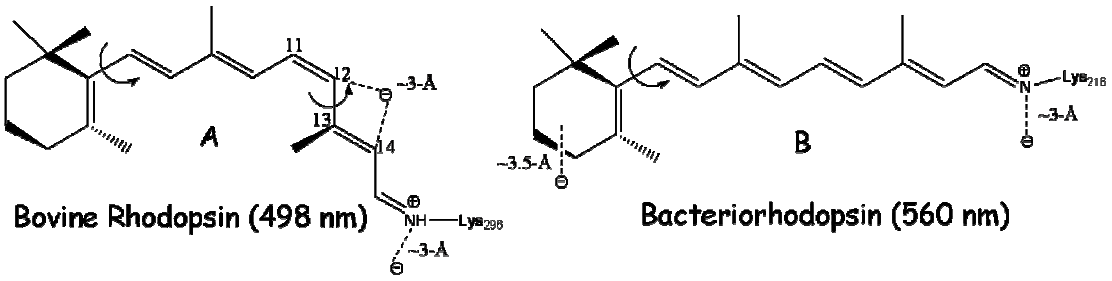

Figure 12 *External point charge model.*

In bovine rhodopsin *(Figure 12-A)*, the existence of a counterion near the protonated nitrogen is assumed. A second negative charge is also located at ~3-Å above C-12. This charge is presumably a member of a charge pair in a salt bridge or possibly the negative end of a neutral dipolar group. In the case of bacteriorhodopsin, a second counterion is located at ~3.5-Å above C-5. The position of the charge depicted in *(Figure 12-B)*, however, is only one example of a location consistent with the experimental results; other locations of the negative charge near the β-ionone ring are also possible.

The external point charges are sensitive to their locations relative to the conjugated chain. These external point charge models accounted for bathochromic shifts of dihydrorhodopsins as well as natural rhodopsins. It was concluded that it is this spatial distribution of charges relative to the retinal SBH^+ moiety that leads to the variation in λ_{max}, of the various pigments and of the intermediates formed during the bleaching process. Although the validity of these models and the identity of the external point charges were not known until the tertiary structures were clarified, they remained as the generally accepted models for further theoretical studies.

1.6.4 Accumulated Evidence

During the past three decades, a number of plausible models have been advanced to account for the spectral tuning of retinal. All rest upon the observation that photoexcitation of 11-*cis*-retinal induces a significant increase in electron delocalization, and a corresponding change in its dipole moment.[107,108] Any protein chromophore interaction that increases delocalization will lead to a smaller energy difference between ground and excited states and therefore a red shift in the absorbance spectrum. Conversely, any interaction that decreases delocalization will

lead to a larger energy difference between ground and excited states and therefore a blue shift in the absorbance spectrum.[112]

Most models propose that a negatively charged amino acid serves as the Schiff's base counterion. Changes in the distance or charge density of the putative counterion have been hypothesized to play a role in generating the differences in absorbance maxima that distinguish the visual pigments from one another, from their photointermediates, and from the reference protonated Schiff base.[172,113,114] Alternatively, the protonated Schiff base in the visual pigment could be paired to a counterion from solution, for instance, chloride, or be stabilized by a surrounding shell of polar residues.

With respect to interactions along the polyene chain, one model proposes that in bovine rhodopsin a negatively charged amino acid selectively stabilizes the photoexcited state by contacting the polyene chain[110,172] near carbon 13. This point charge model is consistent with the red shifts seen in comparing a series of dehydroretinal analogues of bovine rhodopsin with the corresponding N-butylamine salts.[90]

Interactions along the polyene chain that do not involve charged residues have also been considered. Twisting of the chromophore about double or single bonds would produce, respectively, a red or blue shifts;[115-117] polarizable groups near the chromophore would stabilize the photoexcited state by compensatory electronic movements and therefore produce a red shift; and polar groups would produce either a red or blue shift depending upon their orientation with respect to the dipole moment of the chromophore.[118,119] Conformational changes of the 6-s-*cis* bond connecting the polyene chain with the β-ionone ring.[120]

2 Theoretical Framework

Over the past three decades, *ab initio* quantum chemistry has become an essential tool in the study of atoms and molecules and, increasingly, in modelling complex systems such as those arising in biology and materials science. The underlying core technology is computational solution of the electronic Schrödinger equation; given the positions of a collection of atomic nuclei, and the total number of electrons in the system, calculate the electronic energy, electron density, and other properties by means of a well defined, automated approximation (a "model chemistry"). The ability to obtain solutions of sufficient quality to the electronic Schrödinger equation for systems containing tens, hundreds, or even thousands, of atoms has revolutionized the ability of theoretical chemistry to address important problems in a wide range of disciplines; the Nobel Prize awarded to John Pople and Walter Kohn in 1998 is a reflection of this observation.

In its exact form, the electronic Schrödinger equation is a many-body problem, whose computational complexity grows exponentially with the number of electrons, and hence, a brute force solution is intractable. Hartree–Fock theory, a mean field approach, produces reasonable results for many properties but is incapable of providing a robust description of reactive chemical events in which electron correlation has a major role. Thus, a key problem has been the development of treatments of electron correlation that exhibit tractable scaling in computational effort with the size of the system.

Given a well defined theoretical framework of approximation, the next requirement is efficient computational implementation. Considerable sophistication is required to achieve acceptable accuracy and efficiency; the leading quantum chemistry programs are millions of lines of computer code, and mathematical

algorithms to reduce formal scaling of computational effort with system size have an increasingly crucial role in meeting the challenge of handling complex system relevant to practical applications. Below, the most important computational advances are described briefly, and their impact on the ability to address critical problems is discussed.

The treatment of large, condensed phase systems (e.g., proteins in aqueous solution) entirely by *ab initio* methods is extremely expensive computationally. However, it is often the case that a relatively small region of the system can be modelled at the *ab initio* quantum chemical level, whereas the remainder can be treated more approximately [e.g., by means of electrostatics (static point charges), molecular mechanics (MM) or continuum solvation models]. The technologies for coupling quantum chemical methods to these alternative types of models [mixed quantum mechanics QM/MM and self-consistent reaction field (SCRF) approaches] have become an essential component of the theoretical arsenal, enabling realistic modelling of even the most complex molecular structures.

A remarkable range of applications have appeared in the past decade, impacting nearly every aspect of chemistry, biology, and materials science. Continued improvements in the theory and implementation, and reduction in the cost performance of computing, ensure that dramatic progress will continue to be made in the years to come, advancing toward the ultimate goal of theory achieving full partnership with experiment as both an explanatory and predictive methodology.

2.1 *Ab Initio* Quantum Chemistry

The motivation for much of computational quantum chemistry is to determine the electronic energy of molecules, from which useful chemical information such as the structures of molecules and the mechanisms of reactions may be derived. Such calculations can be performed in an *ab initio* fashion, that is, with reference only to fundamental physical constants, by subjecting the laws of quantum mechanics to rigorously defined approximations. The central equation of computational quantum chemistry is the (*time independent*) *electronic Schrödinger equation*[121] solutions of which are the exact non-relativistic energies of the electronic states of a molecule within the *Born-Oppenheimer* (BO) *approximation*.[122] The precise form of this equation is given by:

$$H_{elec}\psi_{elec}(r;R) = E_{elec}\psi_{elec}(r;R) \qquad 2.1$$

where the eigenvalues E_{elec} are the energies associated with the various electronic states of a molecule for a given configuration R of the nuclei, and the operator H_{elec} is known as the *electronic Hamiltonian*.

Both the electronic Hamiltonian H_{elec} and the electronic wavefunction of ψ_{elec} depend explicitly on the coordinates of all electrons *r,* but only parametrically on the nucleus coordinates R; this is what the BO approximation is all about. In the following, since we will be concentrating on the electronic part only, we will drop the subscript and consider the system always in the approximation of a fixed nucleus configuration.

The exact solutions E_{elec} of the electronic Schrödinger equation (Equation 1.1) furnish much of the information sought by practitioners of computational quantum chemistry. Unfortunately, not even the BO approximation renders the Schrödinger equation analytically soluble or even computationally tractable, except for one-electron

systems like the H_2^+ molecule-ion.[123] In order to make *ab initio* methods applicable to systems of chemical interest, additional approximations that address the electron many-body problem must be included.

2.1.1 The Many-Electron Wavefunction

The electronic wavefunction $\psi_R(r)$, describes the simultaneous motion of all the electrons in the system; it is therefore a many-electron wavefunction. In general many-electron wavefunctions are constructed as linear combinations of *n*-electron basis functions, so-called configuration state functions or CSF's)[124]:

$$\psi_i(r) = \sum_k a_{ki}\phi_k(r) \qquad 2.2$$

where $\psi_i(r)$ is the wavefunction of the *i*-th electronic state of the system, $\{\phi_k(r)\}$ are the configuration state functions and $\{a_{ki}\}$ are numerical coefficients which can be optimised, as will be described below, to obtain an accurate description of the system as possible (within the confines of the finite basis expansion approach).

In the majority of applications the CSF's are constructed as antisymmetrised products of one-electron wavefunctions; these are generally atomic or molecular orbitals. CSF's are often defined as linear combinations of these products such that a given CSF is spin and symmetry adapted.

The atomic or molecular orbitals are, in turn, constructed from sets of linearly independent one-electron basis functions:

$$\varphi_i = \sum_{p=1}^{m} c_{pi}\chi_p \qquad 2.3$$

In most applications, these basis functions φ_i, are atom-centred Gaussian type functions. The coefficients of the basis functions are optimised in order to give the best possible description of the atomic or molecular orbitals. More detailed descriptions of

the formulation and optimisation of one- and many-electron wavefunctions are presented in later sections.

2.1.1.1 Configuration Interaction Wavefunctions

The configuration state functions introduced earlier are usually either single Slater determinants or linear combinations thereof. The set of all possible Slater determinants (constructed by considering all possible arrangements of the electrons among the available spin orbitals) therefore forms a set of *n*-electron basis functions for the total electronic wavefunction of the system of interest, $\psi(r)$. If the set of one-electron basis functions (and thus the set of atomic or molecular spin orbitals) is complete (that is, infinite), the resulting infinite set of Slater determinants (CSF's) also forms a complete *n*-electron basis set for $\psi(r)$. This is called the Configuration Interaction (CI) expansion of the wavefunction.[124]

In practice, of course, the set of one-electron basis functions is finite and incomplete and thus the configuration interaction expansion is also finite and can only yield an approximation to the true total wavefunction. Even with a finite one-electron basis set, however, the full set of CSF's for a molecular system even of decent size still contains far too many Slater determinants for such calculations to be computationally feasible. In most applications, therefore, only a subset of these configurations is used. For most molecules, especially near their equilibrium geometries, the wavefunction is dominated by a single CSF. In such cases the Schrödinger equation is first solved subject to the approximation that the wavefunction consists of only this determinant.

This gives both a reference state wavefunction and a convenient set of optimised one-electron orbitals, φ_i, which can be used in the construction of other CSF's. While such single determinant wavefunctions do not account for the effects of electron

correlation (as the independent particle model has been applied), extending them by the inclusion of additional terms in the configuration interaction expansion can correct for this deficiency. Finding solutions of the Schrödinger equation therefore involves finding both the best set of coefficients for the CSF's, $\{a_k\}$, and the optimal set of orbital coefficients, $\{c_{pi}\}$. These coefficients can be obtained by the use of the Variation Principle (described in the next section) or, specifically in the case of the CSF coefficients, by Perturbation Theory[125,126].

2.1.1.2 Variational Principle

Given an approximate wavefunction ψ for a system, the corresponding total energy is, by definition, the expectation value of the Hamiltonian operator:

$$E\psi = \frac{\langle\psi|\hat{H}|\psi\rangle}{\langle\psi|\psi\rangle} \qquad 2.4$$

The Variation Principle or Theorem[127] states that if the energy is stationary with respect to any arbitrary variation, $\delta\psi$, in the wavefunction, i.e.

$$\delta E = 0 \qquad 2.5$$

then the wavefunction is an eigenfunction of the Hamiltonian:

$$\hat{H}\psi = E\psi \qquad 2.6$$

and the lowest eigenvalue, E_0, is an upper bound to the true ground state energy of the system, ε_0:

$$E_0 \geq \varepsilon_0 \qquad 2.7$$

Moreover, according to McDonald's theorem,[128] the higher eigenvalues E_i, are upper bounds to the corresponding excited state energies, ε_i.

The variational flexibility of most approximate wavefunctions is provided by the orbital and CI coefficients c_{pi} and a_k. Variation of these coefficients can be thought of as mixing or rotation between occupied and virtual orbitals (for c_{pi}'s) or among the CSF's (for $\{a_k\}$'s). A "variational" wavefunction, giving the lowest possible energy, is therefore stable under such mixings or rotations.

According to the variational theorem, the energy E_{trial} of a trial wave function satisfying the appropriate boundary conditions is always an upper bound to E_{exact}, the exact ground-state electronic energy. Trial wave functions expressed in terms of freely variable parameters may therefore be optimised, in an energetic sense, by finding those parameters that minimise E_{trial}. Methods that use this principle, for instance Hartree-Fock theory (Section 1.2.1) are said to be *variational*.

In most electronic-structure theories, approximate wave functions are constructed from one-electron wave functions or *spin-orbitals*.[123,129,130] The motivation for this approach is essentially to simplify the many-body problem by allowing the electrons to move independently of one another. Each spin-orbital $\chi(r,\xi)$ is the product of a spatial function or *molecular orbital* (MO) $\psi(r)$, which depends on the spatial coordinates **r** of the electron, with a *spin function*, which depends on the *z*-component of the electron's spin angular momentum as given below

$$\chi(r,\xi) = \begin{cases} \psi^{\alpha}(r)\alpha(\xi) \text{ if } \xi = +\frac{1}{2} \\ \psi^{\beta}(r)\beta(\xi) \text{ if } \xi = -\frac{1}{2} \end{cases} \qquad 2.8$$

2.2 Single-Determinant Methods

Single-determinant or *single-reference methods* approach the exact solution of the electronic Schrödinger equation (Equation 1.1) by improving the description of electronic structure afforded by the Hartree-Fock wave function, which consists of a

single Slater determinant.[123,129,130] These methods are generally appropriate in circumstances where the exact wave function is dominated by a single electronic configuration. This section elaborates on the theoretical approximations involved in single-determinant procedures, and comments upon the issues that may arise in their application to chemical systems.

2.2.1 Hartree-Fock (HF) Theory

Approximate wave functions constructed from spin-orbitals must be antisymmetric with respect to exchange of any two electrons. The simplest such wave function for a system of *n* electrons is the *Slater determinant*,[131] which for orthonormal spin-orbitals takes the form,

$$\Psi \overset{HF-ansatz}{\rightarrow} = \frac{1}{\sqrt{n!}} \begin{vmatrix} \chi_1(1) & \chi_2(1) & .... & \chi_n(1) \\ \chi_1(2) & \chi_2(2) & .... & \chi_n(2) \\ .... & .... & .... & .... \\ \chi_1(n) & \chi_2(n) & .... & \chi_n(n) \end{vmatrix}, \qquad 2.9$$

where $\chi_i(j)$ indicates that electron *j* occupies the *i*-th spin-orbital, and the prefactor is a normalisation constant. Slater determinants form the basis of *Hartree-Fock* (HF) *theory*;[132-135] for a given choice of basis set, the HF wave function is the 'best' Slater determinant in a variational sense. Such wave functions are consistent with chemical intuition, for they correspond to the single *electronic configuration* formed by placing electrons in MOs in an *aufbau* fashion.

HF wave functions may be *restricted* or *unrestricted*, according to whether or not spatial symmetry is enforced between the α and β electrons. For closed-shell systems, the *restricted Hartree-Fock* (RHF) solution comprises a single set of MOs, of which those of lowest energy are doubly occupied, while the remaining higher lying orbitals are unoccupied or *virtual* (Figure 13-a). The extension of restricted methods to

open-shell systems, termed *restricted open-shell Hartree-Fock* (ROHF),[136] also generates a single set of MOs, with the distinction that the occupied MOs may be partitioned into doubly- and singly occupied subspaces (Figure 13-b).

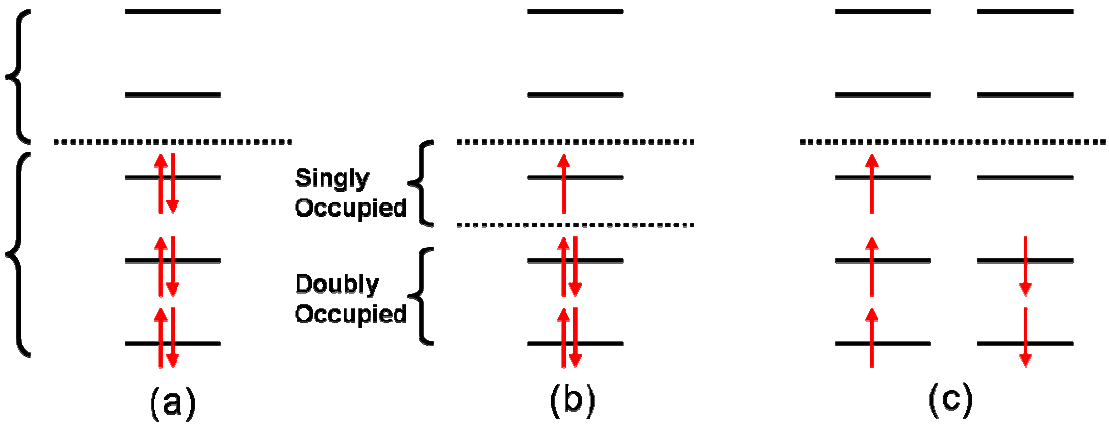

Figure 13 *Schematic representation of restricted (a), restricted open-shell (b) and unrestricted (c) Hartree-Fock solutions.*

In contrast, *unrestricted Hartree-Fock* (UHF)[137,138] wave functions consist of two sets of MOs separately describing the α and β electrons, so that the occupied MOs contain only one electron (Figure 13-c). For singlet states, it is often found that the UHF wave function is associated with a lower energy than the spin-restricted alternative, in which case the RHF wave function is said to possess *singlet-triplet instability*.

However, for such systems UHF methods will often produce the same results as restricted procedures unless the MOs are rotated during the calculation so that they no longer transform as the molecular point group. In practice, this is achieved by using an initial orbital guess in which the HOMO and LUMO are mixed; the resultant method often goes under the extended title of *broken-spin unrestricted Hartree-Fock theory* (BS-UHF).

The RHF approach is generally appropriate for molecules with a closed-shell singlet electronic structure. For open-shell species, however, it is difficult to formulate a general prescription as to when to use ROHF or UHF methodologies. Although ROHF

wave functions correspond to well-defined spin states (doublet, triplet, etc.), the spin polarisation calculated from such wave functions is frequently unphysical. On the other hand, UHF produces a more physically correct description of spin polarisation, but at the expense of introducing the artefact of *spin contamination*.[1] This problem is especially serious when UHF wave functions are used as the starting point for more sophisticated electronic-structure calculations, as we shall see later (Section 2.2.2.3).

In a Restricted Hartree Fock (RHF) calculation the spin orbitals χ are pair wise products of the spatial orbital ϕ (depending on the spatial coordinate $\underline{r}$) and the spin function (depending on the spin coordinate ω), α or β:

$$\chi(\underline{r},\omega) = \begin{cases} \phi(\underline{r})\,\alpha(\omega) \text{ or} \\ \phi(\underline{r})\,\beta(\omega) \end{cases} \qquad 2.10$$

With this ansatz the spin functions α and β can be integrated out. For a numerical treatment the remaining spatial orbitals ϕ are linearly expanded in a finite basis set Q_j of dimension M:

$$\chi_i(\underline{r}) = \sum_j^M k_{ij} Q_j(\underline{r}) \qquad 2.11$$

leading to the Roothaan-Hall equations[139,140]:

$$Fc = Sc\varepsilon, \qquad 2.12$$

where *F* is the Fock matrix with elements,

$$F_{ij} = \langle \chi_i | \hat{F} | \chi_j \rangle \qquad 2.13$$

c is the matrix of eigen vectors which determine the SCF orbitals

$$\varphi = \chi c \qquad 2.14$$

---

[1]UHF wave functions are not pure spin states. The UHF wave function of a doublet radical, for example, is *contaminated* by unphysical contributions from quartet, sextet and other spin states of higher multiplicity.

and *S* is the overlap matrix with elements

$$S_{ij} = \langle \chi_i | \chi_j \rangle \qquad 2.15$$

The Roothaan Hall equation 2.12 must be solved through an iterative procedure called the **Self-Consistent-Field (SCF)** procedure.

2.2.1.1 Self-Consistent Field (SCF) method

The simplest method of determining the electronic structure of molecules by forming approximate solutions to the Schrödinger equation (within the Born-Oppenheimer approximation) is the Hartree-Fock or self-consistent field method (SCF). This method takes the molecular wavefunction (a non-separable function of the coordinates of all N electrons) and approximates this as an antisymmetric product of N one electron functions. Each of these one electron functions (called molecular orbitals) is expanded in an underlying basis set (typically atom centred Gaussian like functions) and the molecular orbitals are then determined by minimising the total energy by varying the expansion coefficients (C).

The simplest N-electron wavefunction is a single antisymmetric product ("Slater determinant") of one electron functions which are orthonormal linear combinations of the atomic orbital basis functions. The computationally most demanding part of the calculation is computing the derivatives of the energy with respect to the molecular orbital coefficients. This is closely related to the Fock matrix (F):

$$F_{ij} = h_{ij} + (1/2) \sum_{kl} \left[2(ij|kl) - (ik|jl) \right] D_{kl} \qquad 2.16$$

where D_{kl} is the density matrix, h_{ij} and $(ij|kl)$ are one and two electron integrals over the underlying basis function.

The *Hartree-Fock* or *self-consistent field method (SCF)* methodology can be summed up as follows:

1) A position is chosen for the atomic nuclei,

2) A certain set of Gaussian basis functions is chosen,

3) An initial guess of the form of the one electron wave functions is generated by choosing the coefficients of the Gaussian basis functions representing each molecular orbital,

4) The density matrix is computed,

5) The Fock Matrix is constructed,

6) The wavefunctions are then solved,

7) Improved molecular orbitals are obtained and used in the first step of the new iteration. Else the process is terminated and continues to next step,

8) The total energy of the system can now be evaluated.

2.2.2 Correlation Energy

The difference between the exact solution of the electronic Schrödinger equation $\hat{H}\left|\Psi_j\right\rangle = E_j^{el}\left|\Psi_j\right\rangle$, E^{el}, and the Hartree Fock limit energy, $E^{(HF-Limit)}$, which is the solution of the Hartree-Fock equations when using a complete basis expansion, is defined as the correlation energy. This definition was originally proposed by Löwdin,[141] who also introduced the concept of the correlation energy, E_{corr}, defined by the equation:

$$E_{corr} = E^{(el)} - E^{(HF-Limit)} \qquad 2.17$$

The obvious way to account for the correlation energy is to use Configuration Interaction (CI). For a given basis set a Full Configuration Interaction (FCI) calculation constitutes a benchmark by which computations of the correlation energy with the same basis set can be judged, i.e. “full CI is the best that one can do”. If the basis set reaches

completeness, the FCI result will be the exact solution $E^{(Schr.)}$. The FCI expansion of an electronic state reads as

$$\left|\Psi^{FCI}\right\rangle = c_0\left|D_0\right\rangle + \sum_{ar} c_a^r \left|D_a^r\right\rangle + \sum_{a<b,r<s} c_{ab}^{rs}\left|D_{ab}^{rs}\right\rangle + ... \qquad 2.18$$

where $\left|D_0\right\rangle$ stands for the ground state configuration and $\left|D_a^r\right\rangle$ denotes a single excitation, *i.e.* a Slater determinant where the spin orbital χ_a which is occupied in the ground state is replaced by the unoccupied (= virtual) spin orbital χ_r. Similarly, $\left|D_{ab}^{rs}\right\rangle$ is a doubly excited determinant where the orbitals χ_a and χ_b are replaced by the virtual orbitals χ_r and χ_s

The number of i-tuply excited determinants for n electrons and 2M spin orbitals, M being the number of spatial basis functions φ, is given by

$$\binom{M}{i}\binom{2M-N}{i} \qquad 2.19$$

From this formula it is clear that the number of configurations in the expansion grows very rapidly with the number of electrons and basis functions making the FCI method only applicable for very small molecules and reduced basis sets. Only truncated CI methods like CIS or CISD, where Single (S) and Double (D) excitations are considered, can be used in general, but they suffer from size inconsistency. Furthermore, CIS gives poor excitation energies.

There are two major phenomena that contribute to the correlation energy. Non-dynamical correlation is the term used for near-degeneracy effects which are not resolved at the Hartree-Fock level. This usually only occurs in systems for which the highest energy (formally) occupied orbitals are close in energy to the (formally) unoccupied orbitals, resulting in several near-degenerate configurations. In such situations the wavefunction will not be dominated by a single configuration

(determinant), and multiconfigurational methods such as MCSCF and CI (see below) must be applied to obtain a good reference state.

While non-dynamical correlation only occurs in special situations, dynamical correlation needs to be considered for all systems. As mentioned earlier, dynamical correlation describes the fact that individual electrons avoid each other. Although the use of a single determinant wavefunction in conjunction with the independent particle model (as for Hartree-Fock SCF theory) neglects this effect, it can be corrected for by the inclusion of additional determinants in the wavefunction such as in CI.

Several methods of varying complexity and accuracy have been proposed in order to account for the dynamical correlation effects; these include the configuration interaction method, Møller-Plesset perturbation theory and coupled cluster theory. Accounting for the correlation of each pair of electrons is naturally quite expensive computationally. In many practical applications, therefore, it is only the correlation of the valence electrons which is explicitly considered while the core electrons are left uncorrelated or "frozen" (the frozen core approximation). The effects of the correlation of the core electrons do need to be considered, however, when high accuracy is required.

The stated aim of most sophisticated *ab initio* methods is to recover a sufficient portion of the correlation energy neglected in the Hartree-Fock approach, in order that chemical processes, such as the breaking of covalent bonds, can be described with greater accuracy. The HF wave function is the usual starting point or *reference wave function* for more advanced methods, because as mentioned it accounts for a significant proportion of the total electronic energy.

2.2.2.1 Multiconfigurational SCF Theory (MCSCF)

In the case of a particular situation involving bond breaking, where the occupied and unoccupied orbitals converge in energy there is a corresponding near-degeneracy amongst the configurations and therefore all near-degenerate Slater determinants Ψ_k, need to be included in the wavefunction in order to properly describe the system:

The complete active space SCF (CASSCF) method[144,142] provides a well defined procedure for choosing *n*-electron configurations in a MCSCF wavefunction.[143-145] As in ROHF, the orbitals are split into three subsets (spaces):

$$\underbrace{\varphi_1 \cdots \varphi_i}_{inactive} \underbrace{\varphi_{i+1} \cdots \varphi_{i+a}}_{active} \underbrace{\varphi_{i+a+1} \cdots \varphi_{i+a+v}}_{virtual} \qquad 2.20$$

where the *i* inactive orbitals are defined as being doubly occupied, the *v* virtual orbitals as unoccupied while the *a* active orbitals have partial occupancy. The relevant configurations are then constructed by considering every possible way (with correct spin and spatial symmetry) of distributing the *n*-2*i* active electrons amongst the *a* active orbitals.

A second order Newton-Raphson type procedure[146] (or an approximate version thereof) is then applied to determine the CI and orbital coefficients such that the generalised Brillouin theorem[147] is satisfied. In other words, on convergence the energy is invariant to rotations between the inactive, active and virtual orbitals.

2.2.2.2 Configuration Interaction (CI)

As outlined in Section 2.1.1 the full many-electron wavefunction for a system can be expressed in terms of the configuration interaction expansion (Equation 2.2). This CI expansion involves all possible determinants which can be constructed by considering every possible arrangement of the available electrons amongst all the

linearly independent molecular orbitals that can be formed from the one particle basis set.

For many systems, however, the many-electron wavefunction ψ, is dominated by a single determinant, in such cases all other configurations can be thought of as a correction, χ, to this reference wavefunction. This correction then accounts for electron correlation.

$$\psi = \psi_0 + \chi \tag{2.21}$$

Application of the Hamiltonian operator followed by projection onto the Hartree-Fock reference state gives:

$$E = E_0 + \left\langle \psi_0 \middle| \hat{H} \middle| \chi \right\rangle \tag{2.22}$$

where E is the total non-relativistic energy of the system and E_0 is the Hartree-Fock reference energy. Thus, according to the definition in Equation (2.17), the correlation energy is simply given by:

$$E_{corr} = \left\langle \psi_0 \middle| \hat{H} \middle| \chi \right\rangle \tag{2.23}$$

This is known as the correlation energy formula. The correction χ can be constructed in a systematic way by generating configurations in the reference determinant by unoccupied spin orbitals.

As the one-electron, viz. molecular orbital (MO), basis has already been optimised in the SCF determination of the Hartree-Fock reference state, the CI coefficients might be expected to show rapid convergence. Unfortunately this is not the case in practice; while the individual coefficients of higher than double excitations do systematically decrease in magnitude, their collective energetic contributions converge slowly with the order of the excitation. This is associated with the difficult problem of

resolving the electron cusp using wavefunctions that do not explicitly depend on inter-electron coordinates.[148]

Although the full CI expansion formally has up to *n*-fold excitation terms (where *n* is the number of electrons in the system), it can be shown that when E_{corr} is evaluated by the correlation energy formula it is only the double excitation terms which contribute. This is because in the orthonormal SCF MO basis the Brillouin condition applies and, according to the Slater-Condon rules, terms with higher than double excitations have zero Hamiltonian matrix elements with the reference state, ψ_0.Thus

$$\begin{aligned} E_{corr} &= \sum_{\substack{i<j,\\ a<b}} \left\langle \psi_0 \middle| \hat{H} \middle| \phi_{ij}^{ab} \right\rangle a_{ij}^{ab} \\ &= \sum_{\substack{i<j,\\ a<b}} \left\langle ij \middle\| ab \right\rangle a_{ij}^{ab} \end{aligned} \qquad 2.24$$

Unfortunately, before E_{corr} can be calculated via this method the coefficients $\left\{a_{ij}^{ab}\right\}$, must be known. In the Full Configuration Interaction (full-CI) method the calculation of $\left\{a_{ij}^{ab}\right\}$, involves the application of the variational principle to solve the appropriate matrix eigenvalue equations for the full configuration interaction expansion of the wavefunction.

This is straightforward in principle but in practice the number of configurations, and thus the computational cost of calculations, rises rapidly with the number of electrons and the size of the MO basis. The computations can be made more efficient by the consideration of spatial and spin symmetry and the application of the Direct CI approach[149,150] (with the Davidson diagonalisation method[151]). Nevertheless, full-CI calculations are still only feasible for small molecules with up to ~10 electrons and modest basis sets (up to about double zeta plus polarisation functions quality).

It is therefore common practice to truncate the CI expansion at the double excitation terms, neglecting triple and higher excitations. While this reduces the size of the problem so that it becomes computationally feasible, the resulting solutions are not size extensive, that is, they do not scale correctly with the number of electrons in the system. This is a serious problem, especially in the context of computing molecular binding energies and intermolecular forces. A useful, although very approximate, way to correct for size extensivity is via the Davidson correction:[152]

$$E_{Dav} = E_{corr}(1 - a_0^{\,2}) \qquad 2.25$$

or via[153]

$$E_{Dav} = E_{corr}\frac{(1 - a_0^{\,2})}{a_0^{\,2}} \qquad 2.26$$

where a_0 is the coefficient of the reference state in the normalised CI expansion. CI can also be extended to multireference wavefunctions, where the reference state is typically a CASSCF wave function. This results in a method of very high accuracy but also high cost. While the multireference CI (MRCI) method is one of the most accurate pure *ab initio* techniques it has not been employed in this work.

2.2.2.3 Møller-Plesset Perturbation Theory (MPPT)

Many-body perturbation theory is an alternative method for recovering electron correlation that is not based explicitly on CI. There are many implementations of this theory, but the most commonly used form is *Møller-Plesset* (MP) *perturbation theory*. MPPT involves the use of perturbation theory to determine the coefficients in the CI expansion. It is based on the assumption that the effects of dynamical correlation can be regarded as a perturbation, $\hat{V}$, to the all-electron Fock operator, $\hat{F}$ (described in **Section 1.2.1.1**). The Hamiltonian is formally partitioned:

$$\hat{H} = \hat{F} + \hat{V} \qquad 2.27$$

where $\hat{V}$ is known as the fluctuation operator.

Starting with the Hartree-Fock wave function as the unperturbed state, the application of Rayleigh-Schrödinger perturbation theory yields the perturbative corrections to the wavefunction $\psi^{(1)}, \psi^{(2)}, \psi^{(3)}$, etc.; these are constructed from the single, double, triple, etc. excitations as specified in the configuration interaction expansion of the wavefunction.

The perturbation corrections to the energy, $E_{(1)}, E_{(2)}, E_{(3)}$.... (to first, second, third,... order) and the corresponding contributions to the coefficients ($\{a_i^a\}, \{a_{ij}^{ab}\}$, etc.) in the CI expansion can thus be determined. As the first order energy correction is simply the expectation value of the perturbing fluctuation operator with respect to the Hartree-Fock reference state, perturbation theory to first order in the energy yields the original Hartree-Fock energy.

The second order energy correction, $E_{(2)}$, in the basis of the occupied (i, j,…) and unoccupied (a, b,…) spin orbitals is found to be:

$$E_2 = \frac{1}{4} \sum_{\substack{i,j \\ a,b}} \frac{\langle ij \| ab \rangle^2}{\varepsilon_i + \varepsilon_j - \varepsilon_{ai} - \varepsilon_b} \qquad 2.28$$

where ε_i, ε_j, … are the Hartree-Fock orbital energies.

$E_{(2)}$ is known as the MP2 correlation energy. Møller-Plesset perturbation theory to second order (in the energy) is widely used as it is computationally inexpensive and thus allows correlated calculations to be performed for relatively large molecules.

Perturbation theory up to fourth order in the energy (MP4) is also commonly used; this requires knowledge of the second order correction to the wavefunction, $\psi^{(2)}$, which has contributions from single, double, triple and quadruple excitations.

Accounting for triple excitations has been found to be more difficult (and expensive) than accounting for the quadruples so they are often neglected, giving MP4 (SDQ) theory. (MP4 theory with triple excitations included is denoted MP4 (SDTQ).) It has been observed that the additional accuracy obtainable by including higher order terms in the perturbation expansion comes at a high additional computational expense; it is therefore more practical to use configuration interaction or coupled cluster methods when higher accuracy is required.

Møller-Plesset perturbation theory can be applied within the framework of both single- and multi-determinant reference states. The most successful implementation of the latter is the complete active space second order perturbation theory (CASPT2) method of Andersson et al.[154,155] Being based on a CASSCF reference state, CASPT2 accounts for both dynamical and non-dynamical correlation. As the formalism is significantly more complex than for single determinant perturbation theory (due to the more complex form of the reference state) the computational effort and cost are also greater.

2.3 Multi-Reference Methods

Due to their multiconfigurational character, electronic excited states cannot be described by a single Slater determinant and, therefore, a multiconfigurational procedure is needed. A solution for computing electronic excited states or for cases where a single determinant is not even a good zeroth order reference wavefunction is the so-called **Multi-Configuration Self-Consistent Field (MCSCF)** approach which consists of a truncated CI expansion where not only the CI coefficients C_i in front of the Slater-determinants $|D_i\rangle$

$$|\phi^{MCSCF}\rangle = \sum_i C_i |D_i\rangle \qquad 2.29$$

are variationally optimized, but also the molecular orbital coefficients $\{c_{pi}\}$ in the basis set expansion. The practical problem lies in the choice of the relevant configurations $|D_i\rangle$. A generally established solution consists of partitioning the molecular orbitals into active and inactive spaces. This is the way how the selection of the configurations is chosen in the **Complete Active Space Self Consistent Field** method **(CASSCF)**.

2.3.1 CASSCF

This methodology has been applied in recent years to study electronic spectra of organic and inorganic molecules. In general, the results have proven that the CASSCF method yields a balanced description of the electronic states and provides reliable predictions of physical properties and transition dipoles. The static part of the correlation energy accounts for the effect of allowing the orbital to be partly singly occupied, like in the CASSCF description, instead of forcing double occupation, like in the HF approximation. The remaining correlation energy is the dynamic correlation which describes the correlated motion of the electrons. The latter part is normally taken into account by subsequent perturbation treatment, CASPT2 or by the Multi-Reference Configuration Interaction (MRCI) method.[156-161] Conventional CI methods like CISD consider only configurations generated by exciting electrons from a single determinant, usually the ground state RHF wave function. A MRCI calculation is based on a previous MCSCF treatment, for example CASSCF.

2.3.1.1 Practical Aspects

The crucial element in performing CASSCF calculations is to correctly choose the active orbital space and the number of active electrons. This task is far from being straightforward, particularly in situations where chemical bonds are elongated and simultaneously the molecule is excited to a higher electronic state. The choice of the

active orbitals requires an insight into the electronic structure of the molecule at all stages of the process under consideration. In some cases this choice is obvious, for example, in the case of rupturing a chemical bond in the ground electronic state, the bonding and the antibonding orbitals for the ruptured bond should be included in the active space. However, in situations where the molecule undergoes a more complex transformation, the choice is often not so clear, and several trials are necessary before the right active space is found.

There are some approximate criteria that one can use in selecting the active space. Generally, to obtain initial orbitals for the CASSCF calculation, UHF natural orbitals are used. UHF natural orbitals are those which provide fractional orbital occupation numbers. The orbitals that should be included in a CASSCF wavefunction are those with occupation numbers that differ from zero or two (i.e. not empty). Typically, valence orbitals with occupation numbers above 0.02 are included in the active space. Also, a single-point CI calculation followed by analysis of the occupation numbers of the natural orbitals derived from the CI density matrix can be used in selecting the active space.

In general, when a more extended range of the potential energy surface (PES) is considered, the natural orbitals analysis should be performed at different geometries to select a uniform active space that provides a balanced treatment along the whole PES. In calculating electronic spectra, the active orbital space is usually determined based on the type of excitation considered. The convergence of the computed transition moment between the calculated states with the size of the active orbital set has been used as a criterion for selecting the active orbitals.

Another possibility is to use the single excitation configuration interaction (SCI) method and select the orbitals that are present in the most important configurations in

the considered states. However, because SCI cannot properly describe the bond dissociation due to its lacking higher excited configurations (even a description of single bond dissociation requires doubly excited configurations in the wave function), the use of this criterion may lead to an inadequate active space. Moreover, even in cases when one is able to select an adequate active space, it may happen that it is computationally intractable due to its size and a smaller space needs to be considered.

An extension of the CAS model is the restricted active space (RAS) concept. As for CAS wave-functions, the orbitals in a RAS calculation are divided into three classes: inactive, active and secondary. In addition, there is a further subdivision of the active orbitals: the RAS1, RAS2, and RAS3 categories. In the construction of the RAS wave-function, restrictions are imposed on the number of electrons or holes in the RAS1 and RAS3 subspaces, i.e. a maximum number of holes may be created in RAS1 and a maximum number of electrons are allowed in RAS3; no constraints are placed on the orbital occupations in RAS2. This has the advantage over the CASSCF method that in general more active orbitals can be considered. A variety of wave-functions can be actually created within the RAS framework.

For example, a multireference singles and doubles CI (MR-SDCI) wave-function with a CAS reference space may be obtained when RAS1 has at most two holes and RAS3 at most two electrons. The RAS concept combines thus the features of the CAS wave-functions with those of more advanced CI wave-functions where dynamical correlation effects are included.

In conclusion, the selection of the active space is a problem that needs to be considered individually on a case-by-case basis. One can use one of the criteria mentioned above or a combination of the criteria. The major virtue of CASSCF is that it is capable of describing the nondynamical electron correlation in a size-consistent and

balanced way in situations when the electronic structure strongly changes, as it happens near transition states and in electronic excitation processes.

However, in most cases it has not been possible to compute with high accuracy the transition energies because the CASSCF wave function includes only a fraction of the electron correlation. To account for the remaining electron correlation effects one need to go beyond the CASSCF level of approximation. One of the most computationally reliable methods available at present is arguably the **multiconfiguration second-order perturbation theory (CASPT2)** method.

2.3.2 CASPT2

The multireference Møller–Plesset (MRMP) method is a single root perturbative technique based on the Rayleigh–Schrödinger perturbation theory. Second-order Many Body Perturbation Theory (MBPT) is the simplest possible treatment of dynamical electron correlation. A second-order perturbation approach to dynamical correlation, with a reference state given by a multiconfiguration CASSCF-type wave-function is referred to as complete active space second-order perturbation theory (CASPT2).[162]

The CASPT2 method computes the first-order wave function and the second-order energy with the CASSCF wave function as the reference function. The zeroth order Hamiltonian is defined using Fock-type one-electron operators, and is constructed in such a way that for the closed-shell single determinant case the CASPT2 method becomes equivalent to the conventional MP2-Møller Plesset second-order perturbation theory. Two different formulations of the zeroth-order Hamiltonian are possible: one that includes only the diagonal part of the Fock matrix PT2D, and one that includes also the nondiagonal elements-PT2F. The latter one was applied in the present study.

In this formulation, the zero-order Hamiltonian is a sum of Fock-type one-electron operators, such that it has $|0\rangle$, the multiconfigurational CASSCF wave-function, as an eigenfunction:

$$\hat{H}_0 = \hat{P}_0 \hat{f}_0 \hat{P}_0 + \hat{P}\ \hat{f}\ \hat{P}, \tag{2.30}$$

where $\hat{P}_0 = |0\rangle\langle 0|$ is a projection operator onto the reference function, $\hat{P}$ is a corresponding projection operator for the rest of the configuration space, and $\hat{f}$ is the CASSCF Fock operator:

$$\hat{f} = \sum_{p,q} f_{pq} E_{pq} = \frac{1}{2} \sum_{p,q} \sum_{\sigma} \langle 0 | \left[a_{q\sigma}^{\perp}, \left[a_{p\sigma}, \hat{H} \right] \right] + |0\rangle E_{pq} \tag{2.31}$$

The CI space is partitioned into four subspaces: 0 – the reference function, *K* – the rest of the CASCI space, *SD* – all singly and doubly excited configuration state functions with respect to the CAS reference, and *X* – the rest of the CI space. This is accomplished by introducing the orthogonal projectors $\hat{P}_K + \hat{P}_{SD} + \hat{P}_X = \hat{P}$, with $\hat{P}_0 + \hat{P} = 1$. The block diagonal structure imposed by the projectors insures that the corrections to the wave-function truncate at a finite level of excitation.

The perturbation part of the Hamiltonian is the difference between the full Hamiltonian and $\hat{H}_0$ Using the so-called internally contracted scheme, the first-order wavefunction correction is written as a linear combination of all single and double excitations from $|0\rangle$:

$$\left|0^{(1)}\right\rangle = \sum_{p,q} C^{(1)}_{p,q \geq r,s} e_{pqrs} |0\rangle. \tag{2.32}$$

In the summation, *q* and *s* are occupied, inactive or active; *p* and *r* are noninactive, i.e. active or secondary. All single and double excitations with respect to $|0\rangle$ are included in the wave-function, except those which have all four indices in the

active space. Such terms belong to the space K and do not interact with $|0\rangle$. The internally contracted formalism reduces considerably the number of terms in the perturbation series, at the cost of greater complexity in the individual terms.

The first- and second-order CASPT energy corrections are calculated as,

$$E^{(1)} = C^{(0)^T} U C^{(0)} \text{ and } E^{(2)} = C^{(1)^T} U C^{(0)}, \quad 2.33$$

where $C^{(0)}$ defines the zero-order state and we used the partitioning of the Hamiltonian matrix $H = H_0 + U$ is used. The first-order wave-function $C^{(1)}$ is obtained as an iterative solution to a set of linear equations of the type:

$$C^{(1)} = -P\left(H_0 - E^{(0)}S\right)^{-1} P U C^{(0)}, \quad 2.34$$

where $P = 1 - C^{(0)}C^{(0)^T}$, $S_{ij} = \langle i | j \rangle$, and $|i\rangle$ refers to one of the contracted configurations $E_{pq}|0\rangle$ or $e_{pqrs}|0\rangle$.

Commonly, all single and double excitations from the reference space are included; this is denoted as multireference singles and doubles CI (MR-SDCI). (MR)CI calculations provide a systematic method for treating electron correlation effects.

It allows one to approach the exact solution following an order-by-order expansion of the wave-function, i.e. singly excited, doubly excited, triply excited, and so on. Perturbation theory provides an alternative systematic approach to recover the correlation energy and it is computationally less expensive than a (MR) CI. This treatment includes a large amount of the dynamical correlation leading to very accurate results for excitation energies (normally the error is in the range 0.0-0.3 eV)

2.3.2.1 Intruder States

Consider a singly or doubly excited state, say $|s\rangle$, that is coupled and quasi degenerate with the reference state $|\alpha\rangle$:

$$\langle s|H|\alpha\rangle \neq 0, \qquad 2.35$$

$$E_s^{(0)} \cong E_\alpha^{(0)}. \qquad 2.36$$

In that case, the second-order energy gives

$$E_\alpha^{(2)} \rightarrow \begin{cases} +\infty ...if\ E_s^{(0)} - E_\alpha^{(0)} \rightarrow 0^- \\ -\infty ...if\ E_s^{(0)} - E_\alpha^{(0)} \rightarrow 0^+ \end{cases} \qquad 2.37$$

where the singularity in $E_\alpha^{(2)}$ is caused by a poor choice of either $E_s^{(0)}\ or\ E_\alpha^{(0)}$. In the limit $(E_s^{(0)}\ or\ E_\alpha^{(0)})$, the second-order energy $E_\alpha^{(2)}$ is infinite, while for the quasi degenerate case, $E_s^{(0)} \cong E_\alpha^{(0)}$ it is very large, positive or negative, yielding usually poor results.

For example, for a state with $(\langle s|H|\alpha\rangle = 0.0005$ a.u) —a weak coupling case— the error is larger than 0.05 a.u. when $(E_s^{(0)} - E_\alpha^{(0)})$ lies within ± 0.000005 a.u. For our purposes, the state $|s\rangle$, in the above example is defined as an intruder state.[163-165] Generally the intruder states are more likely to occur in MRMP when the reference state $|\alpha\rangle$ is a high-lying state, and when a basis set with diffuse functions is used.

Sometimes, for some states no CASPT2 energy is calculated. The reason is that for these states the weight of the CASSCF wave function is significantly lower than for the other states. The low weight indicates that some configurations outside the CAS space have a large contribution to the corrected wave function and should not be treated by perturbation theory but added to the CASSCF wave function expansion instead. As in all perturbational schemes based on Fock-type zeroth-order Hamiltonians, configurations can appear in the first-order wave function with a diagonal matrix element of $\hat{H}_0$ that is very close to (or even lower than) the zeroth-order energy of the reference wave function. This leads to very small (or negative) energy denominators in

the expressions for the corrected energy and wave function, thus causing a breakdown of the perturbation approach, known as the intruder state problem.

A large off-diagonal interaction matrix element between such an intruder state and the reference wave function indicates that it is inevitable to add the configuration to the reference space. On the other hand, it can also happen that the intruder state does not have a large interaction with the reference wave function. Near degeneracy in the zeroth-order Hamiltonian leads to the problem of intruder states. The solution of this problem is to increase the active space. However, this is not always possible, since a larger active space increases the number of configurations and therefore, the computational cost.

Roos and coworkers[163] introduced a method to remove such intruder states by applying a level shift ε to all external configurations treated in the perturbation theory. Subsequently, the second-order estimate for the energy is corrected for the applied level shift. Note that within this method only the energy is corrected, but not the wave function.

The method requires the solution of

$$(\hat{H}_0 - E_0)\Psi_1 = -(\hat{H}_1 - E_1)\Psi_0 \qquad 2.38$$

where Ψ_1, the first-order perturbation to the wave function, is expressed as a large number, typically 100000-1000000, of excitation amplitudes. $\hat{H}_0$ cannot be exactly diagonalized in the representation used, but a good diagonal approximation is used in an iterative scheme and a converged solution is usually obtained in half a dozen iterations or so. The corresponding equation with a constant denominator shift ε - the *level shift* of the LS-CASPT2 method - is then

$$(\hat{H}_0 - E_0 + \varepsilon)\tilde{\Psi}_1 = -(\hat{H}_1 - E_1)\Psi_0, \qquad 2.39$$

where

$$\hat{H}_0\Phi_i = \varepsilon_i\Phi_i (i \in \{1....M\}),$$

$$\tilde{\Psi}_1 = \sum_{i=1}^{M} \tilde{C}_1\Phi_i,$$

$$\tilde{C}_i = -\frac{V_i}{\Delta_i + \varepsilon}$$

$$\tilde{E}_2 = -\sum_{i=1}^{M} \frac{\left|\left\langle \Phi_i \middle| \hat{H}_1\Psi_0 \right\rangle\right|^2}{\varepsilon_i - E_0 + \varepsilon} = -\sum_{i=1}^{M} \frac{|V_i|^2}{\Delta_i + \varepsilon}$$

The tilde denotes quantities affected by the level shift. The resulting second-order energy $\tilde{E}_2$ depends on ε. This is of course the intention, close to a singularity. However, away from the singularity, i.e. when no denominator is very small, Roos and Andersson minimized the effect on the energy by using a level shift correction. They defined

$$E_2^{LS} = \tilde{E}_2 - \varepsilon\left(\frac{1}{\tilde{\omega}} - 1\right), \qquad 2.40$$

where $\tilde{\omega}$ is the weight of the CASSCF reference function Ψ_0 in the (normalized) wavefunction through first order. This energy is much less sensitive to the shift than $\tilde{E}_2$ is.

When applied to excited states, a small shift merely moves the singularity. A large shift may cause new divergences, and too large shifts are unacceptable since the potential function is affected in regions further away from the singularities. Therefore, based on our experience the extent of using level shift to avoid the intruder state problem depends on a case by case basis. Throughout this thesis, a level shift of 0.3 a.u is applied and therefore the energies presented in the results section can be compared with the experiment and thereby the accuracy of the applied quantum chemistry method can be judged.

2.4 Technical Details

In short, my thesis work is based on the theoretically refined 2.2-Å, 2.6-Å crystal structures of rhodopsin and bathorhodopsin, while for isorhodopsin an independent quantum mechanical model was prepared. The wave function of the whole binding pocket including the chromophore was calculated with Gaussian[166] using DFT (B3LYP in a 6-31G** basis set) on which natural and Mulliken population analysis were performed.

All the reported calculations were performed using the MOLCAS-5.4[167] and/or 6.2[168] quantum chemistry software packages. Ground and excited state energies were calculated with the CASSCF method. The starting orbitals for each and every CASSCF calculation was taken from the SCF orbitals and strictly no recycled old orbital files was used. Six-root state-averaged wave functions were expanded in an atomic natural orbital basis set with the contraction C,N,O[4s3p1d]/H[2s]. The active space was (12,12), i.e., all pseudo π-electrons and valence pseudo π-orbitals were considered. Second-order corrections to the CASSCF energies were calculated with CASPT2. All core orbitals were kept frozen during the calculations. To avoid the effect of intruder states, the level shift was set uniformly to 0.3 au unless and until specified otherwise. CASPT2-corrected state energies were combined with transition dipole moments calculated by the CAS state interaction method (CASSI)[169] to obtain oscillator strengths. All excitations were assumed to be vertical.

3 Theme

High-level quantum mechanical studies of the photophysical properties of an interesting and biologically relevant class of proteins known as rhodopsin is at the focus of my thesis. In particular, I have studied the spectral tuning process of the retinal chromophore in three different forms of rhodopsin, namely dark-adapted rhodopsin, its first isolable light-adapted photo-intermediate bathorhodopsin and isorhodopsin, an artificial pigment generated by incorporating 9-*cis*-retinal into opsin. It is tempting to compare the absorption maxima of these three pigments *(Figure 14)* with those of the three cone pigments responsible for trichromatic color vision *(Figure 1)*.

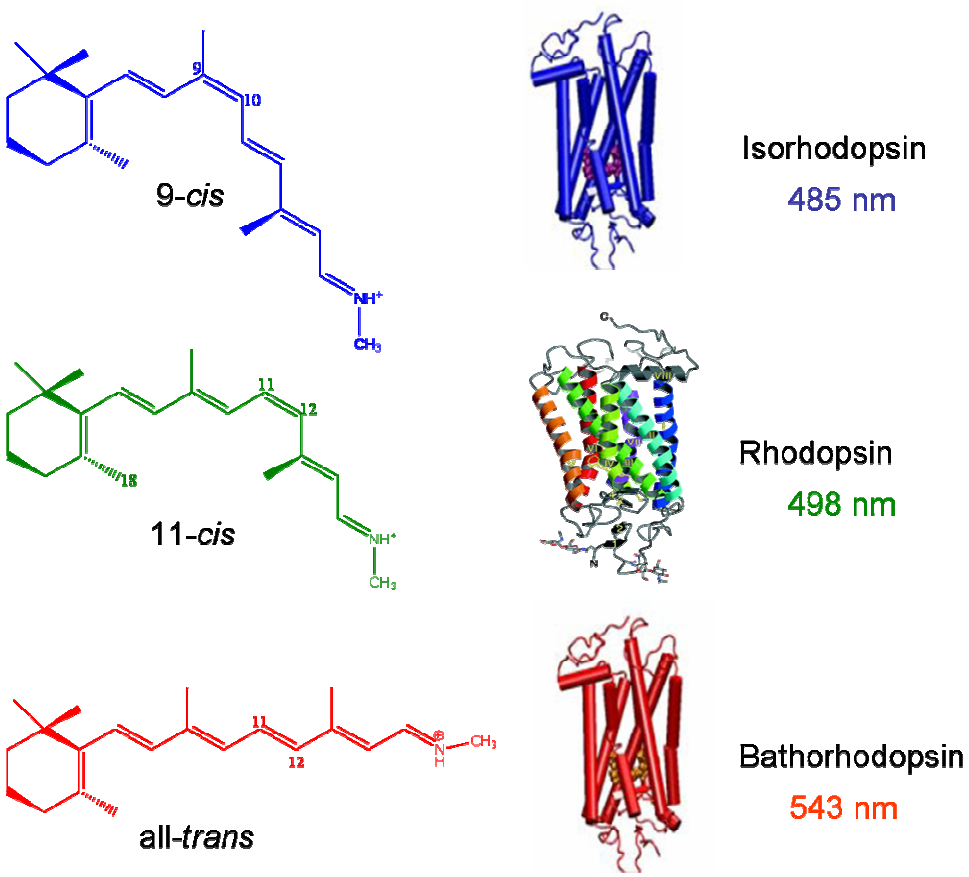

Figure 14 *Absorption maximum of the 9-cis-, 11-cis- and the all-trans- retinal protonated Schiff base chromophore in isorhodopsin, rhodopsin and bathorhodopsin.*

Isorhodopsin absorbs at 485 nm (blue like), while rhodopsin absorbs at 498 nm (green like), and bathorhodopsin peaks at 543 nm (red like). However, the similarities stop here, as unlike the cone pigments these three pigments contain three different chromophores distinctly different from one another. Unravelling the origin of wavelength regulation mechanism in these pigments strongly depends on understanding the characteristics of the chromophore-protein interaction at a molecular level.

Models for the binding pocket of these three pigments based on the best available crystal structure data have been employed throughout my thesis. A step-wise probe has been initiated, starting with the retinal chromophores in *vacuo* **(vac)**; followed by calculations on their distorted conformations in the protein **(dist)**; to which the counterion is attached giving the relevant *"ion-pair"* structures **(ip)**; which when embedded into their respective protein pockets result in the protein embedded chromophores **(pe)**. In order to see the larger picture, the role of the so-called residual effect is pitted against the counterion effect, while the effect of a mutant on the absorbance in conjunction with the reason for the presence of two water molecules near to the Schiff base binding site were also studied.

As the applicability of theory to the calculation of absorption maxima was rigorously tested, an *out-of-the-box* solution for negating the effect of counterion was unearthed which the author believes, if confirmed by experiments can have wide ranging implications on the pharmacological activity of GPCRs in humans and animals.

3.1 Spectral Tuning in Rhodopsin

Rhodopsins (and rhodopsin-like systems) have been the subject of very intensive experimental and theoretical investigations for the last thirty-five years. The

unquestionable successes of the first decades of investigations led to the optimistic opinion that one would soon be able to truly describe the structure and mechanisms of the action of different retinal-based systems.[8] However, recent years have taught us a lesson in humiliation: arguments have accumulated against the principal rhodopsins paradigms. The arguments based on our research supplement this opinion. We are returning to the basic questions which were at the beginning of "rhodopsin research".

Theoretical studies of electronic spectra date back to the early days of quantum chemistry. Yet, despite this early start, most quantum mechanical studies have been confined to isolated molecules in the gas phase, while most experimental studies involve molecules in solutions.[170-173] Thus, the development of methods capable of evaluating the spectra of molecules in solutions as well as in pigments is one of the challenges of modern quantum chemistry.

The protonated Schiff base formed between n-butylamine and 11-*cis*-retinal absorbs at 440 nm in CH_3OH,[102,103] however, in bovine rhodopsin, in which retinal is covalently bound to Lys296 the absorption maximum is shifted to 498 nm.[5,6] The origin of the anomalous spectroscopic properties of the visual pigments and their photoproducts is one of the intriguing problems confronting research on the physiochemical mechanism of vision. In fact, Pitt has suggested that no simple theory exists which can "explain" these spectra.[174] In principle, the red shift of +58 nm or the so-called "opsin shift" can be explained in the language of molecular orbital theory by simply considering various kinds of electrical interactions between the opsin binding site and the ground and lowest excited state of the protonated Schiff base imine.

3.1.1 Chromophore – Protein Interplay

There is considerable support for the suggestion that electrostatic interactions between the chromophore and charged or dipolar groups on the opsin are responsible

for wavelength regulation in visual pigments. The excitation of the protonated Schiff base (PSB) of retinal has been studied in terms of valence bond or resonance theory[103,175,176] which predicts that in the ground state the positive charge is located on nitrogen, whereas in the lowest excited state the charge is delocalized on alternate carbon atoms (*Figure 15*).

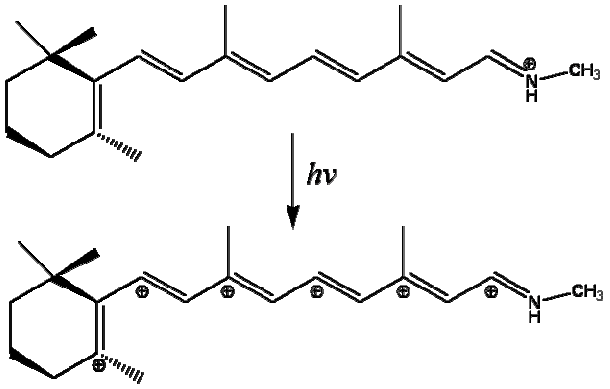

Figure 15 *Positive charge located on nitrogen in the ground state and delocalized on alternating carbon atoms in the excited state.*

If negatively charged groups, such as COO^-, O^-, or S^-, are distributed throughout the binding site, these electron-rich centres can lower the energy of the first excited state by stabilizing the delocalized positive charge of this state, and thus shift the absorption maximum toward the red.

In the discussion below, we shall be concerned with the behaviour of electrons in the highest filled molecular orbital, a π-bonding orbital, and the lowest (in the ground state) unfilled orbital, a π* antibonding molecular orbital. To simplify the arguments, let us assume that an electron in the π orbital is delocalized over all 12 atoms of the π system in the chromophore, and that in the π* orbital the electron is essentially located around the iminium nitrogen atom, rendering it nearly neutral (in the Franck-Condon state, as a result of the electric dipole transition oriented in the long axis of the polyene).[177]

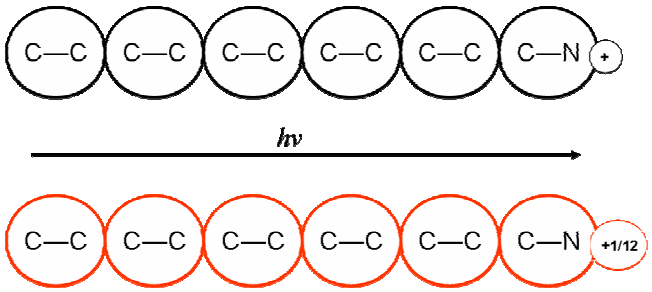

Figure 16 *Schematic molecular orbital representations of the highest energy π orbital during excitation of the retinal cation. Black circles indicate doubly (electron) occupied ground state, red circles indicate orbital is half-filled, nitrogen is neutralized, leaving a residual charge of +1/12 on all atoms ideally. The arrow indicates the electric dipole transition moment accompanying photoexcitation of an electron to the not shown (π*) orbital polarized primarily around nitrogen.*

In the ground state, two electrons occupy the highest π orbital and the iminium nitrogen carries a unit positive charge.[178] In the excited π,π* state, one electron occupies the π orbital while the other now occupies the π* orbital with most of the charge density around nitrogen**.** Thus, in the π,π* state, each of the twelve atoms in this simple model (including nitrogen) of the π system carries a 1/12 e positive charge (*Figure 16*). It is then appropriate to consider what factors determine the energy needed to promote an electron in the π orbital to the π* orbital, or in state terminology, the energy difference between the ground and π,π* singlet excited state.

The problem can be considered by one of the two reasonable approaches. (1) The energies of the ground and excited π,π* states are determined by the energy of the isolated chromophore plus the sum of electrostatic and induced dipole interactions between the state and its environment. (2) Alternatively, one can consider the energy of the system as a unit rather than the sum *E* (vacuum) and *E* (interactions). Thus the position and behaviour of an electron are "localized" in such a way as to obtain the lowest possible potential energy with respect to electrical interactions.

Let us then determine in a qualitative way how the energy difference between the ground and π,π* states changes as we successively consider the cationic chromophore in the following different environments **(A)** *in the vacuum or the gas*

phase; **(B)** *in the protein environment which induces significant geometric distortions;* **C)** *as an anion tightly bound to the iminium nitrogen;* **D)** *interacting with static point charges capable of inducing dipole interactions;* **E)** *in mutants where native amino acid side chain groups of the protein environment are mutated;* **F)** *in a dehydrated protein environment involving step-wise removal of water molecules;* **G)** *with the charge of the protein, modulated presenting a "hostile" anionic environment.* We thus propose an alternative spectroscopic model which attempts to predict the behaviour of the chromophore in several specific environmental situations, after which experimental data of others and ourselves will be given and discussed in light of the model.

3.1.2 Vacuo

Upon π-π* excitation in vacuo where the chromophore is sealed off from any external influence, the electron density is shifted towards the iminium nitrogen atom. This excited state, with a life time too short for vibrational relaxation, and its energy relative to the ground state determines the absorption spectrum. The energy required for excitation can be calculated by standard molecular orbital methods.

3.1.2.1 Reference Point

The reference point for spectral tuning was considered to be the solution spectrum of the chromophore in methanol compared to that of the pigment. The red shift of 58 nm – the so called "opsin shift" – remained the point of departure for extensive theoretical investigations as long as there was no rhodopsin structure available. Modelling the reference point proved to be a nightmare for theory since it involves many difficulties, the most important being the aspect of encountering a mobile anion in solution compared to a static anion inside the protein.

Now that we know the structure of rhodopsin in atomic detail, it makes much more sense to calculate the electronic spectrum "bottom up", starting with the chromophore in *vacuo*, where it is completely devoid of any environmental influence, and then adding the different perturbations which the chromophore undergoes as a consequence of binding to the protein. This approach was keenly adapted in several research groups in the last couple of years (*Figure 17*).[179-184]

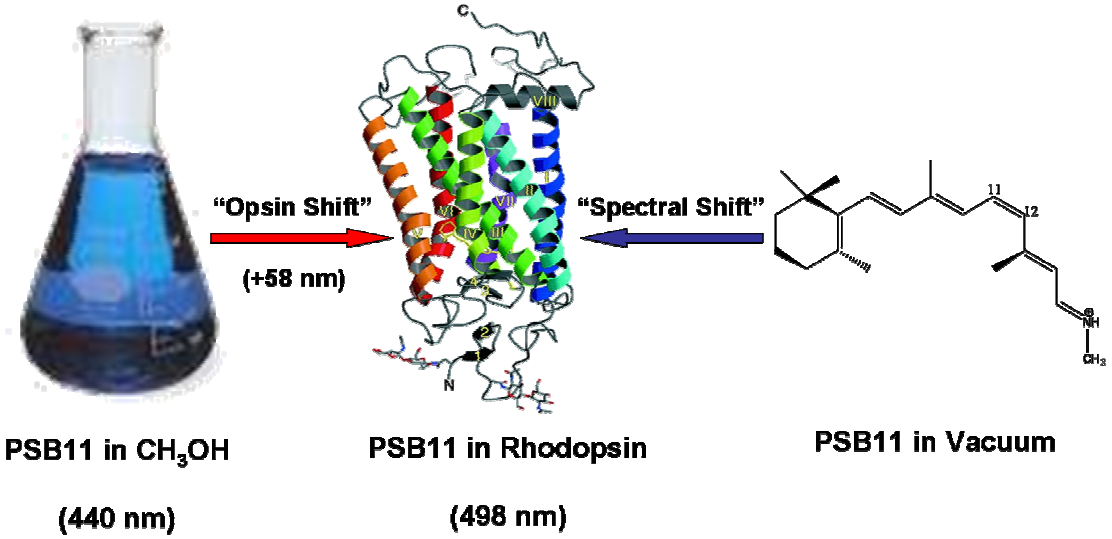

Figure 17 *Schematic representation of the protonated Schiff base of 11-cis-retinal chromophore in different environments.*

However, perusal of the literature suggests that theoretical values do not agree on the absorption maximum of this reference point. The earliest semi-empirical calculations by Blatz,[170] Suzuki,[171] Honig and coworkers,[172] converged on a value around 600 nm. Some 30 years later, with an exponential development of computational resources and with the structure of rhodopsin known in atomic detail the situation has become less clear-cut than in the beginning, with values now ranging from 544 to 720 nm.

Fortunately, the experimentalists seem to have clarified the picture. Recently, Andersen and his co-workers have provided data for the absorption cross section of retinal and retinal derived organic cations in the gas phase, providing the much

needed reference data to test the theoretical results against.[185-187] Apart from providing a stern test for theory, they obviate the misleading comparison between retinal absorption properties in the protein and in a solvent and lay the basis for reconsidering the molecular mechanisms of color tuning in the large family of retinal proteins.

3.1.2.2 Stern Test for Theory

A set of six different retinal chromophores was chosen for the study namely, protonated and deprotonated Schiff bases of 11-*cis*-, 9-*cis*- and all-*trans*-retinal (*Figure 18*). An intermediate state where the proton charge is moved to the next neighbouring heavy atom (SBN^+T), is also considered. To cover the short-wavelength region of retinal Schiff base spectra, we also include the neutral species *cis*- and *trans*-SB whose absorbance in the nonpolar solvent 3-methylpentane peak at 353 nm.[173]

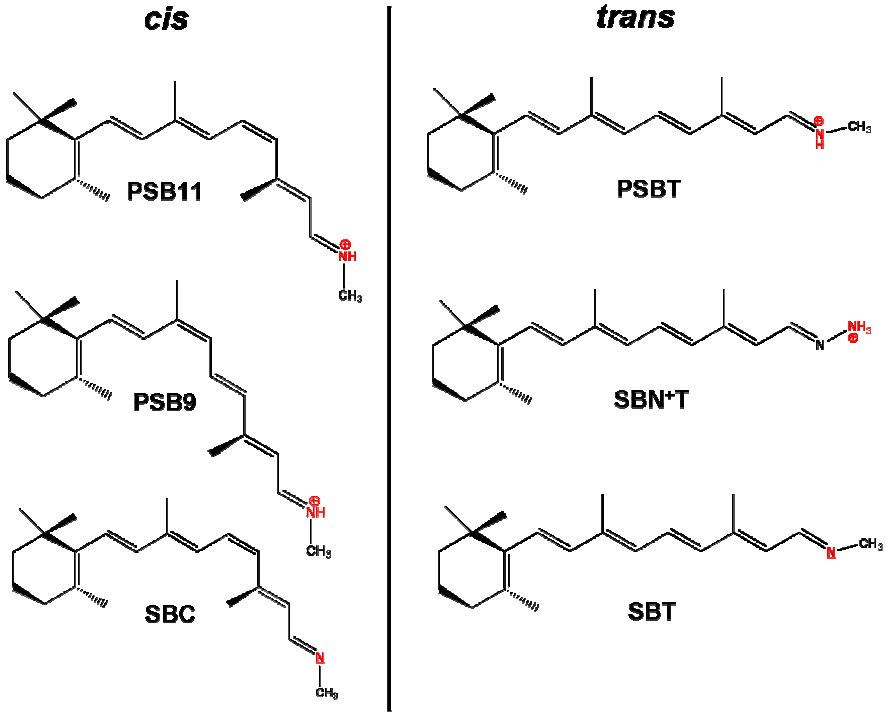

Figure 18 *Schematic representations of 11-cis- and all-trans-retinal Schiff base chromophore and their derivatives.*

Geometry optimization at the CASPT2 level for systems of this size is still prohibitive in cost. We therefore resorted to MP2 and its analytical gradients, which allow for an efficient geometry search with a correlated wave function. Starting with the DFT-optimized structures,[188] the chromophores were reoptimized with MP2 using a 6-31G** basis set.[166] In view of the huge computational requirements, the *n*-butyl group in the experimental gas-phase study was reduced to methyl (the solvent spectra of the two PSBs are essentially identical)[189] and $N(CH_3)_3^+$ to NH_3^+.

All six chromophores after optimization exhibit strong bond alternation (*Figure 19*), which is, however, significantly reduced between C9 and N16 in the three positively charged systems. A further reduction is observed in PSB11, PSB9 and PSBT, where the positive charge is part of the π-system.

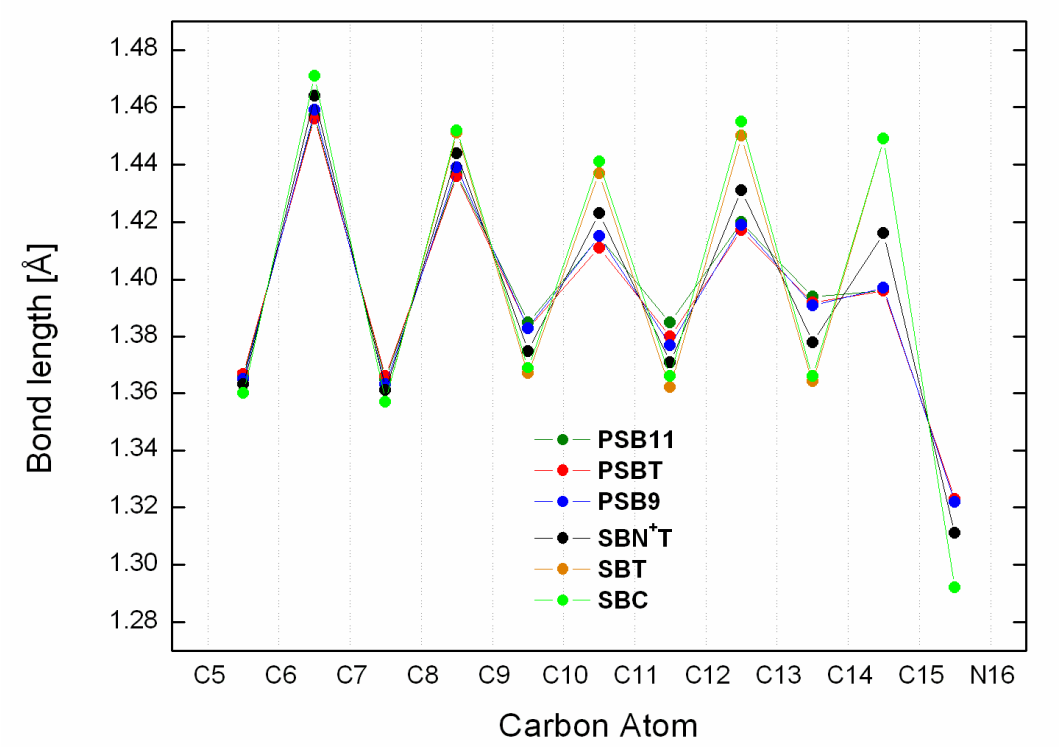

Figure 19 *Bond lengths along the conjugated carbon chain.*

Once the proton charge is moved from PSBT to SBN^+T, gradual increase in BLA pattern of the single bonds can be observed starting from C10─N16, which compensates for the decrease in their double bonded neighbouring counterparts.

However, strong deviations are seen once the proton is completely removed, thus reversing the BLA completely.

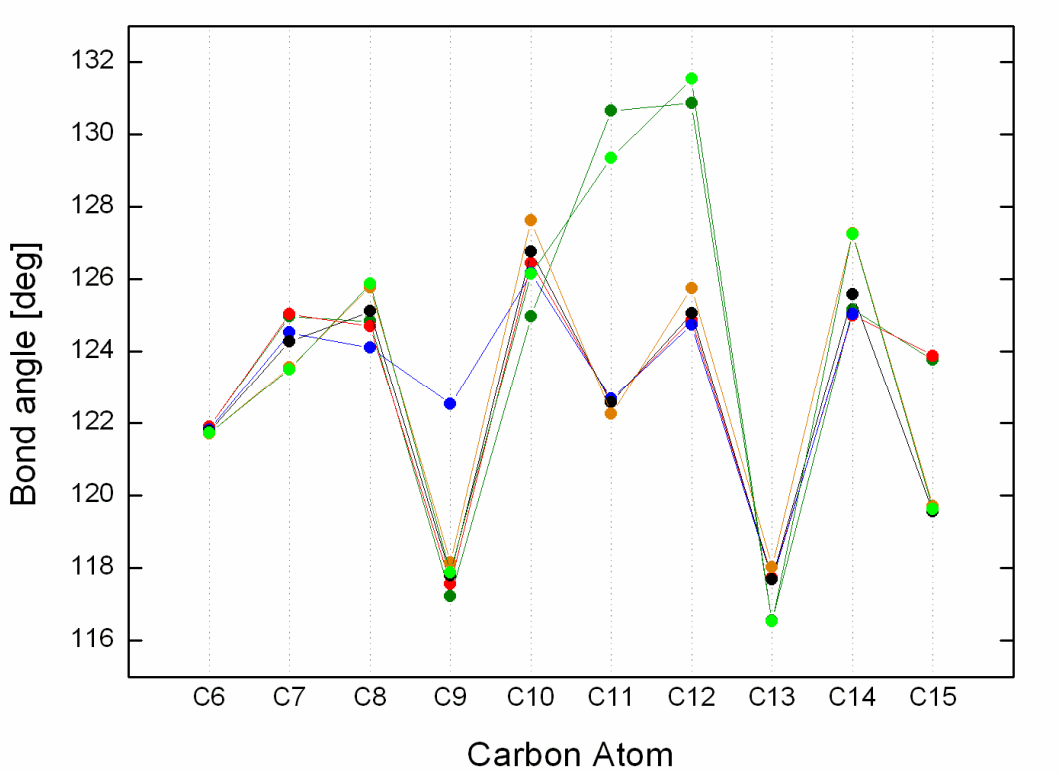

Figure 20 *Bond angles along the conjugated carbon chain.*

Bond angles (*Figure 20*) centered at odd numbered carbon atoms are always smaller than their direct neighbours. This anomaly which has been observed both experimentally[190] and from computational studies[191] of cyanine type dyes can be correlated with hybridization changes due to alternating atomic charges.[192] The small values at C9 and C13 result from the spacious methyl substituents at these positions, and the angles at C11 and C12 are widened to ease the strain of the 11-*cis*- and 9-*cis*-configurated double bonds in their respective chromophores.

Dihedral angles (*Figure 21*) determine the conformation of the chromophore more than bond lengths and bond angles. Also, dihedral angles react more sensitively to changes in the environment because of the small force constants involved. From C7 to N16, all chromophores are essentially planar with the exception of PSB11 and

SBC, which are twisted by 7° and 3° about the C11═C12 and the C12─C13 bonds, along with a further 9° twist in SBC about the C13═C14 bond, respectively, which moves the C13-N16 fragment away from the bulky β-ionone ring.

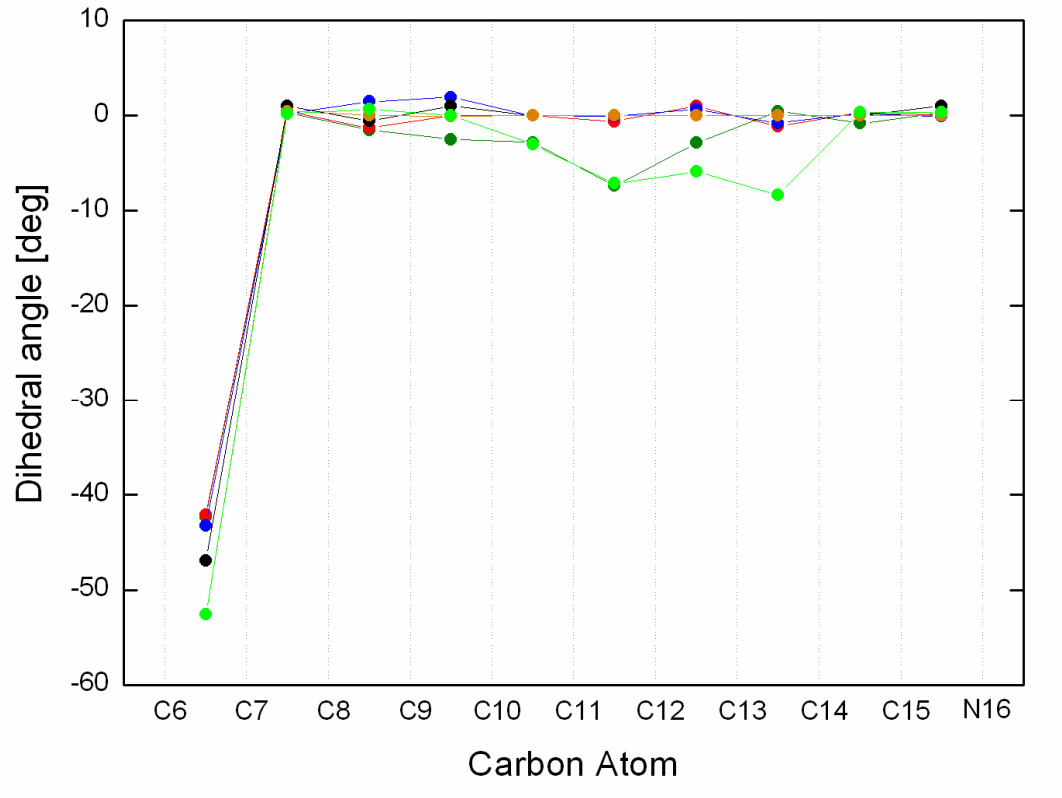

Figure 21 *Dihedral angles along the conjugated carbon chain showing the deviations from either the cis (0°) or trans (180°) configuration.*

Note also the negative twist angle of the C6─C7 bond, which indicates the distorted *s-cis*- orientation of the β-ionone ring relative to the polyene chain.

3.1.2.3 Absorption Maximum in *Vacuo*

In the following, we show that CASPT2 theory at a very high level of sophistication is able to quantitatively reproduce the experimental gas phase absorption maxima of the retinal chromophores shown in *Figure 18*. Ground and excited state energies were calculated with the CASSCF method as provided by the MOLCAS set of routines. Six-root state-averaged wave functions were expanded in an atomic natural orbital basis set with the contraction C,N[4s3p1d]/H[2s]. The active

space was (12,12), i.e., all pseudo π-electrons and valence pseudo π-orbitals were considered. Second-order corrections to the CASSCF energies were calculated with CASPT2. All core orbitals were kept frozen during the calculations. To avoid the effect of intruder states, the level shift was set uniformly to 0.3 au. These parameters are identical to the ones that were used in earlier studies on retinal model chromophores and on the rhodopsin binding pocket. A summary of the calculations is given in Table 1.

TABLE 1 *CASPT2 energies, oscillator strengths, main contributing configurations with weight, and dipole moments for the ground state S_0 and two main excited states of the six retinal chromophores shown in Scheme 1 and experimental wavelengths (in bold, nm) of the optical transitions.*

Model	State	CASSCF[a]	CASPT2[a,b]	f	Configuration[c]	μ[d]	λ(Exp)
	S_0	-868.3623	-871.2306	-	$(6a)^2(7a)^0$ *75*	22.75	
PSB11	S_1	2.71 (457)	2.05 (**606**)	1.12	$(6a)^1(7a)^1$ *61*	6.70	**610**[e]
	S_2	3.50 (354)	2.84 (436)	0.13	$(6a)^0(7a)^2$ *28*	19.45	390
	S_0	-868.3709	-871.2370	-	$(6a)^2(7a)^0$ *76*	22.20	
PSB9	S_1	2.77 (447)	2.09 (**593**)	1.05	$(6a)^1(7a)^1$ *63*	6.64	
	S_2	3.66 (339)	2.96 (419)	0.18	$(6a)^0(7a)^2$ *27*	18.40	
	S_0	-868.3713	-871.2380	-	$(6a)^2(7a)^0$ *75*	24.45	
PSBT	S_1	2.71 (457)	2.07 (**600**)	1.32	$(6a)^1(7a)^1$ *61*	7.17	**600**[d]
	S_2	3.50 (354)	2.85 (435)	0.14	$(6a)^0(7a)^2$ *28*	20.04	385
	S_0	-884.3239	-887.2138	-	$(6a)^2(7a)^0$ *67*	35.48	
SBN^+T	S_1	4.26 (291)	2.56 (**484**)	0.9	$(6a)^1(7a)^1$ *45*	19.82	**487**[d]
	S_2	3.67 (338)	2.76 (449)	0.2	$(6a)^0(7a)^2$ *27*	30.02	
	S_0	-868.0040	-870.8470	-	$(6a)^2(7a)^0$ *69*	2.02	
SBT	S_1	6.09 (204)	3.47 (**357**)	1.2	$(6a)^1(7a)^1$ *68*	3.94	**353**[f]
	S_2	4.20 (295)	3.62 (342)	0.0	$(6a)^0(7a)^2$ *27*	1.96	
	S_0	-867.9949	-870.8399	-	$(6a)^2(7a)^0$ *69*	2.10	
SBC	S_1	6.09 (204)	3.58 (**346**)	0.96	$(6a)^1(7a)^1$ *61*	4.06	**353**[f]
	S_2	4.20 (295)	3.61 (343)	0.00	$(6a)^0(7a)^2$ *27*	2.33	

[a] S_0 energies are in a u., S_1 and S_2 energies are in eV relative to S_0, in parentheses: wavelengths in nm. [b] Only π-type MO's are counted; weights (in italics) are in %. [c] Dipole moments in Debye. [d] Ref (185). [e] (186). [f] (173).

The ground state is mainly closed shell in all cases, with 67-76% contribution from that configuration, $6a^27a^0$. With a calculated dipole moment of ~25.0 D, the charge distribution is highly unsymmetrical for the free protonated Schiff base. The excited state with high oscillator strength ($f \geq 0.9$) always involves, with weights ranging from 45% to 69%, the HOMO to LUMO configuration ($6a^17a^1$). This is the

state which is lowered most in energy relative to the ground state by the CASPT2 treatment, averaging 2 eV in all complexes except **SBC** and **SBT,** where it is 3 eV. For simplicity of formulation, we will refer to this states which is the lowest excited energy state in all complexes as the S_1 state in the following discussion. Excitation into S_1 is associated with a strong change of the dipole moment, both in magnitude and in orientation (*Figure 22*).

The next higher state S_2 is mostly doubly excited HOMO to LUMO ($6a^0 7a^2$) plus equal contributions of HOMO-1 to LUMO ($5a^1 7a^1$) and HOMO to LUMO+1 ($5a^1 7a^1$) excitation. There is no intensity in this state, and the dipole moment is almost identical to the ground state.

Since the different isomers profit differently from the increased π electron conjugation, it is not surprising that the relative energies change appreciably. The agreement between calculated and experimental $S_0 \rightarrow S_1$ energies is extremely good, especially in view of the fact that the calculations cover a wavelength range from 350 nm for the neutral Schiff base to 600 nm for the protonated chromophore. The hypsochromic shift of 116 nm, or 0.49 eV, from **PSBT** to **SBN$^+$T** is a consequence of the positive charge being moved from the Schiff base nitrogen to the neighbouring atom where it is no longer part of the conjugated system and can interact only electrostatically with the chromophore.

However, this interaction is very effective judging from the further 0.91 eV energy shift for the **SBN$^+$T** to **SBT** transformation. These data highlight the extraordinary sensitivity of the retinal chromophore to the environment, where the movement of one positive charge suffices to shift the absorbance maximum by almost 1.4 eV or 243 nm. With respect to the formally forbidden S_2 state, the situation is less

clear-cut. In the protonated species **PSB11** and **PSBT**, we find this state 0.8 eV above S_1, somewhat smaller than the value (1.2 eV) determined by Andersen.[185]

In the neutral **SBT**, **SBC** species, this gap is significantly reduced, to 0.15 eV, 0.03 eV but S_2 is still above S_1. In their study of a six double bond polyene Schiff base, Palmer et al. found this state 0.4 eV below S_1,[193] in line with results on other polyene hydrocarbons.[194] Grossjean and Tavan, in their semi empirical studies on retinal models[195] have demonstrated the importance of electron correlation for the correct description of the $S_1 \rightarrow S_2$ gap.

Most recently, the gas phase absorption maximum of neutral Schiff base chromophores have also been measured, albeit with a conspicuous spectator positive charge far away from the Schiff base iminium nitrogen atom, and found to peak at 388 nm.[196] The 31 nm difference in the calculated value could be due to the presence of spectator charge in the experimental set-up or due to the exclusion of lone pair of electrons from the active space in our computational set-up. Hufen et al.[205] found the switch of the S_1 and S_2 states in the five double bond model retinal Schiff bases using the same computational setup. The state inversion of S_1 and S_2 is also established for long polyenic systems: in 1,3,5,7-octatetraene, the largest polyene for which exact CASPT2 calculations are available,[197] the lowest excited state is the forbidden 2^1A_g state which corresponds to the S_2 state in **SB**. The strongly allowed 1^1B_u state refers to the S_1 state.

It appears that the setup that we have applied in our CASPT2 treatment (size of the active space) is not sufficient to correctly describe the S_2 state, especially in the neutral species. Apparently this is sufficient for treating the S_2 state in the reduced retinal model compounds but needs enlargement for more extended systems. It must be noted that theoretical calculations predict the low-lying S_2 state to be strongly two-

photon allowed in virtually all polyenes, whether polar, nonpolar, linear, or non-linear, provided that a strongly one-photon allowed S_1 state is nearby.[198]

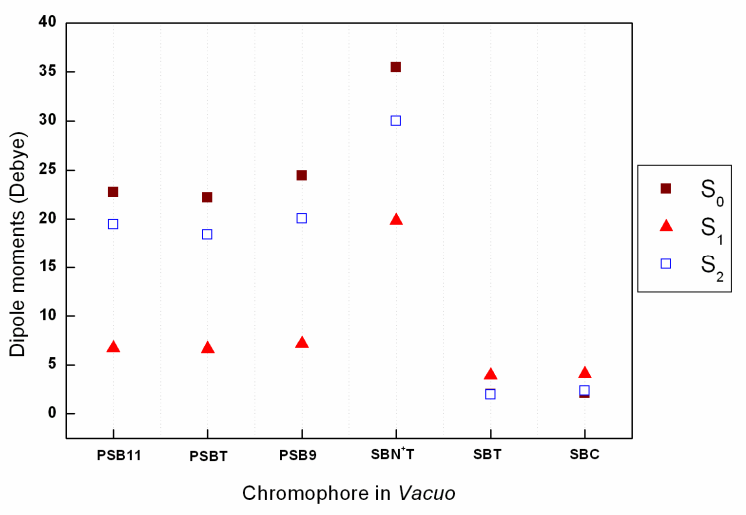

Figure 22 Dipole moments (in Debye) of retinal Schiff base model chromophores in vacuo.

A key to understanding the spectral shifts is the change in the dipole moment as the chromophore is promoted to an excited state *(Figure 22).* This change is small in the case of the neutral system **SBT** but large in the presence of a positive charge and when the excitation is to S_1: In **SBN$^+$T**, the moment decreases by almost 50%, and in **PSBT** and in **PSB11** the decrease is even larger. This loss in Coulomb energy stabilizes the excited state and results in huge bathochromic shifts. Excitation to S_2 states leads to a small but almost constant decrease of the dipole moment, and accordingly the S_0 to S_2 absorbance is largely unaffected by differences in the charged environment.

We have shown that the CASPT2 method with a basis set that optimally treats correlation and polarization effects is able to quantitatively reproduce the response of retinal Schiff base absorption spectra to polar perturbations. The huge computational resources necessary to perform this kind of calculations will be prohibitive for their use as standard application. However, these calculations provide the necessary

benchmark data for the calibration of the embedded QM part in any of the widely used QM/MM schemes.

3.1.3 Binding Pocket

Three mechanisms are generally discussed in connection with the phenomenon of spectral tuning in retinal proteins: a) internal twisting of the chromophore, b) effect of the counterion, and c) the polar environment due to the binding pocket.[172,178] In this section, by employing the same theoretical platform we show that the three contributions discussed above add up quantitatively to the experimentally observed spectral shift of the chromophore from the vacuum to the rhodopsin molecule.

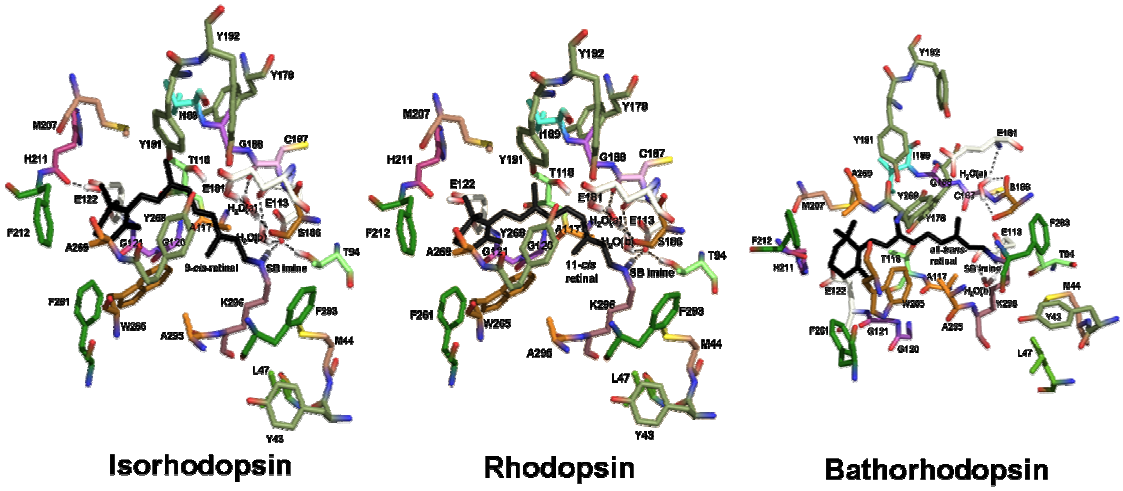

Figure 23 *SCC-DFTB optimized binding pockets of isorhodopsin, rhodopsin and bathorhodopsin containing the.chromophore (in black). Shown are the 28 amino acids within 4.5-Å distance of the chromophore and two water molecules close to the counterion.*

The chromophore binding pocket based on chain-B of the 2.2-Å and 2.6-Å crystal structure of rhodopsin (PDB:1U19)[199] and bathorhodopsin (PDB:2G87)[200] was chosen for our studies (*Figure 23*). The binding site contains 28 amino acid residues, namely: Tyr43, Met44, Leu47, Thr94, Glu113, Ala117, Thr118, Gly120, Gly121, Glu122, Tyr178, Glu181, Ser186, Cys187, Gly188, Ile189, Tyr191, Tyr192, Met207,

His211, Phe212, Phe261, Trp265, Tyr268, Ala269, Phe293, Ala295, Lys296, and two water molecules (Wat2a and Wat2b) respectively.

These residues are within 4.5-Å distance from any atom within the retinal skeleton. Except for the counterion Glu113, all amino acids were considered neutral and as a consequence the binding pocket remains uncharged. The complete amino acid residues were considered, while unsaturated valencies from the peptide backbone were filled with hydrogen atoms.

To obtain the isorhodopsin binding pocket, **PSB9$_{vac}$** was put into the place of **PSB11$_{dist}$** and the whole pocket including the chromophore was minimized with SCC-DFTB code giving the structure described elsewhere in detail.[201] Incidentally the geometrical parameters of this theoretical model of isorhodopsin have been found to be in reasonable agreement with experimental model published recently.

3.1.3.1 Effect of Geometric Distortion

It has been shown recently that the most significant shifts of the absorption maximum of the retinal Schiff base chromophore to longer wavelengths are observed when formal double bonds are twisted from planarity.[202] In this section, we will discuss how the 11-*cis-, all-trans- and 9-cis*-retinal chromophores get deformed as a consequence of entering into the binding pocket and the corresponding effect of geometric distortion on the absorption maximum.

X-ray crystallographic studies of rhodopsin have shown that the non-bonded interaction with five atoms from Thr118, Ile189, Tyr191, and Tyr268 within 4.5-Å distance from C19 is one of the crucial factors for stabilizing the **PSB11$_{dist}$** in the dark state. A careful look at the BLA pattern, bond angles and dihedral angles (*Figure 24, 25, 26*), reveal the out-of-plane distortion induced by the protein mainly at the central

isomerizing region from C10 to C13, in particular a large pre-twist (14°) is observed on the C11═C12 double bond.

Perusal of *Figure 24* shows that the *zig-zag* bond length alternation (BLA) pattern which is more visible from the C9─C15 retinal backbone is underestimated as the π-electron conjugation benefits strongly from correlation energy, which is partly included in the DFT methodology. As a consequence, the MP2 optimized structures are biased towards delocalization of conjugated double bonds and tend to reduce BA relative to Hartree–Fock (HF) methodology, which puts more emphasis on the description of electrons as pairs. A strong reduction in BLA toward the terminal C15═N16 double bond reveals the accumulation of the positive charge at that position

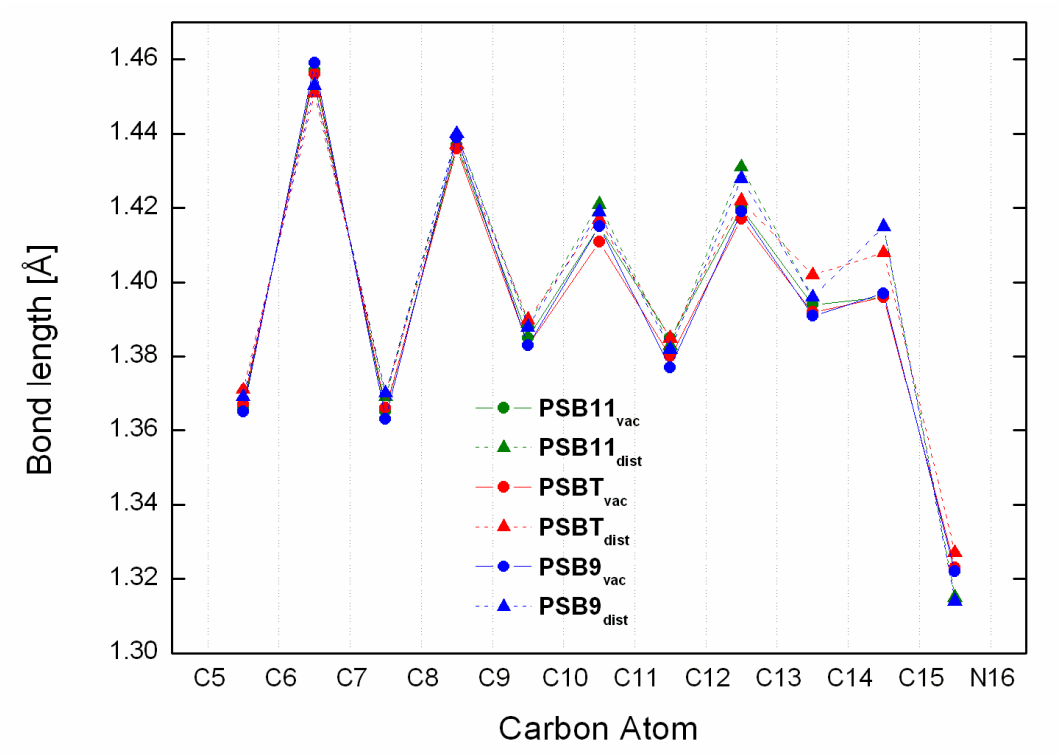

Figure 24 *Bond lengths along the conjugated carbon chain of the retinal chromophores in vacuo and in protein.*

CASSCF methodology has been found to overestimate BLA. It appears that the limited space in which the excited configuration state functions in the CASSCF

treatment are expressed is not of sufficient size to remedy the correlation error inherent in the HF method.

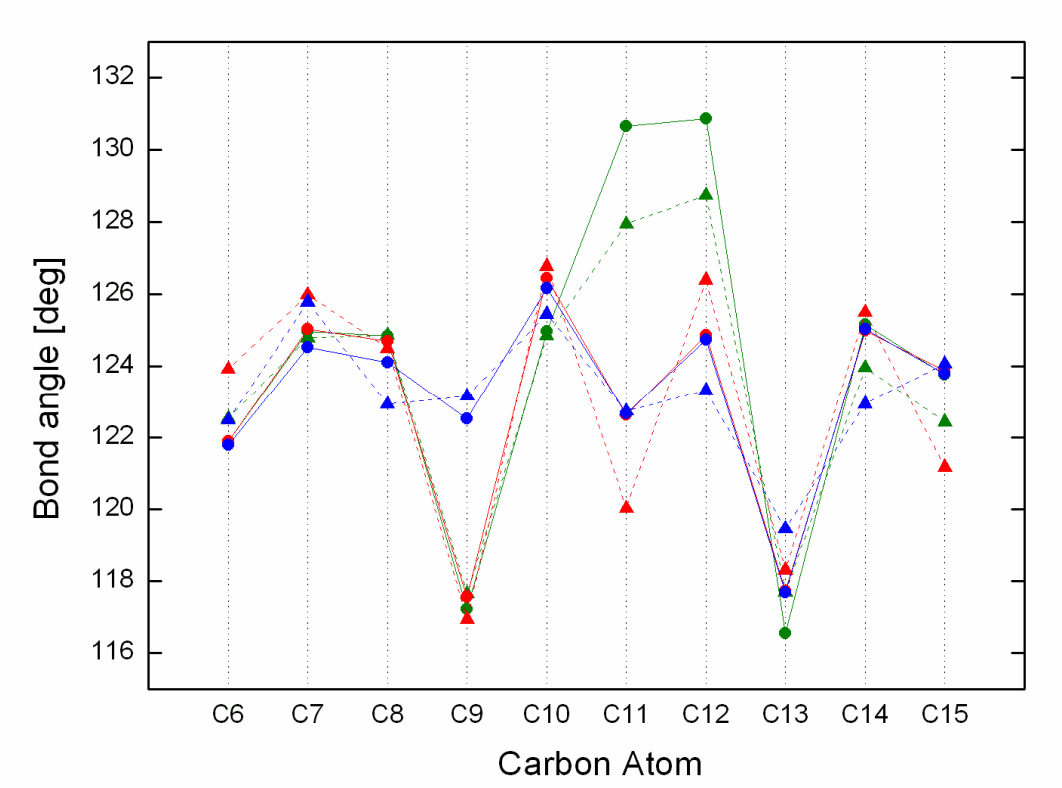

Figure 25 *Bond angles along the conjugated carbon chain of the retinal chromophores in vacuo and in protein.*

A strong twist of 30° about the C13═C14 double bond is followed by a 22° twist about the primary isomerizing C11═C12 as well as the C9═C10 double bonds. A relatively stronger 18° twist at the terminal C15═N16 position clearly indicates that this strong non-planar distortion of the chromophore, including the sense of rotation, is mainly determined by a combination of two effects: the fitting of both ends to the protein matrix which imposes a distance constraint and the bonding arrangement acting as a torque at the Schiff base terminus an aspect recently explored by Sugihara et al.[203] The 10° twist of the C6─C7 bond in the β-ionone ring is further accompanied by 13°, 6° twists of the C7═C8, C8─C9, bonds (*Figure 26*).

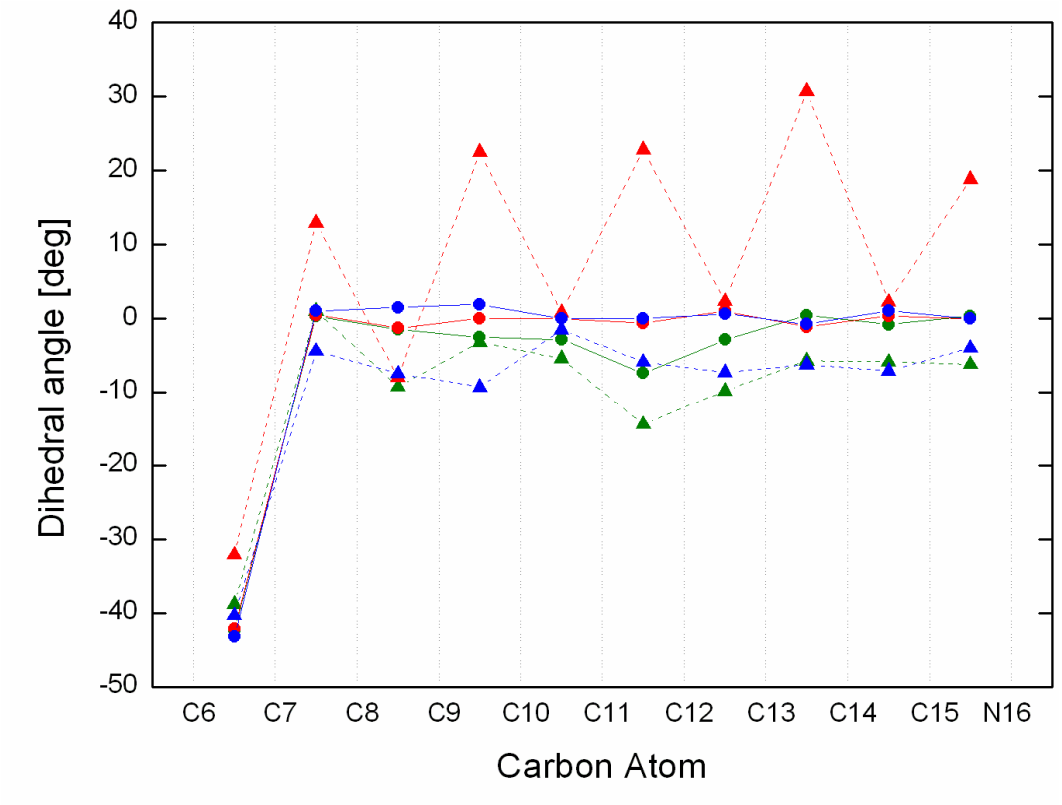

Figure 26 *Dihedral angles along the conjugated carbon chain showing the deviations from either cis (0°) or trans (180°) configuration of the retinal chromophores in vacuo and in protein.*

In **PSB11$_{dist}$**, a strong twist of 8° about the C8─C9 precedes the 7° twist about the primary isomerizing C11═C12 double and C12─C13 single bond. It is closely followed by ~6° twist at the C15═N16, C14─C15, C13═C14 bonds. Note in particular, the dihedral angle of the C10─C11═C12─C13 bond is negative which confirms the strong chiral discrimination exerted by the protein pocket.

In the case of **PSBT$_{dist}$**, the effects of the binding pocket are drastically different. All double bonds of the trans geometry are strongly twisted and the sum of deviation from planarity (from C7 to N16) is 109° in strong contrast to the single bonds which are essentially planar (the sum being 15°). In contrast, the amount of deviation is only 30° for both the single and double bonds. Bond length alternations increase considerably along the polyene chain extending uptil C15═N16 terminal double bond.

In **PSB9$_{dist}$**, bond length alternations are similar to that of **PSB11$_{dist}$**. A twist of 7.5° about the C9═C10 isomerizing double bond and 6.7° at the C12─C13 single bond are most prominent as the chromophore remains essentially planar. It is closely followed by ~6° twist at the C8─C9, C11═C12, C14─C15 bonds.

TABLE 2 *CASPT2 energies, oscillator strengths, main contributing configurations with weight, and dipole moments for the ground state S_0 and two main excited states (S_1, S_2) of the distorted retinal isomers and their corresponding optical transitions.*

Model	State	CASSCF[a]	CASPT2[a,b]	f	Configuration[c]	μ[d]
PSB11$_{dist}$	S_0	-868.3398	-871.2185	-	$(6a)^2(7a)^0$ *74*	16.41
	S_1	2.66 (467)	1.93 (**643**)	0.96	$(6a)^1(7a)^1$ *60*	11.42
	S_2	3.45 (359)	2.77 (447)	0.14	$(6a)^0(7a)^2$ *27*	13.34
PSB9$_{dist}$	S_0	-868.3474	-871.2240	-	$(6a)^2(7a)^0$ *74*	16.65
	S_1	2.72 (456)	2.01 (**617**)	1.00	$(6a)^1(7a)^1$ *61*	10.72
	S_2	3.58 (346)	2.88 (431)	0.16	$(6a)^0(7a)^2$ *26*	13.15
PSBT$_{dist}$	S_0	-868.3247	-871.2095		$(6a)^2(7a)^0$ *76*	12.21
	S_1	2.29 (542)	1.91 **(649)**	1.43	$(6a)^1(7a)^1$ *61*	8.83
	S_2	3.16 (392)	2.56 (484)	0.08	$(6a)^0(7a)^2$ *30*	10.17

[a] S_0 energies are in a u., S_1 and S_2 energies are in eV relative to S_0, in parentheses: wavelengths in nm. [b] Only π-type MO's are counted; weights (in italics) are in %. [c] Dipole moments in Debye.

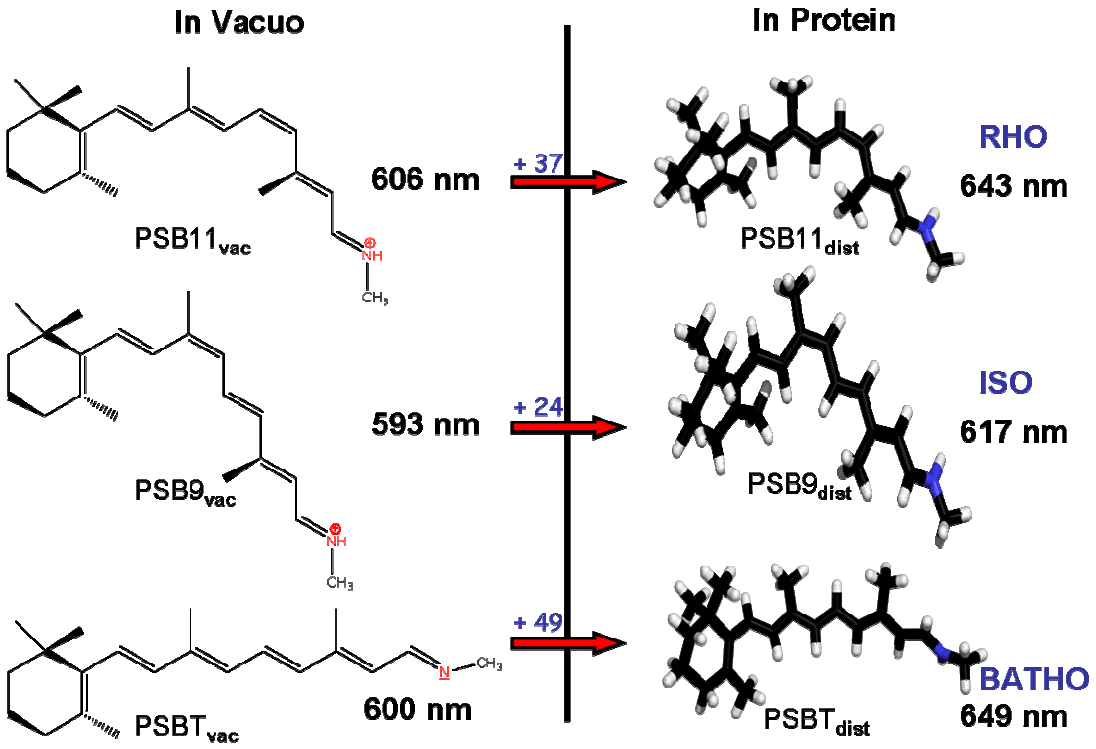

Figure 27 *Absorption maximum of protonated retinal Schiff base chromophores in vacuo and in protein environments.*

Comparion of the absorption maxima for **PSB11$_{vac}$**, **PSB9$_{vac}$**, **PSBT$_{vac}$**, (see Table 1) with that of their distorted counterparts (see Table 2) clearly shows that the sum of all distortions in rhodopsin, isorhodopsin and bathorhodopsin add up to calculated red shifts of 37, 24 and 49 nm, respectively (*Figure 27*). In addition to the spectral shift we note a reduction of the oscillator strength and of the ground state dipole moment, both a consequence of the somewhat compressed geometry of the bound chromophore relative to the fully stretched geometry *in vacuo*.

The only exception to this is **PSBT$_{dist}$**, where the reduction in length of the carbon chain is compensated by an increase in stabilisation of the delocalised positive charge in the excited state resulting in its slighty higher oscillator strength. We further note that the dipole moment is significantly reduced in the S_1 state relative to S_0, a consequence of the massive flow of negative charge from the conjugated carbon chain towards the positive nitrogen following excitation to the ionic S_1 state.

3.1.3.2 Effect of the Counterion

Thus far, attention has been focused on the cationic chromophore – the protonated retinal Schiff base. The influence of the anion (the conjugate base of the protonated acid) obviously cannot be ignored since it is certainly a perturbing factor in the microenvironment. When the chromophore is attached to its counterion (Glu-113), an ion-pair environment is formed (**PSB11$_{ip}$**, **PSB9$_{ip}$**, **PSBT$_{ip}$**) which possess permanent dipole moments.[204]

The dipoles will in the ground state orient themselves around the positively charged nitrogen in a fashion in which maximum favourable electrostatic interactions can be achieved. Elsewhere along the chromophore the dipoles will be largely randomly oriented with little effect on the total energy. Excitation to the **π-π*** Franck-Condon state results in a new charge distribution, as reorientation of the permanent

dipoles cannot occur in such a short time, the excited state thus ends up greeting a hostile environment. The reduction of charge at the nitrogen atom (*Figure 16*), induces greater electrostatic repulsion between the dipoles than their attraction to the smaller (ideally +e) charge.

TABLE 3 *CASPT2 energies, oscillator strengths, main contributing configurations with weight, and dipole moments for the ground state S_0 and two main excited states (S_1, S_2) of the retinal chromophore ion-pair and their corresponding optical transitions.*

Model	State	CASSCF[a]	CASPT2[a,b]	f	Configuration[c]	μ[d]
$PSB11_{ip}$	S_0	-1056.6899	-1060.0803		$(6a)^2(7a)^0$ *65*	10.22
	S_1	4.92 (252)	2.55 **(486)**	0.82	$(6a)^1(7a)^1$ *62*	20.79
	S_2	3.41 (363)	2.93 (423)	0.00	$(6a)^0(7a)^2$ *29*	10.03
$PSB9_{ip}$	S_0	-1056.6885	-1060.0794		$(6a)^2(7a)^0$ *64*	11.10
	S_1	4.96 (250)	2.60 **(477)**	0.84	$(6a)^1(7a)^1$ *61*	21.80
	S_2	3.53 (351)	3.04 (408)	0.00	$(6a)^0(7a)^2$ *28*	10.59
$PSBT_{ip}$	S_0	-1056.6667	-1060.0584		$(6a)^2(7a)^0$ *61*	11.13
	S_1	4.66 (266)	2.38 **(521)**	0.82	$(6a)^1(7a)^1$ *55*	22.99
	S_2	3.08 (402)	2.70 (459)	0.00	$(6a)^0(7a)^2$ *27*	10.96

[a] S_0 energies are in a u., S_1 and S_2 energies are in eV relative to S_0, in parentheses: wavelengths in nm. [b] Only π-type MO's are counted; weights (in italics) are in %. [c] Dipole moments in Debye.

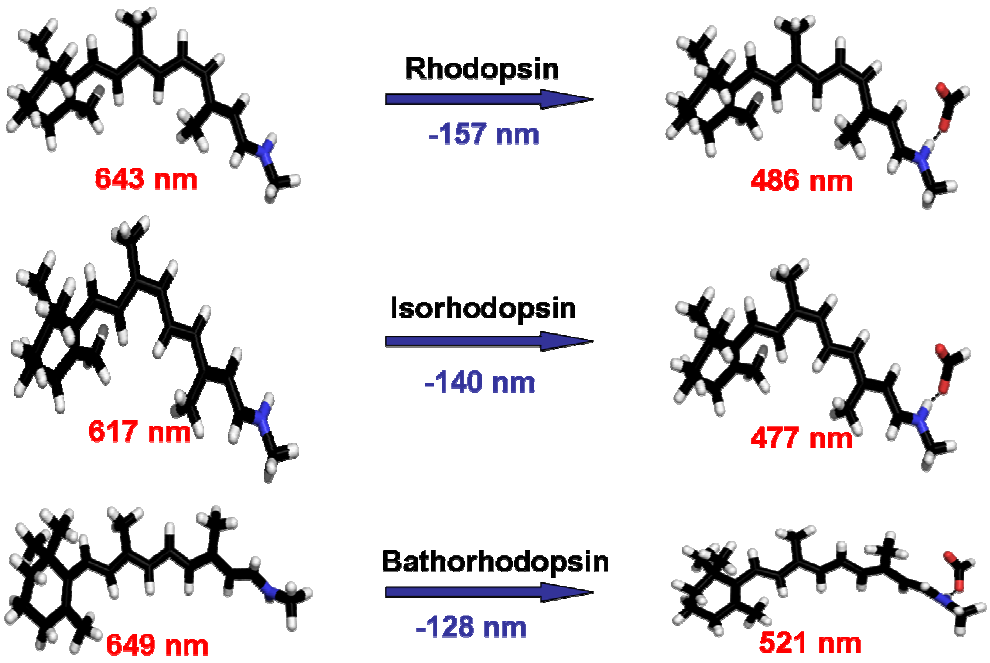

Figure 28 *Effect of counterion on the absorption maximum of rhodopsin, isorhodopsin and bathorhodopsin.*

Due to the effects discussed above the excited state charge density is moved against the negative charge of the counterion during the S_0-S_1 excitation which raises the energy of the excited state, resulting in a significant blue shift of the absorption maximum relative to vacuum (*Figure 28*).

Perusal of Table 3 shows that there is a huge increase of the S_0 to S_1 energy gap by 0.62 eV, 0.59 eV, 0.47 eV shifting the absorbance of the respective chromophore - ion pairs to 486, 477, 521 nm into the range of the rhodopsin, isorhodopsin and bathorhodopsin absorption maximum (498, 485, 543 nm). The decrease of the oscillator strength indicates that the motion of the electron charge being excited is further restricted. It must also be noted that the position of the counterion relative to the Schiff base iminium nitrogen atom remains more or less unchanged in all three pigments.

This is conceivable considering the fact that in the ion pair this charge must be shifted against the negatively charged counterion. This shift is also the reason for the increased dipole moment of the S_1 state relative to S_0 (*Figure 29*). The major part of the calculated blue shift is due to the destabilization of the S_1 state in the presence of the counterion caused by increased electrostatic repulsion.

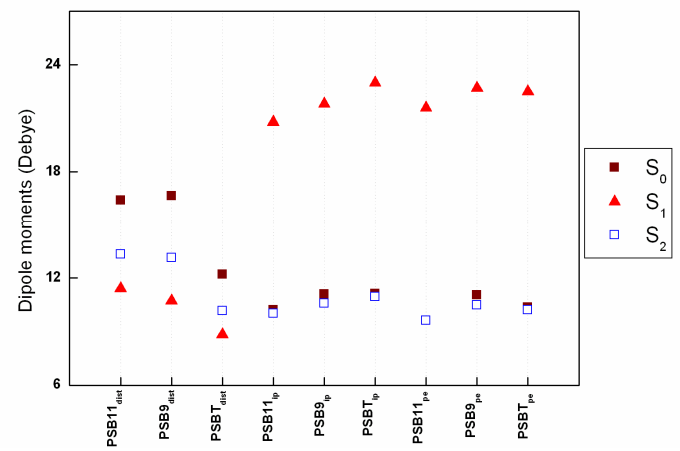

Figure 29 *Dipole moments for the chromophore-counterion (ion-pair) models.*

There is another effect, *viz*. the increased double bond fixation of the conjugated chain as the positive charge of the chromophore becomes localized by the counterion. Calculations on model retinal have shown, however, that this effect contributes no more than 10% to the total shift.[205]

Circular dichroism spectroscopy can be used to monitor the overall shape of an inherently chiral chromophore; specifically, the absolute conformation of enantiomeric or pseudoenantiomeric geometries may be distinguished. The α bands of rhodopsin, isorhodopsin and bathorhodopsin calculated on the basis of the quantum mechanical geometries agree in sign and magnitude with those determined experimentally.[206] The calculated rotatory strengths of +0.27 au for **PSB11$_{ip}$**, +0.15 au for **PSB9$_{ip}$** and -0.39 au for **PSBT$_{ip}$** shows that the spectral manifestation of this sign is the circular dichroism (CD) of the optical transition (α-band) which is positive in rhodopsin and isorhodopsin (somewhat smaller in magnitude due to the induced fit of the chromophore[207]) and negative in the latter.[208] Both the sign inversion of the rotatory strength and its marked increase in bathorhodopsin, a consequence of configurational change and the prominent helical geometry of the chromophore, are correctly reproduced by the calculations.

3.1.3.3 Residual Effect Vs Counterion Effect

The chromophore is surrounded by hydrophilic and hydrophobic residues inside the rhodopsin binding pocket. Mutational studies have clearly shown that the neighbouring amino acids are critical for understanding the retinal related diseases in sick humans and animals. However, so far there has been no concrete evidence for predicting and rationalising the residual effect with reference to the counterion effect on the electronic spectrum.

The point charges for the binding pocket have been calculated using the sophisticated Natural Population Analysis (NPA)[209] with 6-31G** basis. NPA is based on the transformation of the molecular wave function into natural bonding orbitals. It has been developed as a tool to obtain a molecular charge distribution which is less dependent on the choice of the basis set. Charges obtained from conventional Mulliken population analysis[210] and from CHARMM formalism[211] are tested against NPA. While the former, like the NPA charges, are derived from an explicitly calculated wave function, the latter are transferable parameters. The effect of the environment should be described better by the quantum-mechanically derived charges compared to the environment insensitive CHARMM charges.

Table 4 *CASSCF and CASPT2 corrected state energies, oscillator strengths, main contributing configuration with weight, and dipole moments for the ground state S_0 and two main excited states S_1, S_2.*

Model	State	CASSCF[a]	CASPT2[a,b]	f	Configuration[c]	μ[d]
5.PSB11 QM	S_0	-519.2764	-520.9352		$(5a)^2(6a)^0$ *76*	18.43
	S_1	3.24 (383)	2.28 (**544**)	0.84	$(5a)^1(6a)^1$ *56*	8.13
	S_2	3.69 (336)	3.10 (400)	0.19	$(5a)^0(6a)^2$ *27*	17.15
5.PSB11+E113[†] QM	S_0	-992.6450	-995.7568		$(5a)^2(6a)^0$ *67*	7.85
	S_1	5.14 (241)	2.71 (**457**)	0.83	$(5a)^1(6a)^1$ *61*	14.61
	S_2	3.55 (349)	3.16 (392)	0.00	$(5a)^0(6a)^2$ *29*	7.46
5.PSB11+E113 QM/NPA	S_0	-519.4299	-521.0772		$(5a)^2(6a)^0$ *66*	24.04
	S_1	4.72 (263)	2.77 (**447**)	0.69	$(5a)^1(6a)^1$ *48*	13.20
	S_2	3.56 (348)	3.13 (396)	0.00	$(5a)^0(6a)^2$ *30*	23.92
5.PSB11+E113 QM/Mulliken	S_0	-519.4003	-521.0488		$(5a)^2(6a)^0$ *66*	23.40
	S_1	4.57 (271)	2.58 (**480**)	0.77	$(5a)^1(6a)^1$ *55*	10.25
	S_2	3.57 (347)	3.13 (396)	0.00	$(5a)^0(6a)^2$ *30*	23.26
5.PSB11+E113 QM/CHARMM	S_0	-519.4780	-521.1240		$(5a)^2(6a)^0$ *67*	24.99
	S_1	4.97 (249)	2.87 (**432**)	0.86	$(5a)^1(6a)^1$ *56*	13.70
	S_2	3.55 (349)	3.14 (395)	0.00	$(5a)^0(6a)^2$ *30*	24.87

[a] S_0 energies are in a.u., S_1 and S_2 energies are in eV relative to S_0. [b] In parentheses: wavelengths in nm. [c] Only π-type MO's are counted; weights (in italics) are in % [d] Dipole moments in Debye. [†] Full E113 as atoms.

The results are tabulated in Table 4. The 544 nm for the reduced **5.PSB11$_{dist}$** will serve as a reference point for analysing the residual spectral shifts. The quality of the point charges can be gauged from entries-2 & -3. The pure quantum chemical calculation of chromophore-counterion electrostatic interaction results in a blue shift

of 97 nm (note that the complete counterion backbone is included in this calculation). The full counterion when mimicked as NPA point charges in entry 3 reproduces the spectral shift within 10 nm or 0.06 eV accuracy *(Figure 30)* while atomic charges from Mulliken, and CHARMM formalism fall short by approximately 30 nm.

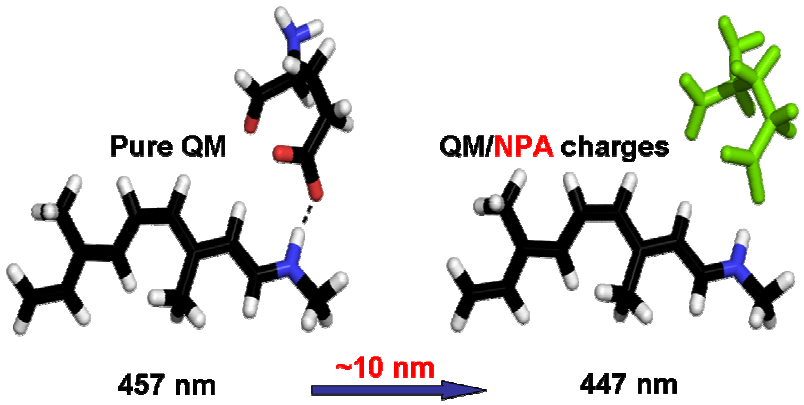

Figure 30 *Quality of NPA point charges as counterion is mimicked.*

The residual spectral shift in rhodopsin (*Figure 31*) and bathorhodopsin (*Figure 32*) is calculated based on the interaction of that residue and the chromophore alone as discussed below. Note that the spectral shifts in bathorhodopsin are given in parentheses. Glu113 emerges as the single largest contributor with a -87 (-91) nm blue shift. This is not surprising considering the fact that it is the only ionic group inside the binding pocket. Our calculations show that the EII loop comprising of Ser186, Cys187, Gly188, Ile189 contribute a sum of -43 (-39) nm blue shift. Until recently, the role of the extracellular loop II has been primarily associated with the counterion-switch mechanism.[222]

In this section the results of a study are described in which a truncated five double bond retinal model chromophore (**5.PSB11$_{dist}$**, **5.PSBT$_{dist}$**) and the NPA atomic point charges of the binding pocket consisting of 30 residues were used to study the residual effect on the electronic spectrum of rhodopsin. Our findings show that the binding pocket is evenly spaced between red and blue shifting residues, while

the anionic Glu-113 remains the primary counterion required for balancing the positive charge on the cationic retinal. Most importantly, a blue shifting role by the extracellular (EII) loop is identified.

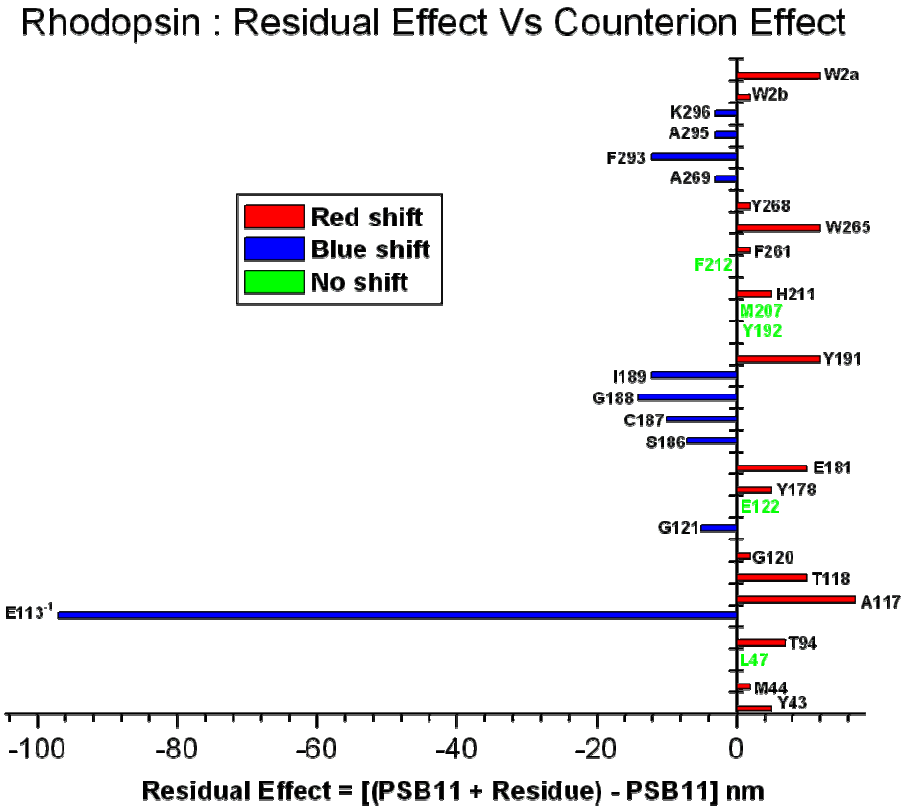

Figure 31 *The spectral shift of each residue inside the rhodopsin binding pocket is based on the interaction of that residue and the chromophore alone.*

Ala117 leads the list of red shifting residues with +17 (+13) nm. This strong interaction is caused by its close proximity to the retinal chromophore.[212] Thr118 and Thr94 are the second largest contributors with +10 (+7) and +7 (+5) nm respectively. Thr118 has been observed to interact with C9-methyl group,[213] whereas theoretical results point to a possible role for Thr94 in stabilising the counterion salt bridge.[221] Of the eight aromatic residues, both Tyr191 and Trp265 induce +12 (+10) nm red shift individually, whereas Phe293 accounts for a -12 (0) nm blue shift in the dark state and remains inactive in bathorhodopsin. This could be due to the strong interaction of Tyr191 with Thr118 and strategic positioning of a hydrophobic Phe293 near to the

Schiff base terminal in rhodopsin while it moves away from the orientation of the iminium nitrogen atom in bathorhodopsin.

The binding site contains only two water molecules, one of which (Wat2a) produces a strong +12 nm (+2) compared to a weak but consistent +2 nm shift by Wat2b from rhodopsin to bathorhodopsin. The indifferent shift of Wat2a is due to its strategic positioning in rhodopsin where it can perturb the chromophore along the polyene chain[214] thus inducing a strong shift, and then move further away from the retinal proximity in bathorhodopsin resulting in a weak interaction. Wat2b is primary involved in stabilizing the iminium nitrogen atom through hydrogen bonding[221] and hence results in a weak contribution. Specific details about the role of the two water molecules on the electronic spectrum will be discussed in a separate section.

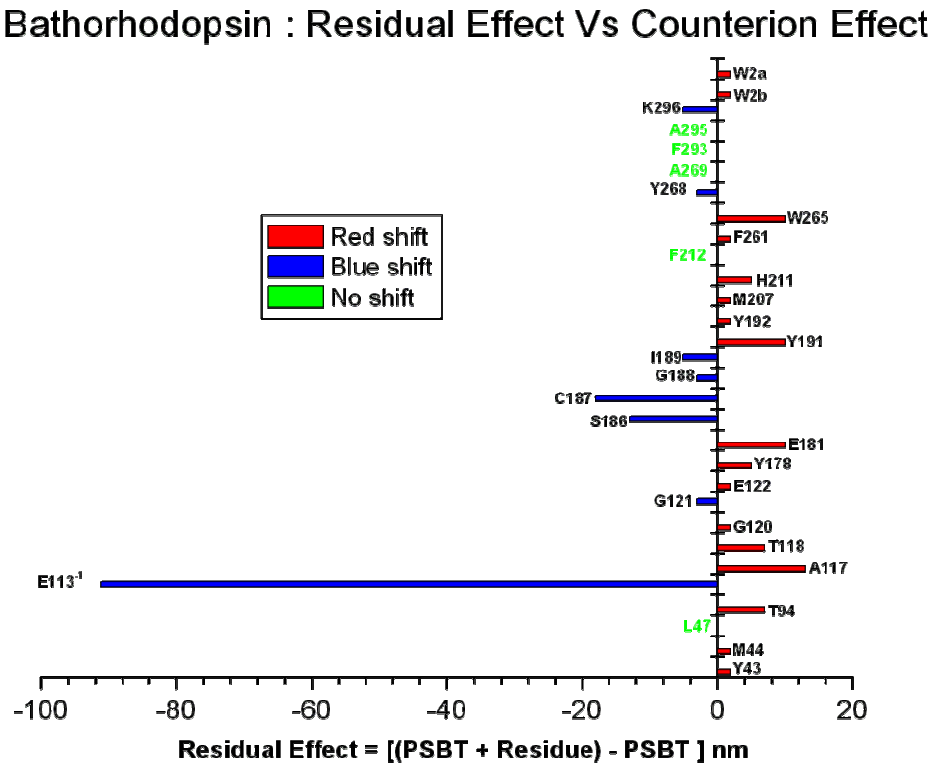

Figure 32 *The spectral shift of each residue inside the bathorhodopsin binding pocket is based on the interaction of that residue and the chromophore alone.*

Glu181 in its protonated state is calculated to induce +10 nm in agreement with Glu181Gln mutant experiments.[215] Glu122, Phe212, and Met207 do not have any

effect on the λ_{max} due to the lack of interaction with the omitted β-ionone ring. Deprotonated Glu181 induces a very small -7 nm blue shift compared to the -97 nm from Glu113, whereas a charged Glu122 exerts a +27 nm red shift due to the partial stabilisation of the positive charge deposited at the other end of the polyene chain in the excited state. Gly121, Ala269, Ala295 and Lys296 each induce negligible -3 nm blue shifts. Tyr43, Met44, Tyr178, Tyr192, His211, Phe261 each account for red shifts for up to +5 nm.

Tyr268 close to the β-ionone ring induces +5 nm in rhodopsin as it stabilizes the excited state, while the shift is inversed as it is displaced further away in the bathorhodopsin pocket. Leu47 and Tyr192 remain more or less inactive as they are positioned far away from establishing any contact with the chromophore both in the rhodopsin and the bathorhodopsin pockets. In summary, 15 residues account for a red shift, while 10 residues induce a blue shift and 5 residues remain ineffective in rhodopsin. On the other hand, 17 residues induce red shift, 8 residues induce blue shift and 5 residues remain neutral in bathorhodopsin.

The spectral shifts serve as a predictive tool to monitor the movement of amino acids from one intermediate state to another. In conclusion, we have presented a viable theoretical framework, where the reduced retinal chromophore is treated quantum mechanically and each of the 30 residues mimicked by static point charges. It is apparent that in the case of uncharged (neutral) amino acids, the opsin is specifically designed to carry evenly spaced residues with 10 (8) residues inducing blue shift, 15 (17) residues inducing red shift and 5 residues inducing no shift in both the rhodopsin and bathorhodopsin binding pockets.

Most importantly, the functional role of the two water molecules in red shifting the absorption maximum is observed. E181 and E122 are found to be neutral;

in agreement with experimental FTIR measurements.[89] A key role for the EII loop in blue shifting the absorption maximum has been identified. The strategic positioning of the EII loop above the counterion, suggests that it may act as a shield by negating the impact of the neighbouring red shifting residues, paving the way for the counterion engage itself in an intimate *ion-pair* relationship with the retinal.

3.1.3.4 Effect of the Polar and/or Non-Polar Amino Acids

The process of spectral tuning is completed by the addition of atomic charges to the protein embedded systems (**$PSB11_{pe}$**, **$PSB9_{pe}$**, **$PSBT_{pe}$**). Compared to the chromophore-counterion system (see Table 3), perusal of Table 5 reveals that the perturbation due to the charges is rather small. There is a red shift of 0.08 eV or 16 nm, 0.07 eV or 13 nm, and 0.02 or 4 nm in the absorbance and also the charge distribution as measured by the dipole moments does not change significantly compared to chromophore/counterion system. The net effect of the charges is, however, to bring the calculated absorbance very close to the experimental absorption maximum of rhodopsin, isorhodopsin and bathorhodopsin (*Figure 33*).

Table 5 *CASSCF and CASPT2 corrected state energies, oscillator strengths, main contributing configuration with weight, and dipole moments for the ground state S_0 and two main excited states S_1, S_2.*

Model	State	CASSCF[a]	CASPT2[a,b]	f	Configuration[c]	μ[d]	λ(Exp)
$PSB11_{pe}$	S_0	-1057.3938	-1060.7835		$(6a)^2(7a)^0$ *65*	9.64	
	S_1	4.83 (257)	2.47 **(502)**	0.79	$(6a)^1(7a)^1$ *62*	21.59	**498**
	S_2	3.41 (363)	2.89 (429)	0.00	$(6a)^0(7a)^2$ *29*	9.64	
$PSB9_{pe}$	S_0	1057.3868	-1060.7773		$(6a)^2(7a)^0$ *64*	11.06	
	S_1	4.84 (256)	2.53 **(490)**	0.80	$(6a)^1(7a)^1$ *60*	22.70	**485**
	S_2	3.50 (354)	3.00 (413)	0.00	$(6a)^0(7a)^2$ *28*	10.50	
$PSBT_{pe}$	S_0	-1057.3648	-1060.7560		$(6a)^2(7a)^0$ *61*	10.37	
	S_1	4.53 (274)	2.36 **(525)**	0.77	$(6a)^1(7a)^1$ *49*	22.50	**543**
	S_2	3.10 (400)	2.71 (457)	0.00	$(6a)^0(7a)^2$ *27*	10.22	
$PSB11_{pe}$ + E122Q	S_0	-1057.3937	-1060.7833		$(6a)^2(7a)^0$ *65*	9.29	
	S_1	4.92 (252)	2.55 **(486)**	0.79	$(6a)^1(7a)^1$ *62*	19.95	**481**
	S_2	3.42 (363)	2.92 (425)	0.00	$(6a)^0(7a)^2$ *29*	9.17	

[a] S_0 energies are in a.u., S_1 and S_2 energies are in eV relative to S_0. [b] In parentheses: wavelengths in nm. [c] Only π-type MO's are counted; weights (in italics) are in % [d] Dipole moments in Debye.

We have also performed a mutant calculation, where glutamic acid at position 122 (E122) is replaced by a glutamine (Q122) and the whole binding pocket is reoptimized fixing only the peptide backbone. The resulting chromophore structure in the mutant binding pocket is more or less similar to the chromophore in the original binding pocket and the calculated absorption spectra is 16 nm blue shifted compared to the 17 nm observed through experimental mutagenesis studies by Nathans.[216] Since the resultant absorbance spectra is relatively close to that of native bovine rhodopsin, we rule out a significant role for such neutral residues in spectral tuning. We strongly believe that at any given amount of time, removing or mutating a single neutral amino acid in rhodopsin can only lead to shift of anywhere in between 15 to 20 nm, however, it must be noted that within our computational set-up mutant pigments can also be studied with high accuracy.

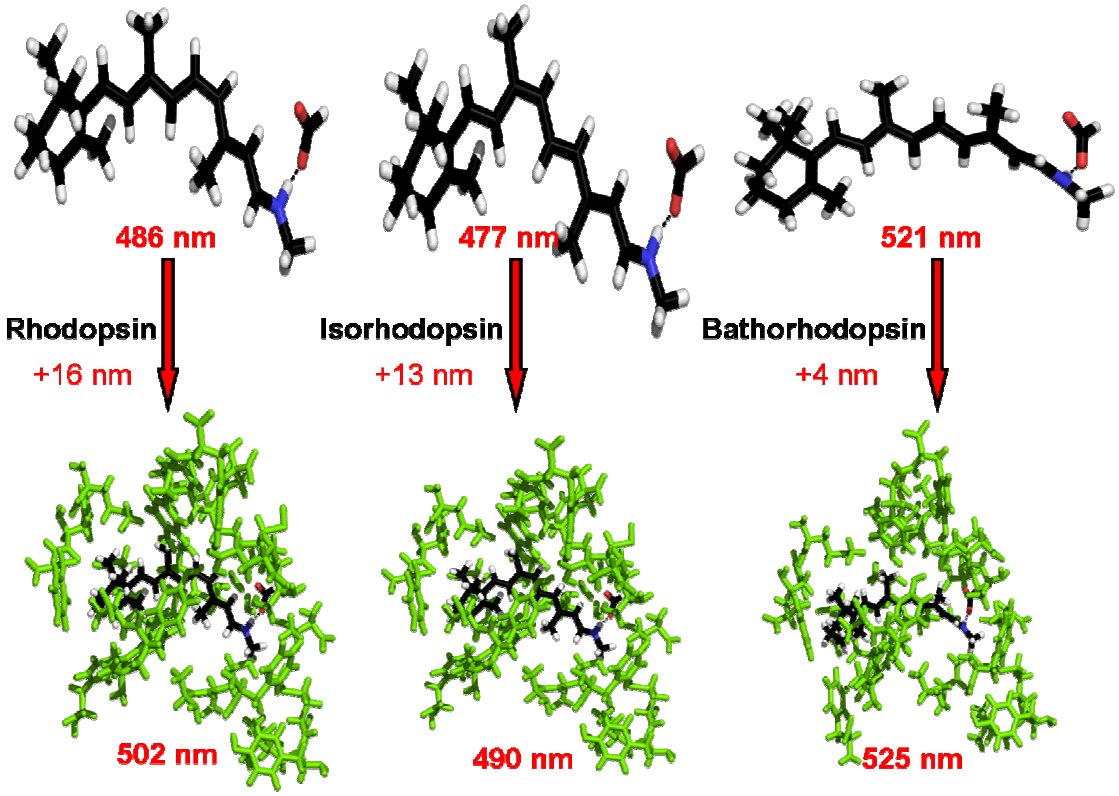

Figure 33 *Effect of the binding pocket on the absorption maximum of rhodopsin, isorhodopsin and bathorhodopsin.*

3.1.4 Retinal "Sees" the Water

Water molecules in protein cavity have been the subject of continuing interest due to their profound role in facilitating the evolution of key biological networks.[217-219] The visual protein rhodopsin contains two water molecules (Wat2a, Wat2b) near the protonated Schiff base binding region. As a consequence of steric strain, one end of the retinal chain is held fixed by its β-ionone ring,[220] while the other end is in electrostatic contact with its primary counterion (Glu113)[75-77]–a viable connection found to be stabilised by Wat2b.[221] The other water molecule Wat2a, is engaged to the extracellular loop (EII) consisting of Glu181, Ser186, Cys187, Gly188, and Ile189 residues via hydrogen bonded networks generally agreed to be involved in a so-called counterion switch mechanism from position 113 to 181 during the formation of Metarhodopsin-I.[222]

The functional role of water molecules in intraprotein proton transfer has confirmed that water molecules are as essential for biological functions as amino acids.[223] Experimental studies have shown that three water molecules are present in the active centers of *bacteriorhodopsin*[32,224] and *halorhodopsin,*[33,225] respectively. QM/MM calculations[226] along with FTIR probes[227] have shown that the hydrogen bonding interaction of Wat402 is stronger with Asp85 than with Asp212 in bR. In the case of hR, it was suggested that hydration of chloride ion is stabilized by weak hydrogen bonds of waters.[228] However the critical role of water molecules in the spectral tuning mechanism of rhodopsins has been left unexplored.

It is difficult to predict *a priori* which direction the presence or absence of water molecule will cause the absorption maxima to shift. In the case of the Wat2a and Wat2b in rhodopsin, due to lack of strong theoretical evidence little is understood so far. Arguments in this communication are basically the result of the calculation of

spectral shifts due to the Wat2a and Wat2b residues in the presence and absence of the counterion, polar and/or non-polar amino acids lining the rhodopsin binding pocket. By employing a step-wise procedure, we have attempted to find answers to the following questions: (1) What is the role of Wat2a and Wat2b on the electronic spectrum? (2) Do the water molecules actively participate in altering the ground and excited state energies of the retinal chromophore? (3) Is the effect of water molecules additive or selective? (4) To what extent are the water molecules involved in stabilizing the chromophore-counterion salt-bridge?

TABLE 6 *CASPT2 calculated energies, oscillator strengths, main contributing configurations with weight, and dipole moments for the ground S_0 and excited states S_1, S_2, of retinal chromophore models shown in Scheme A, B and C*

Model	State	CASSCF[a]	CASPT2[a,b]	f	Configuration[c]	μ[d]
PSB11$_{dist}$ + Wat2a[†]	S_0	-944.3714	-947.4692	-	$(5a)^2(6a)^0$ *77*	15.83
	S_1	2.39 (518)	1.83 (**677**)	1.05	$(5a)^1(6a)^1$ 61	12.34
	S_2	3.40 (365)	2.70 (459)	0.14	$(5a)^0(6a)^2$ *30*	12.01
PSB11$_{dist}$ + Wat2b	S_0	-944.3740	-947.4641	-	$(5a)^2(6a)^0$ *76*	15.59
	S_1	2.61 (476)	1.83 (**677**)	0.94	$(5a)^1(6a)^1$ *59*	9.95
	S_2	3.44 (360)	2.76 (449)	0.00	$(5a)^0(6a)^2$ *31*	12.09
PSB11$_{dist}$ + Wat2a + Wat2b	S_0	-1020.4055	-1023.7179	-	$(5a)^2(6a)^0$ *77*	14.82
	S_1	2.35 (527)	1.82 **(681)**	1.07	$(5a)^1(6a)^1$ *61*	10.68
	S_2	3.38 (366)	2.68 (463)	0.00	$(5a)^0(6a)^2$ *30*	10.34
PSB11$_{ip}$ + Wat2a	S_0	-1132.7271	-1136.3341	-	$(5a)^2(6a)^0$ *65*	9.61
	S_1	4.84 (256)	2.49 (**498**)	0.81	$(5a)^1(6a)^1$ *61*	20.85
	S_2	3.42 (362)	2.93 (423)	0.00	$(5a)^0(6a)^2$ *29*	9.44
PSB11$_{ip}$ + Wat2b[†]	S_0	-1132.7349	-1136.3419	-	$(5a)^2(6a)^0$ *65*	9.67
	S_1	4.86 (255)	2.52 (**492**)[¶]	0.81	$(5a)^1(6a)^1$ *62*	20.63
	S_2	3.42 (363)	-	-	-	9.40
PSB11$_{ip}$ + Wat2a + Wat2b	S_0	-1208.7717	-1212.5951	-	$(5a)^2(6a)^0$ *65*	8.52
	S_1	4.78 (259)	2.46 (**504**)	0.80	$(5a)^1(6a)^1$ *61*	20.44
	S_2	3.43 (361)	2.93 (423)	0.00	$(5a)^0(6a)^2$ *29*	8.30
PSB11$_{pe}$	S_0	1056.6899	-1060.7835		$(6a)^2(7a)^0$ *65*	9.64
	S_1	4.92 (252)	2.47 **(502)**	0.79	$(6a)^1(7a)^1$ *62*	21.59
	S_2	3.41 (363)	2.89 (429)	0.00	$(6a)^0(7a)^2$ *29*	9.64
PSB11$_{pe}$ – Wat2a	S_0	-1057.3879	-1060.7774		$(6a)^2(7a)^0$ *65*	9.11
	S_1	4.95 (250)	2.55 **(486)**	0.81	$(6a)^1(7a)^1$ *62*	19.83
	S_2	3.40 (364)	2.89 (429)	0.00	$(6a)^0(7a)^2$ *29*	9.10
PSB11$_{pe}$ – Wat2b	S_0	-1057.3741	-1060.7653		$(6a)^2(7a)^0$ *65*	9.45
	S_1	4.86 (255)	2.49 **(498)**	0.79	$(6a)^1(7a)^1$ *62*	21.11
	S_2	3.41 (364)	2.90 (428)	0.00	$(6a)^0(7a)^2$ *29*	9.45
PSB11$_{pe}$ – (Wat2a + Wat2b)	S_0	-1057.3681	-1060.7590		$(6a)^2(7a)^0$ *65*	8.92
	S_1	4.99 (249)	2.57 **(482)**	0.81	$(6a)^1(7a)^1$ *63*	19.29

	S_2	3.40 (365)	2.89 (429)	0.00	$(6a)^0(7a)^2$ *29*	8.91

[a]S_0 energies are in au. S_1 and S_2 energies are in eV relative to S_0, in parentheses: wavelengths in nm. [b]Only π-type MO's are counted; weights (in italics) are in %. [c]Dipole moments in Debye. [†]Stable isomer [†]Reference 238

In Table 1, the calculated ground- and excited-state energies (including the forbidden S_2 state), oscillator strengths and dipole moments, are listed for different retinal-water complexes under investigation. In the absence of the counterion (see Scheme A), the charge distribution is highly unsymmetrical for the distorted free protonated Schiff base **($PSB11_{dist}$)** which absorbs at 643 nm. When Wat2a and Wat2b are allowed to interact individually with **$PSB11_{dist}$**, each of the water molecules contributes an identical bathochromic shift of 34 nm pushing the λ_{max} to 677 nm.

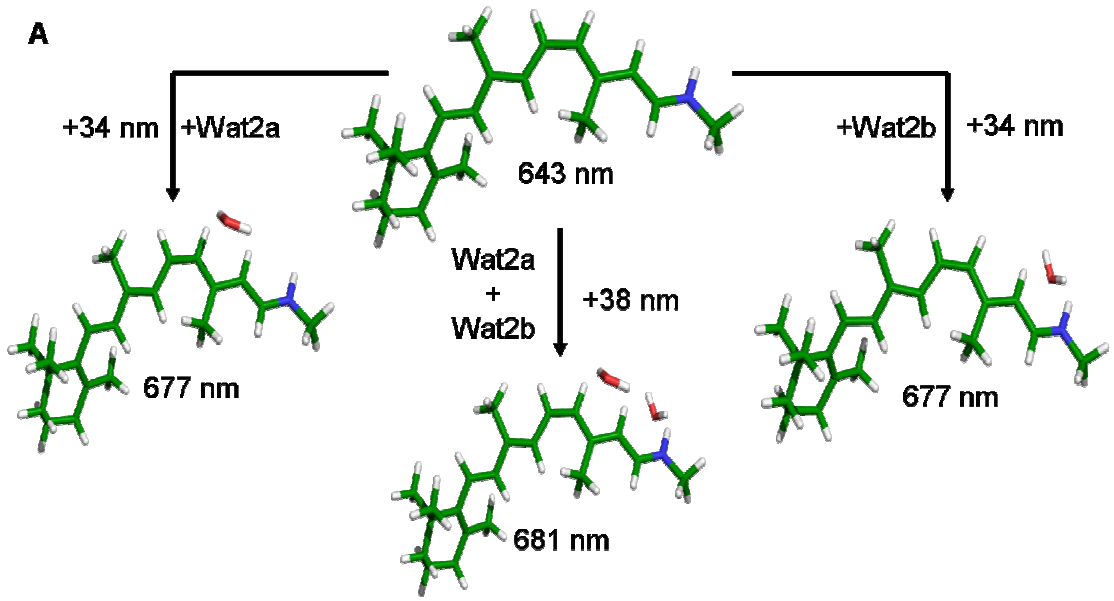

Scheme A *Schematic representation of the individual and cumulative effects of Wat2a and Wat2b on the electronic spectrum of rhodopsin in the absence of counterion.*

It should be noted that, the **$PSB11_{dist}$+Wat2a** complex is 3.2 kcal·mol^{-1} more stable than the **$PSB11_{dist}$+Wat2b** counterpart; an aspect also reflected in the slight increase of the S_0 dipole moment for the former. This stabilizing effect could be due to the strategic presence of Wat2a within ~3.5-Å distance to the strongly twisted isomerizing region (C11=C12 double bond) which may induce a non-bonded

interaction. Notice that, the magnitude of the S_1 dipole moment very similar to that of S_2 due to the characteristic presence of Wat2a.

The cumulative effect of the two water molecules is only +4 nm higher (+38 nm) than their respective individual spectral shifts. Thus the chromophore fails to discriminate against the location of the two water molecules in the absence of the counterion as the spectral shifts are non-additive in good agreement with the findings from Kusnetzow et al. where the effect of each residue inside the binding site is calculated based on the interaction of that residue and the chromophore alone.[229]

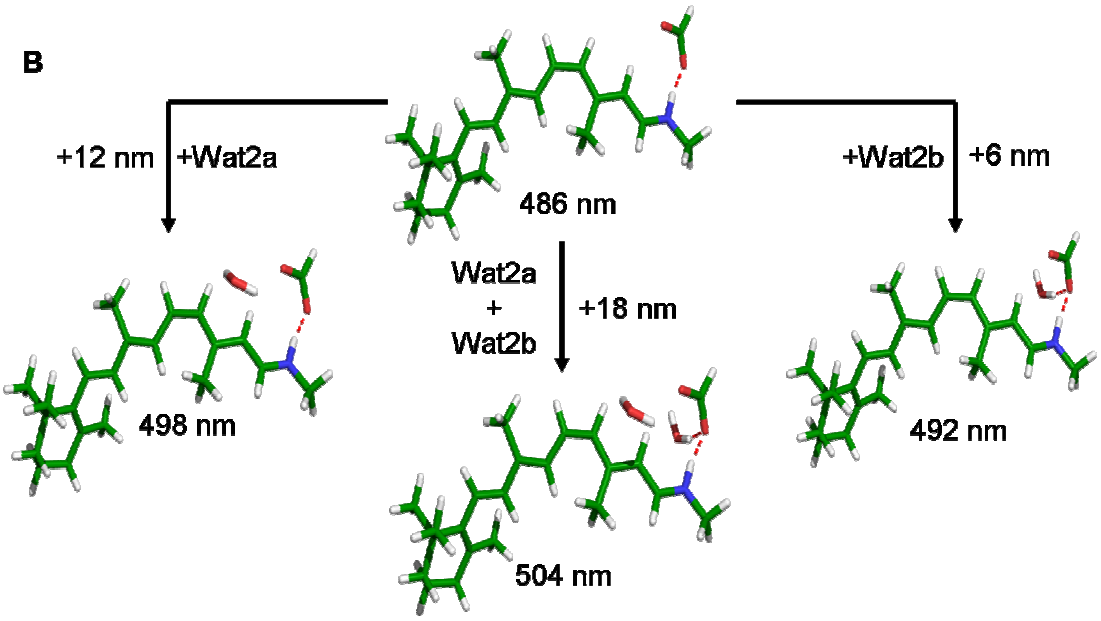

Scheme B *Schematic representation of the individual and cumulative effects of Wat2a and Wat2b on the electronic spectrum of rhodopsin in the presence of counterion.*

In the presence of the counterion (see Scheme B), the **PSB11$_{ip}$+Wat2b** isomer is calculated to be 4.9 kcal·mol^{-1} more stable than **PSB11$_{ip}$+Wat2a** complex, indicating a strong preference for Wat2b over Wat2a, by the chromophore. A strong reduction in the extent of electron delocalization is observed upon excitation, as there are no longer any formal charges available. The counterion anchors the positive charge on the Schiff base iminium nitrogen atom and shifts the excited state charge density against the negative charge of the counterion. As a consequence, the S_0-S_1

energy gap is raised and a strong blue shift is induced as the λ_{max} is pushed to 486 nm. The strong red shift calculated in the absence of counterion is drastically reduced as the individual interaction of Wat2a and Wat2b result in weak red shifts of 6 and 12 nm, respectively. Surprisingly, the individual effect adds up to produce an 18 nm shift identical to the cumulative effect of the two water molecules.

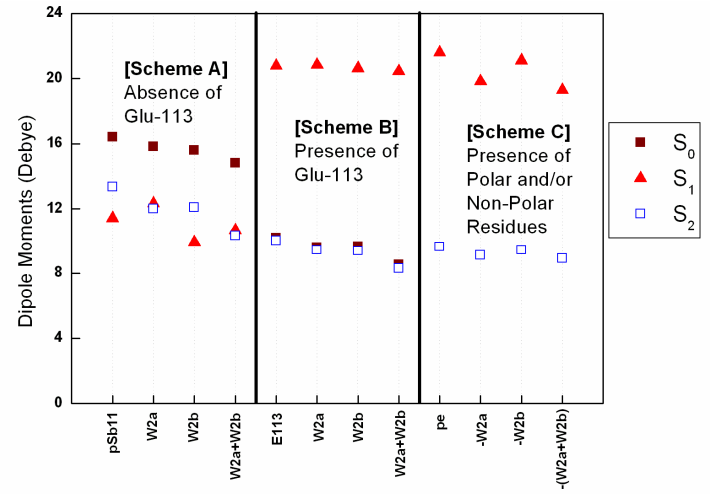

Figure 34 *Dipole moments of the retinal complexes in Scheme A, B, C.*

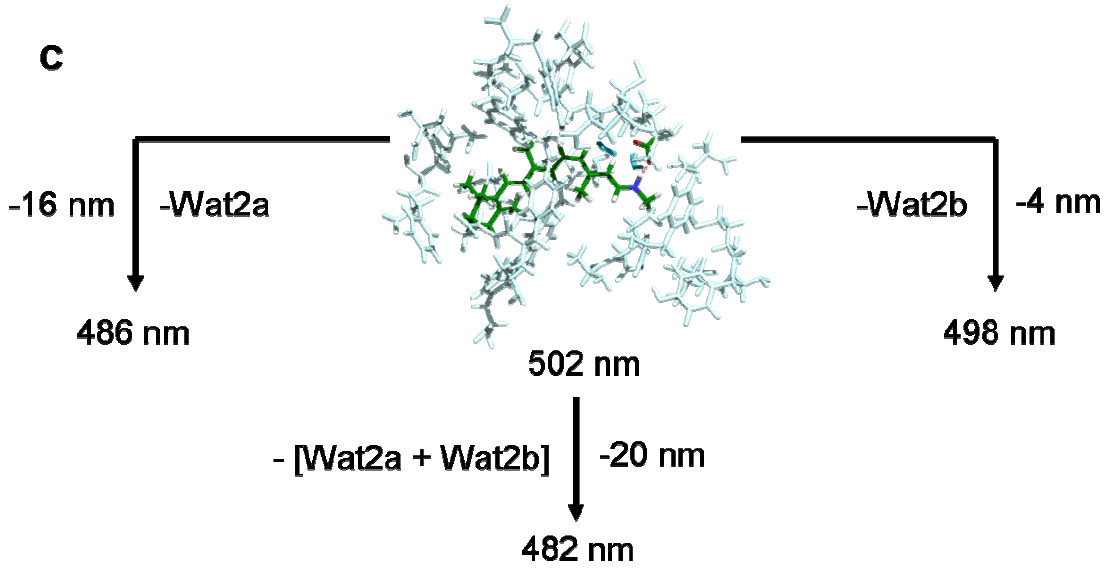

Scheme C *Schematic representation of the individual and cumulative effects of Wat2a and Wat2b on the electronic spectrum of rhodopsin in the presence of polar and/or non-polar amino acids.*

In order to further substantiate this observation, an independent dehydrated rhodopsin binding pocket models were prepared in which the two water molecules

(mimicked as NPA point charges in the protein embedded chromophore) are removed one after another in the presence of polar and/or non-polar amino acids including the counterion (see Scheme C). The calculated λ_{max} of the 486, 498 and 482 nm indicates the stepwise removal of Wat2a, Wat2b and both together, in strong support to our findings from Scheme B. The absence of the water species **(PSB11$_{pe}$-Wat2a-Wat2b)** destabilizes the retinal protein cavity by 15.4 kcal·mol^{-1} relative to **PSB11$_{pe}$**, which further confirms the physiological relevance of the two water molecules.

In conclusion, we have demonstrated the key role of water molecules in manipulating the ground and excited state energies of the retinal chromophore. It is apparent that, the electrostatic contact of the chromophore with the counterion can significantly modulate the influence of the neutral residues like water molecules on the electronic spectrum. Most importantly in the presence of the counterion, an additive spectral shift is calculated and hydrogen bonded Wat2b is preferred over Wat2a for stabilizing the chromophore-counterion salt-bridge. The results clearly show that the retinal "sees" water through the eyes of the counterion in rhodopsin.

Our results strongly support the emerging paradigm that water molecules are as essential for biological functions as amino acids. It remains to be seen, if similar calculations can pinpoint the exact role of water molecules in archael rhodopsins like *b*R, *s*RI, and *s*RII.

3.1.5 Mechanism of Energy Storage & Origin of Bathochromic Shift

Photochemical events in rhodopsin can conveniently serve as testing grounds for wide ranging theoretical investigations, since they concern the mechanism of energy storage required for driving the kinetics of the visual cascade. In this connection it may be recalled that several of the early rhodopsin photo-intermediates are characterised by their peculiar red-shifted absorption maxima, e.g. a 45 nm red-

shift as rhodopsin (498 nm) is transformed to bathorhodopsin (543 nm). Microcalorimetric measurements[230] have revealed that this early photo-intermediate alone can carry 35 kcal·mol^{-1} out of the total 57 kcal·mol^{-1} photonic energy.

Little is understood with respect to this particular evolution of a biological network which interlinks the energy storage process with that of the bathochromic shift. Early investigations from retinal models have proposed the distribution of negative charge along the retinal carbon skeleton[172] and charge separation between the chromophore-counterion salt-bridge network upon photoisomerization as the major source, until the mechanism of distortion of the conjugated retinal backbone was put forward by Warshel et al.[231] Later a combination of these two mechanisms has been proposed by Birge et al.[232]

A logical place to start our investigation is to focus on the ground state energies of the different retinal complexes, which can provide evidence on how the photonic energy is stored in bathorhodopsin. From the perusal of *Figure 36* and the results from our calculations given in Table 7, it is interesting to note that the stability of the *cis* and *trans* isomers in *vacuo* (4.65 kcal·mol^{-1}) is inverted as **PSB11$_{dist}$** enters into the protein environment (5.65 kcal·mol^{-1}). On the other hand, **PSB9$_{vac}$** is higher in energy than **PSB11$_{vac}$** by 4.0 kcal·mol^{-1} for the reasons discussed above. The gap remains around 3.4 kcal·mol^{-1}, caused by protein distortion which affects mainly the native chromophore.

The binding pocket stabilizes the geometrically distorted chromophore via by fitting the β-ionone ring at one end of the hydrophobic pocket, while facilitating the formation of a salt-bridge at the other end of the retinal tether with the counterion (E113). The chromophore/counterion (**PSB11$_{ip}$**, **PSBT$_{ip}$**) electrostatic interaction contributes a further 8.1 kcal·mol^{-1} raising the S_0 energy gap between to 13.75

kcal·mol^{-1}. This is conceivable as the excited state charge mobility is restricted in the presence of counterion compared to a free unsymmetrical polyene, where we notice the displacement of negative charge toward the Schiff base nitrogen atom from the β-ionone ring in the S_1 state. The counterion anchors the proton on the Schiff base terminus, thus increasing the stiffness of an already distorted retinal backbone[233] an aspect also observed by ^{13}C NMR measurements.[234]

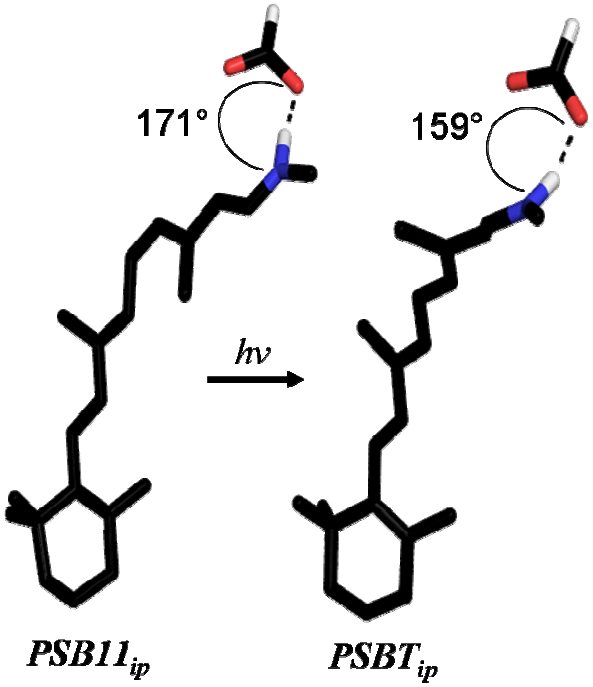

Figure 35 *Dihedral ange deviation in the salt-bridge network as $PSB11_{ip}$ is transformed to $PSBT_{ip}$.*

Due to the *cis-trans* isomerization, considerable portion of energy of about 5.0 kcal·mol^{-1} (calculated by *M. Sugihara*) is retained at the salt-bridge network due to the deviation of 12° (see *Figure 35)* as rhodopsin is transformed to bathorhodopsin. In the presence of the binding pocket, the S_0 energy difference is further raised to 17.3 kcal·mol^{-1} which is almost 50% of the stored energy. The increase in the counterion distance by 0.3-Å observed experimentally[200] in the conversion of rhodopsin to bathorhodopsin can further increase the energy by another 7.3 kcal·mol^{-1} which shows

that between 18.9 to 11.6 kcal·mol^{-1} of the missing energy should be stored via steric interaction between the highly strained chromophore and the binding pocket. Accordingly, the presence of protein charges places **PSB9$_{pe}$** comfortably around 4 kcal·mol^{-1} over **PSB11$_{pe}$** in very good agreement with photocalorimetric measurements on the two pigments.[235,236]

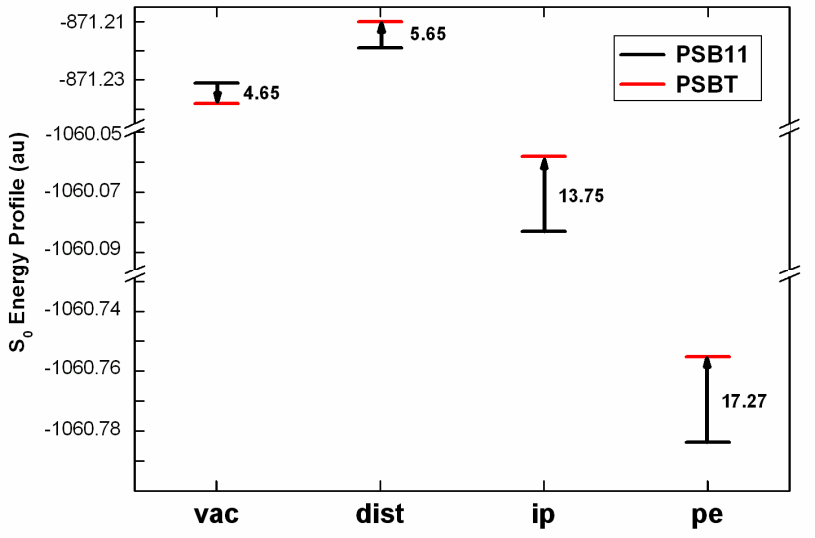

Figure 36 *The calculated CASPT2 ground state (S_0) energies in au of **PSB11** (—) and **PSBT** (—) models in vacuo and in protein environment. In bold, energy difference in kcal·mol^{-1}.*

The response of the ground and the excited states to the external perturbation from the protein environment is popularly referred to as spectral tuning. The $S_0 \rightarrow S_1$ excitation characterising the lowest lying excited state is normally referred to as the *'ionic'* state, while the formally forbidden $S_0 \rightarrow S_2$ energy gap dominated by a weak double excitation is the *'covalent'* state (*Figure 37*). As we have already seen, the calculated primary λ_{max} absorption band of **PSB9$_{dist}$**, **PSB11$_{dist}$** and **PSBT$_{dist}$** are 593, 643 and 649 nm, respectively.

Table 7 *Calculated energies, oscillator strengths f and dipole moments μ of retinal model chromophores.[a] In bold, wavelength of the allowed optical transition (in nm).*

Model	State	PSB9		PSB11		PSBT	
		CASPT2[c,d]	f	CASPT2[b,d]	f	CASPT2[c,d]	f
vac	S_0	-4.02		-871.2306		-4.65	
	S_1	48.2 **(593)**	1.05	47.3 **(606)**	1.12	47.6 **(600)**	1.32
dist	S_0	-3.45		-871.2185		+5.65	
	S_1	46.3 **(617)**	1.00	44.5 **(643)**	0.96	44.1 **(649)**	1.43

ip	S_0	+0.56		-1060.0803		+13.75	
	S_1	59.9 **(477)**	0.84	58.8 **(486)**	0.82	54.9 **(521)**	0.82
pe	S_0	+3.89		-1060.7835		+17.27	
	S_1	58.3 **(490)**	0.80	57.0 **(502)**	0.79	54.4 **(525)**	0.77

[a]See text for abbreviations. [b]S_0 energies in au; [c]S_0 energies relative to the corresponding S_0 energy of PSB11, in kcal·mol^{-1}. [d]S_1 energies relative to S_0 in kcal·mol^{-1}.

Comparison of the **"vac"** and **"dist"** chromophore models clearly shows that the calculated red shift of 24, 37 and 49 nm relative to their **PSB9$_{vac}$** (593 nm), **PSB11$_{vac}$** (606 nm) and **PSBT$_{vac}$** (600 nm) is due to geometric distortion, while only +6 and -26 nm spectral shifts are calculated between the distorted isomers. It must be noted, while the extent of internal twisting accounts for the stability of **PSB11$_{dist}$** over **PSBT$_{dist}$**, it fails to hold true for the origin of the 45 nm bathochromic shift as rhodopsin is transformed to bathorhodopsin.

Recently, the counterion (E113) has been shown to be the origin of spectral tuning in rhodopsin.[237] The calculated λ_{max} of 486 nm (2.55 eV) for **PSB11$_{ip}$** and 521 nm (2.38 eV) for **PSBT$_{ip}$**, shows a clear difference of 35 nm bathochromic shift as against the 45 nm observed experimentally. Since both chromophores are strongly twisted with only a small increment of 0.03-Å in the position of the counterion (observed theoretically[238]) between the two chromophore – ion pair systems, we propose that the electrostatic interaction of the chromophore with E113 is designed to achieve dual function, to raise the energy of the distorted all-*trans* ion-pair and thus lower the $S_0 \rightarrow S_1$ energy gap leading to the 35 nm red shift.

For **PSB11$_{pe}$**, the calculated λ_{max} of 502 nm is convincingly close to the experimental value of rhodopsin (498 nm). The agreement is not quite as good in the case of **PSBT$_{pe}$** (525 vs. 543 nm), but there may be a reason for this: there is a curious discrepancy between the experimental and the calculated distance of the counterion and the chromophore. It should be noted that other recent computational studies on the rhodopsin photo-intermediate[183,239] have failed to account for the origin of

bathochromic shift, which is a key photophysical property to characterise bathorhodopsin.

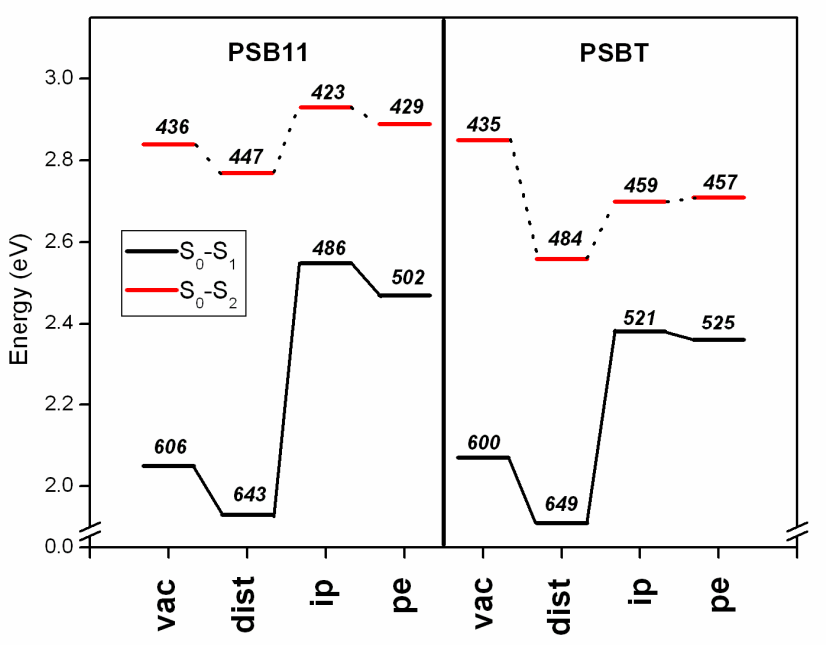

Figure 37 *CASPT2 calculated $S_0 \rightarrow S_1$ (—), $S_0 \rightarrow S_2$ (—), energy gap for the different retinal complexes in table 1. Numbers in italics are absorption maxima in nm.*

In the case of isorhodopsin, the 13 nm blue-shift (calc. 12 nm) relative to rhodopsin can be traced back to the less distorted chromophore in *vacuo* (the **PSB9$_{vac}$** chromophore is essentially planar) and the significantly smaller red shift suffered through distortion by the protein pocket – a consequence of steric misfit in the binding site of isorhodopsin.[207]

In conclusion, our results provide information essential for understanding the electronic excitation of rhodopsin on a molecular level. The counterion appears to be the key player in two aspects: (i) enhancing the stored photonic energy in the chromophore and (ii) controlling the conspicuous bathochromic shift evident in the early photo-intermediate. We demonstrate that 16% of the energy is locked as strain in the distorted polyene, while 15% is exclusively retained in the dynamics of the salt-bridge network. The chromophore-counterion interaction accounts for 9% and the charges of the binding pocket induce a further 10%. It is apparent that there is a strong

discrepancy between the calculated and the experimental energy of bathorhodopsin relative to rhodopsin. This could be due to the reduced binding pocket models which we have consistently used in our study. However, more work is clearly needed before definite statements can be made for understanding the energy storage mechanism in detail.

3.1.6 How to Annul the Counterion

It is now clear that the origin of spectral tuning in rhodopsin lies with the counterion. Recently, Andruniów et al.[183] and Coto el al.[240] using a CASSCF/CASPT2/AMBER set-up postulated a counterbalancing role of the opsin environment against the counterion which is in complete contrast to our results. We do not, however, believe that their data in any way rules out the blue shift induced by the counterion. In any case, the model proposed by them is incompatible with the known experimental gas-phase studies as well as our theoretical results discussed here. This could be due to the poor description of the active site with a smaller 6-31G* basis set which does not allow a definitive conclusion.

Moreover, it is difficult to see how all the neutral residues can counterbalance a charged counterion which is already engaged with the cationic chromophore via the salt-bridge network. Common sense would suggest that the only way to counterbalance or annul the counterion is to remove or mutate it. However, we show that by creating another counterion in the β-ionone ring region, the excited state positive charge is effectively anchored and the primary counterion effect is annulled. In other words, in an electrically neutral binding pocket only a charged residue can counterbalance the counterion.

We have chosen the bathorhodopsin structure as the basis of our study (*Figure 38*), as the intrinsic character of the all-*trans*-retinal makes it more feasible for

capturing the proton charge. Since it is close to the β-ionone ring region, deprotonated E122 has been chosen to play the role of the second counterion.

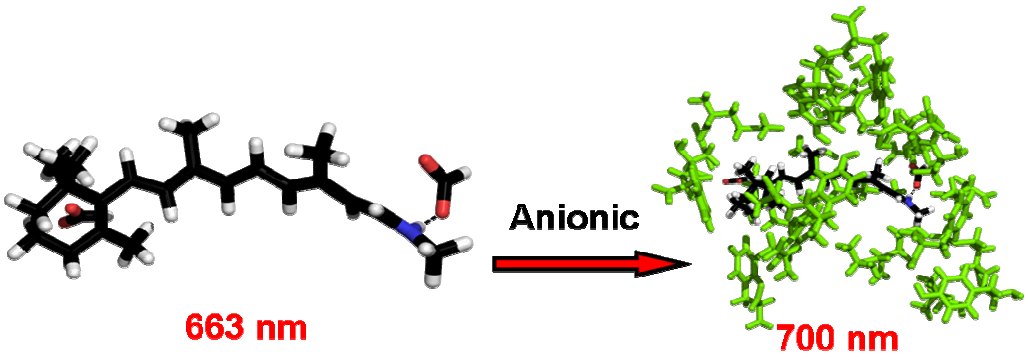

Figure 38 *Anionic bathorhodopsin binding pocket containing* $PSBT_{dist}$*, E113 and E122 in deprotonated forms surrounded by the rest of the amino acids mimicked as NPA point charges.*

Perusal of the results in Table 8 shows that the dipole moments of the S_0 and the S_2 excited states are three times greater in magnitude compared to those of their cationic **($PSBT_{dist}$)** and neutral **($PSBT_{ip}$)** counterparts (Table 2, 3). However, it is interesting to note that the dipole moment of the S_1 state remains more or less unaffected compared to **$PSBT_{ip}$**.

TABLE 8 *CASPT2 calculated energies, oscillator strengths, main contributing configurations with weight, and dipole moments for the ground* S_0 *and excited states* S_1*,* S_2*, of retinal chromophore models shown in Figure 38.*

Model	State	CASSCF[a]	CASPT2[a,b]	f	Configuration[c]	μ[d]
$PSBT_{ip}^{-1}$	S_0	-1245.0099	-1248.9941	-	$(5a)^2(6a)^0$ *62*	37.51
	S_1	3.77 (329)	1.83 (**663**)	0.65	$(5a)^1(6a)^1$ 50	22.84
	S_2	3.06 (405)	2.55 (486)	0.01	$(5a)^0(6a)^2$ *29*	36.85
$PSBT_{pe}^{-1}$	S_0	-1246.1709	-1250.1598	-	$(5a)^2(6a)^0$ *61*	37.74
	S_1	3.52 (352)	1.77 (**700**)	0.68	$(5a)^1(6a)^1$ *51*	21.28
	S_2	3.09 (401)	2.20 (563)	0.02	$(5a)^0(6a)^2$ *29*	36.21

[a] S_0 energies are in au. S_1 and S_2 energies are in eV relative to S_0, in parentheses: wavelengths in nm. [b] Only π-type MO's are counted; weights (in italics) are in %. [c] Dipole moments in Debye

The absorption maximum of **$PSBT_{ip}^{-1}$** is red shifted by 20 nm relative to the bare chromophore **$PSBT_{dist}$**, which shows that the blue shift of ~140 nm induced by the primary counterion in **$PSBT_{ip}$** is more than neutralised by the presence of another counterion near the β-ionone ring region. It is possible that the stabilization of the

delocalized positive charge by E122 lowers the excited state energy as much as the ground state is lowered by E113, thus the energy difference (1.83 eV vs. 1.91 eV) will be approximately equivalent to that in vacuo with spectra to the red. Inclusion of the protein charges further induces a 37 nm bathochromic shift and pushes the λ_{max} of the anionic bathorhodopsin to 700 nm.

It may be useful to compare this value of 700 nm with that of 640 nm of the O state of bacteriorhodopsin which also contains an anionic binding pocket encircling a distorted all-*trans*-retinal chromophore electrostatically linked to a *soft* dual counterion complex (Asp-212, Asp-85) mediated by a pentagonal water cluster.

4 Conclusion

We have theoretically demonstrated the wavelength dependence of retinal Schiff base absorbencies on the protonation state of the chromophore at the multiconfigurational level of theory using second order perturbation theory (CASPT2) within an atomic natural orbital (ANO) basis set on MP2 optimized geometries. Quantitative agreement between calculated and experimental absorption maxima is obtained for protonated and deprotonated Schiff bases of 11-*cis*- and all-*trans*-retinal PSBs and intermediate states covering a wavelength range from 610 to 353 nm. These data will serve as reference points for the calibration of the embedded QM part in any of the widely used QM/MM schemes.

Employing the same CASSCF/CASPT2/ANO computational platform we have investigated the origin of spectral tuning in the visual protein rhodopsin, its early primary photo-intermediate bathorhodopsin and in the artificial analogue isorhodopsin. Employing the best structural data available we have shown that the absorption spectrum of rhodopsin can be calculated *ab initio* and with great accuracy

using a high-level quantum-mechanical platform. We have presented a roadmap in the form of a structural template to investigate the electronic spectrum of rhodopsin.

Starting with the chromophore in vacuo **(vac)** different perturbations are added in the form of protein mediated geometric distortion **(dist)**, plus electrostatic interaction with the counterion **(ip),** and finally the influence of the polar and/or non-polar amino acids mimicked as NPA point charges forms the protein embedded system **(pe)** We have demonstrated that by far the largest effect is exerted by the counterion. Since the protein environment provides and stabilizes the chromophore distortion necessary for the selective and ultrafast transformation from rhodopsin to bathorhodopsin we conclude that this is its primary role and that spectral tuning by the binding pocket is not the goal pursued by evolution. Clearly, the complete protein was not included in the calculation and no polarization effects were considered. However, the results obtained from multiconfigurational perturbation treatment make it highly probable that the lowest-lying excited state is correctly described and hence the qualitative outcome must certainly remain the same.

Our study on isorhodopsin and bathorhodopsin provides essential information for understanding the electronic excitation of rhodopsin at a molecular level. The counterion appears to be the key player in enhancing the stored photonic energy in the chromophore and controls the conspicuous bathochromic shift evident in the early photo-intermediate, while the effect of geometric distortion accounts for the blue shift in isorhodopsin. It reveals a possible explanation for the relation between the photo-reactivity and the protein assistance, and gives insights into manipulating the sophisticated biological function.

Our calculations on the individual residual effect against the counterion effect on the electronic spectrum can serve as a predictive tool to monitor the movements of

amino acids from one intermediate state to another. Our analysis of the role of water molecules in the binding site may provoke further studies on other related rhodopsins like bR, sRI and sRII where more than one water molecule is present inside the binding pocket. Recently the crystal structure of lumirhodopsin[241] and metarhodopsin II[242] have also been resolved, and it remains to be seen if our step-wise approach can hold good for elucidating the photophysical properties of these rhodopsin intermediates in detail.

The adaptive changes in the spectral sensitivity of rod photoreceptors can be traced to amino acid substitutions in rod opsin.[243] In invertebrate visual pigments, the position homologous to bovine rhodopsin E113 is occupied by a tyrosine (Y) or phenylanine (F) residue in the visible and UV-absorbing invertebrate pigments. This site has been proposed as the invertebrate counterion, and the F/Y polymorphism may be responsible for the difference in absorption between the visible and UV pigments of invertebrates.[244,245]

To sum up, faced with well-nigh universal problems, organisms everywhere may tend to gravitate toward common solutions. This aspect is governed by natural selection, the process described a century ago by Darwin and Wallace. It has sometimes been argued that natural selection is "not enough"-not enough to account for the evolution of an apparatus as complicated as the vertebrate eye. But one cannot dismiss natural selection just because it works better than one thinks it should. A hypothesis should be damned for its failures, not its successes; cases in which evolution have appeared to work to the net disadvantage of organisms.

5 References

[1] Oesterhelt, D. and Stoeckenius. W. *Proc. Nat. Acad. Sci. U.S.A.* **10**, 2853-2857 (1973).

[2] Wald, G. *Science,* **162,** 230-239 (1968), and references cited therein

[3] Hubbard, R. and Wald, G. *J. Gen. Physiol.* **36,** 269-315 (1952).

[4] Hubbard, R., Brown. K. P. and Kropf. A. *Nature*. **183**, 442-450 (1959).

[5] Hubbard, R., *Nature*. **221**, 432-435 (1969).

[6] Yoshizawa, T. and Wald. G. Nature. 197, 1279-1286 (1963).

[7] Knowles A. and Datnall J. A. in **"The Eye"**, Vol.2B, H. Davson, Ed., Academic Press, New York, 1977, 8-9.

[8] Honig, B. and Ebrey. T. G. *Annu. Rev. Biophys. Bioeng.* **3**, 151-177 (1974).

[9] Spudich, J. L., Yang, C. S., Jung, K. H. and Spudich, E. N. *Annu. Rev. Cell. Dev. Biol.* **16**, 365-392 (2000) and references cited therein.

[10] Sakmar. T. P., Menon, S. T., Marin, E. P. and Awad, E. S. *Annu. Rev. Biophys. B Biomol. Struct*. **31**, 443-484 (2002) and references cited therein.

[11] Nathans, J. *Neuron.* **24**, 299-312 (1999).

[12] Nakanishi, K. *Pure. Appl. Chem.,* **57**, 769-776 (1991).

[13] Nakanishi, K. *Pure. Appl. Chem.,* **63**, 161-170 (1991).

[14] Lagnado, L. and Baylor, D. *Neuron* **8**, 995-1002 (1992).

[15] Lagnado, L. and Baylor, D. *Nature* **367**, 273-277 (1994).

[16] Pugh Jr., E. N and Lamb, T. D. *Biochim. Biophys. Acta*. **1141**, 111-149 (1993).

[17] Yarfitz, S. and Hurley, J. B. *J. Biol. Chem*. **269**, 14329-14332 (1994).

[18] Yau, K, W. Invest. *Opthal. Vis. Sci.* **35**, 9-31 (1991).

[19] Bownds, M. D. and Arshavsky, V. Y. *Behav. Brain Sci*. **18**, 415-424 (1995).

[20] Koutalos, Y., Nakatani, K. and Yau, K. W. *J. Gen. Physiol*. **106**, 891-921 (1995).

[21] Tranchina, D. *J. Gen. Physiol*. **111**, 3-6. (1998).

[22] Sun, H., Macke, J. P. and Nathans, J. *Proc. Nat. Acad. Sci. U.S.A.* **94**, 8860-8865 (1997).

[23] Radlwimmer, F. B. and Yokoyama, S. *Gene* **218**, 103-109 (1998).

[24] Kojima, D., Okano, T., Fukada, Y., Shichida, Y., Yoshizawa, T. and Ebrey, T. G. *Proc. Nat. Acad. Sci. U.S.A.* **89**, 6841-6845 (1992).

[25] Lythgoe, J. and Patridge, J. *J. Exp. Biol*. **146**, 1-20 (1989).

[26] Grigorieff, P, Pelosi, P, Passarelli, V. and Barsanti, L. *Biochim. Biophys. Acta.* **1117**, 55-59 (1992).

[27] Kimura, Y, Vassylyev, D. G, Miyazawa, A, Kidera, A, Matsushima, M, et al. *Nature* **389**, 206-211 (1997).

[28] Pebay-Payroula, E., Rummel, G., Rosenbuch, J. P. and Landau, E. M. *Science* **277**, 1676-1781 (1997).

[29] Luecke, H., Richter H. T. and Lanyi, J. K. *Science* **280**, 1934-1937 (1998).

[30] Essen, L., Siegert, R., Lehmann, W. D. and Oesterhelt, D. *Proc. Nat. Acad. Sci. U.S.A.* **95**, 11673-11678 (1998).

[31] Luecke, H., Schobert, B., Richter, H. T., Cartailler, J. P. and Lanyi, J. K. *Science* **286**, 255-261 (1999).

[32] Luecke, H., Schobert, B., Richter, H. T., Cartailler, J. P. and Lanyi, J. K. *J. Mol. Biol.* **291**, 899-911 (1999).

[33] Kolbe, M., Besir, H., Essen, L-O. and Oesterhelt, D. *Science* **288**, 1390-1396 (2000).

[34] Palczewski, K., Kumasaka, T., Hori, C. A. Behnke, H., Motoshima, B. A., Fox, I., Le Trong, I., Teller, D. C., Okada, T., Stenkamp, R. E., Yamamoto, M., and Miyano, M. *Science* **289**, 739-745 (2000).

[35] Teller, D. C., Okada, T., Behnke, C. A., Palczewski, K. and Stenkamp, R. E. *Biochemistry* **40**, 7761-7772 (2001).

[36] Okada T., Fujiyoshi Y., Silow M., Navarro J., Landau E. M. and Shichida Y. *Proc. Natl. Acad. Sci. U.S.A.* **99**, 5982-5987 (2002).

[37] Li, J., Edwards, P. C., Burghammer, M., Villa, C. and Schertler, G. F. *J. Mol. Biol*. **343**, 1409-1438 (2004).

[38] Okada, T., Sugihara, M., Bondar, A. M., Elstner, M., Entel, P. and Buss, V. *J. Mol. Biol.* **342**, 571-583 (2004).

[39] Baldwin, J. M., Schertler, G. F. and Unger, G. F. *J. Mol. Biol.* **272**, 144-164 (1997).

[40] Baldwin, J. M. *EMBO J*. **12**, 1693-1703 (1993).

[41] Tang, L. and Ebrey, T. G. *Isr. J. Chem.* **35**, 193-209 (1995).

[42] Luecke, H., Schobert, B., Lanyi, J. K., Spudich, E. N. and Spudich, J. L. *Science* **293**, 1499-1502 (2001).

[43] Bownds, D., Nature **216**, 1178-1181 (1967).

[44] Bayley, II., Huang, K. S., Radharkrishnan, R., Ross, A. H., Takagaki, Y. and Khorana, H. G. *Proc. Natl. Acad. Sci. U.S.A.* **78**, 2225-2229 (1981).

[45] Khorana, H. G., Gerber, G. E., Herlihy, W. C., Gray, C. P., Anderegg, R. J., et al. *Proc. Natl. Acad. Sci.U.S.A.* **76**, 5046-5050 (1979).

[46] Ovchinnikov, Y. A., Abdulaev, N. G., Feigina, M. Y., Kiselev, A. V. and Lobanov, N. A. *FEBS Lett.* **100**: 219-224 (1979).

[47] Ovchinnikov, Y. A. *FEBS Lett*. **148**, 179-191 (1982).

[48] Hargrave, P. A., McDowell, J. H., Curtis, D. R., Wang, J. K., Juszczak, E., Fong, S. L., Rao, J. K. M. and Argos, P. *Biophys. Struct. Mech.* **9**, 235-244 (1983).

[49] Nathans, J. and Hogness, D. S. *Cell* **34**, 807-814 (1983).

[50] Nathans, J., Thomas, D. and Hogness, D. *Science* **232**, 193-202. (1986).

[51] Wald, G. and Brown. P. K. *Proc. Nat. Acad. Sci. U.S.A.* **36**, 84-92 (1950).

[52] Hubbard. R. and Kropf, A. *Proc. Nat. Acad. Sci. U.S.A.* **44**, 130-139 (1957).

[53] Pullmann, A. and Pullmann, B. *Proc. Nat. Acad. Sci. U.S.A.* **8**, 7-14 (1960).

[54] Wald, G. and Hubbard. R. *Proc. Nat. Acad. Sci. U.S.A.* **36**, 85-102 (1950).

[55] Hubbard. R. and Wald, G. *Proc. Nat. Acad. Sci. U.S.A.* **37**, 69-79 (1951).

[56] Lin, S. W., Groesbeek, M., van der Hoef, I., Verdegem, P., Lugtenburg, J. and Mathies, R. A. *J. Phys. Chem. B* **102**, 2787-2806 (1998).

[57] Verdegem, P. J. E., Bovee-Geurts, P. H. M., de Grip, W. J., Lugtenburg, J. and DeGroot, H. J. M. *Biochemistry* **38**, 11316-11324 (1999).

[58] Mathies, R. A., and Lugtenburg, J. (2000) The primary photoreaction of rhodopsin, in *Handbook of Biological Physics* (Stavenga, D. G., DeGrip, W. J. and Pugh, E. N., Jr., Eds.) Vol. **3**, Chapter 2, pp 55-90, North-Holland, Amsterdam.

[59] Feng, X., Verdegem, P. J. E., Lee, Y. K., Sandstro¨m, D., Ede´n, M., Bonvee-Geurts, P., DeGrip, W. J., Lugtenburg, J., de Groot, H. J. M. and Levitt, M. H. *J. Am. Chem. Soc*. **119**, 6853-6857 (1997).

[60] Han, M. and Smith, S. O. *Biochemistry* **34**, 1425-1432 (1995).

[61] a) Stam, C. H. and MacGillavry, C. H. *Acta Crystallogr*.**16**, 62-68 (1963); b) Stam, C. H. *Acta Crystallogr., Sect. B* **28**, 2936-2945 (1972).

[62] Terstegen, F. and Buss, V. *Chem. Lett.* **6***,* 449-450 (1996).

[63] Terstegen, F., Carter, E. A. and Buss, V. *Intern. J. Quantum Chem.* **75**, 141-145 (1999).

[64] Callender, R. H., Doukas, A., Crouch, R. and Nakanishi, K. *Biochem*. **15**, 1621-1629 (1976)

[65] Kakitani, H., Kakitani, T. and Yomosa, S. *J. Phys. Soc. Jpn*. **42**, 996, (1977).

[66] Han, M. *Biochemistry* **36**, 7280- (1997).

[67] Tan, Q., Lou, J., Borhan, B., Karnaukhova, E., Berova, N. and Nakanishi, K. *Angew. Chem. Int. Ed. Engl.* **36**, 2089-2093, (1997).

[68] Lou, J., Hashimoto, M., Berova, N. and Nakanishi, K. *Org. Lett*. **1**, 51-54, (1999).

[69] Buss, V., Kolster, K., Terstegen, F. and Vahrenhorst, R. *Angew. Chem. Int. Ed. Engl.* **37**, 1893-1895 (1998).

[70] Buss, V. *Chirality* **13**, 13-23 (2001).

[71] Fujimoto, Y., Fishkin, N., Pescitellli, G., Decatur, J., Berova, N. and Nakanishi, K. *J. Am. Chem. Soc*. **124**, 7294–7302 (2002).

[72] Tang, J. and Albrecht, A. C. 1970. *Raman Spectroscopy, ed*. H. A. Szymanski, Vol. **2**, pp. 33-38. New York: Plenum.

[73] Behringer, J. 1974. *Molecular Spectroscopy, ed*. R. F. Barrow, D. A. Long, D. J. Millen, Vol. **2**, pp-100-172. London: Chemical Society.

[74] Spiro, T. G. *Biochim. Biophys. Acta* **416**, 169-189 (1975).

[75] Lewis, A. and Spoonhower, J. 1974. *Spectroscopy in Chemistry and Biophysics*, ed. S. Chen, S. Yip, pp. 347-375. New York: Academic.

[76] Mendelsohn, R. *Nature* **243**, 22-29 (1973).

[77] Oseroff, A. R., Callender, R. H. *Biochemistry* **13**, 4243-4248 (1974).

[78] Lewis, A., Spoonhower, J., Bogomolni, R., Lozier, R., Stoeckenius, W. *Proc. Natl. Acad. Sci.U.S.A.* **71**, 4462-4466 (1979).

[79] Lewis, A., Fager, R. S. and Abrahamson, E. W. *J. Raman. Spectrosc*. **1**, 465-470 (1973).

[80] Sakmar, T. P.; Franke, R. R. and Khorana, H. G. *Proc. Nat. Acad. Sci. U.S.A.* **86**, 8309-8313 (1989).

[81] Zhukovsky, E. A. and Oprian, D. D. *Science* **246***,* 928-930 (1989).

[82] Nathans, J. *Biochemistry* **29**, 937-942 (1990).

[83] Harris, W. A., Stark, W. S. and Walker, J. A. *J. Physiol. (London)* **256**, 415-439 (1976).

[84] Ovchinnikov, Y. A., Abdulaev, N. G., Zolotarev, A. S., Artamonov, I. D., Bespalov, 1. A., Dergachev, A. E. and Tsuda, M. *FEBS Lett*. **232**, 69-72 (1988).

[85] Koutalos, Y. and Ebrey, T. G. *Biophys. J.* **55**, 379- (1989).

[86] Strader, C. D., Sigal, I. S., Candelore, M. R., Rands, E., Hill, W. S. and Dixon, R. A. F. *J. Biol. Chem*. **263**, 10267-10271 (1988).

[87] Wang Q, Schoenlein, W. R., Peteanu, L. A., Mathies, R. A. and Shank, C, V. *Science* **266***,* 422-424 (1994).

[88] Birge, R. R., Murray, L. P., Pierce, B. M., Akita, H., Nair, V. B., Findsen, L. A. and Nakanishi, K. *Proc. Nat. Acad. Sci. U.S.A.* **82**, 4117-4121 (1985).

[89] Fahmy, K., Jäager, F., Beck, M., Zvyaga, T. A., Sakmar, T. P. and Siebert, F. *Proc. Nat. Acad. Sci. U.S.A.* **90**, 10206-10210 (1993).

[90] Fahmy, K., Siebert, F. and Sakmar, T. P. *Biophys. Chem.* **56**, 171-181 (1995).

[91] Feng, X, Vergegem, P. J., Eden, M., Sandstrom, D. and Lee, Y. K., *Biomol. Nucl. Magn. Res.* **16**, 1-8 (2000).

[92] Klein-Seetharaman, J., Getmanova, E. V., Loen, M. C., Reeves, P. J. and Khorana, H. G. *Proc. Nat. Acad. Sci. U.S.A.* **96**, 13744-13749 (1999).

[93] Kliger, D. S. and Lewis, J. W. *Isr. J. Chem.* **35**, 289-307 (1995).

[94] Lewis, J. W., Szundi. I. and Kliger, D. S., *Biochemistry* **39**, 7851-7855 (2000).

[95] Lin, S. W. and Sakmar, T. P. *Biochemistry* **35**, 11149-11159 (1996).

[96] Lin, S. W., Sakmar, T. P., Franke, R. R., Khorana, H. G. and Mathies, R. A. *Biochemistry* **31**, 5105-5111 (1992).

[97] Palings, I., Pardoen, J. A., van der Berg, E., Winkel, C., Lugtenburg, J. and Mathies, R. A. *Biochemistry* **26**, 2544-2556 (1987).

[98] Popp, A., Ujj, L. and Atkinson, G. H. *Proc. Nat. Acad. Sci. U.S.A.* **93**, 372-376 (1996).

[99] Sakmar, T. P. and Fahmy, K. *Isr. J. Chem*, **35**, 325-337 (1995).

[100] Nakayama, T. A. and Khorana, H. G. *J. Biol. Chem.* **265**, 15762-15769 (1990).

[101] Nakayama, T. A. and Khorana, H. G. *J. Biol. Chem.* **266**, 4269-4275 (1991).

[102] Zhang, H., Lerro, K. A., Yamamoto, T., Lien, T. H., Sastry, L, et al*., J. Am. Chem. Soc.* **116**, 10165-10173 (1994).

[103] Han, M., Lin, S. W., Minkova, M., Smith, S. O. and Sakmar, T. P. *J. Biol. Chem.* **271**, 32337-32342 (1996).

[104] Ridge K. D., Battacharya, S., Nakayama, T. A. and Khorana, H. G. *J. Biol. Chem.* **267**, 6770-6775 (1992).

[105] Kochendoerfer, G. G., Lin, S. W. and Sakmar, T. P. Mathies, R. A. *TIBS.* **24**, 300-305 (1999).

[106] Lin, S. W. and Sakmar, T. P. *Novartis Found. Symp*. **224**, 124-135 (1999).

[107] Kropf, A. and Hubbard, R. *Ann. NY Acad. Sci.* **74**, 266-280 (1958).

[108] Mathies, R. and Stryer, L. *Proc. Nat. Acad. Sci. U.S.A.* **73***,* 2169-2173 (1976).

[109] Ottolenghi, M. and Sheves, M. *J. Membrane. Biol.* **112**, 193-212 (1989).

[110] Honig, B., Dinur, U., Nakanishi, K., Balogh-Nair, V., Gawinwicz, M. A., Arnboldi, M. and Motto, M. G. *J. Am. Chem. Soc.* **101**, 7084-7086 (1979).

[111] Sheves, M. and Nakanishi, K. *J. Am. Chem. Soc.* **105**, 4033-4039 (1983).

[112] Hubbard, R. and Sperling, L. (1973) *Exp. Eye Res.* **17***,* 581-589 (1973).

[113] Baasov, T. and Sheves, M. *Biochemistry* **25***,* 5249-5258 (1986).

[114] Fukada, Y., Okano, T., Shichida, Y., Yoshizawa, T., Trehan, A., Mead, D., Denny, M., Asato, A. E. and Liu, R. S. H. *Biochemistry* **29***,* 3133-3140 (1990).

[115] Warshel, A. and Karplus, M. *J. Am. Chem. Soc.* **96**, 5677-5689 (1974).

[116] Kakitani, K. and Kakitani, H. *Biophys. Struct. Mechanism* **5**, 55-73 (1979).

[117] Blatz, P. E. and Liebman, P. A. (1973) *Exp. Eye Res.* **17**, 573-580 (1973).

[118] Irving, C. L., Byers, G. W. and Leermakers, P. A., *Biochemistry,* **19**, 858-864 (1970).

[119] Hays, T. R., Lin, S**.** H. and Eyring, H. *Proc. Natl. Acad. Sci. U.S.A.* **77***,* 6314-6318 (1980).

[120] Hu, J., Griffin, R. G. and Herzfeld, J. *Proc. Nat. Acad. Sci. U.S.A.* **91**, 8880-8884 (1994).

[121] Schrödinger, E. *Phys. Rev.*, **28**, 1049-1070 (1926).

[122] Born, M., and Oppenheimer, J. R. *Ann. Physik*. **84**, 457-484 (1927).

[123] Jensen, F. *Introduction to Computational Chemistry*, John Wiley and Sons, Chichester (1998), and references therein.

[124] Shavitt, I. in *Methods of Electronic Structure Theory*, H. F. Schaefer, III, Ed.; Plenum Press: New York, **1977**, p. 189.

[125] Møller, C. and Plesset, M. S. *Phys. Rev.*, **46**, 618-622 (1934).

[126] Binkley, J. S. and Pople, J. A. *Int. J. Quantum Chem.*, **9**, 229-236 (1975).

[127] Hurley, A. C. *Introduction to the Electron Theory of Small Molecules*; Academic Press: London, **1976**, 17.

[128] McDonald, J. K. L. *Phys. Rev.*, **43**, 830-833 (1933).

[129] Szabo, A. and Ostlund, N. S. *Modern Quantum Chemistry: Introduction to Advanced Electronic Strucutre Theory*, Macmillan, New York (1982).

[130] Hehre, H., Radom, L., Schleyer, P. v. R. and Pople, J. A. *Ab Initio Molecular Orbital Theory*, Wiley, New York (1986).

[131] Slater, J. C. *Phys. Rev.*, **34**, 1293-1323 (1929).

[132] Hartree, D. R. *Proc. Cam. Phil. Soc.*, **24**, 89-132 (1928).

[133] Hartree, D. R. *Proc. Cam.Phil. Soc.*, **24**, 111-132 (1928).

[134] Hartree, D. R. *Proc. Cam. Phil. Soc.*, **24**, 246- (1928).

[135] Fock, V. Z. Z. *Phys.*, **61**, 126- (1930).

[136] Hurley, A. C. *Introduction to the Electron Theory of Small Molecules*; Academic Press: London, **1976**, 242.

[137] Pople J. A. and Nesbet, R. K. *J. Chem. Phys.*, **22**, 571-578 (1954).

[138] Löwdin, P. O. *Phys. Rev.*, **97**, 1509-1520 (1955).

[139] Roothaan, C. C. J. *Rev. Mod. Phys.*, **23**, 69-89 (1951).

[140] Hall, G. G. *Proc. Roy. Soc. London*, **A205**, 541- (1951).

[141] Löwdin, P. O. *Adv. Chem. Phys.*, **2**, 207- (1959).

[142] Roos, B. O. in *Ab initio Methods in Quantum Chemistry II*, K. P. Lawley, Ed.; *Advances in Chemical Physics*, I. Prigogine and S. A. Rice, Eds.; Vol. LXIX; J. Wiley & Sons Ltd.: Chichester, UK, **1987**, p. 399.

[143] Wahl A. C. and Das, G. in *Methods of Electronic Structure Theory*, H. F. Schaefer, III, Ed.; Plenum Press: New York, **1977**, p. 51.

[144] Roos, B. O., Taylor, P. R. and Siegbahn, P. E. M. *Chem. Phys.*, **48**, 157-173 (1980).

[145] Roos, B. O. in *European Summerschool in Quantum Chemistry*, Vol. 2, **2000**, p. 287.

[146] Roos, B. O. in *European Summerschool in Quantum Chemistry*, Eds.; Vol. 2, **2000**, p. 313.

[147] Guest M. F. and Saunders, V. R. *Mol. Phys.*, **28**, 819-828 (1974).

[148] Knowles, P. J. in *Cambridge Summer School in Quantum Chemistry Lecture Notes*; University of Cambridge, **1996**, p. 27.

[149] Siegbahn, P. E. M. in *European Summerschool in Quantum Chemistry*, Eds.; Vol. 1, **2000**, p. 269.

[150] Jensen, F. *Introduction to Computational Chemistry*; John Wiley & Sons: Chichester, UK, **1999**, 109.

[151] Davidson, E. R. *J. Compnt. Phys.* **17**, 87- (1975).

[152] Langhoff, S. R. and Davidson, E. R. *Int. J. Quantum Chem.* **8**, 61-72 (1974).

[153] Siegbahn, P. E. M. *Chem. Phys. Lett.* **55**, 386-394 (1978).

[154] Andersson, K., Malmqvist, P.-Å., Roos, B. O., Sadlej, A. J. and K. Wolinski, *J. Phys. Chem.* **94**, 5483-5488 (1990).

[155] Andersson, K., Malmqvist, P.-Å. and Roos, B. O. *J. Chem. Phys.* **96**, 1218-1226 (1992).

[156] Werner, H. J. and P. J. Knowles, *J. Chem. Phys.* **89**, 5803-5814 (1988).

[157] Siegbahn, P. E. M. *Chem Phys*. **25**, 197- (1977).

[158] Siegbahn, P. E. M. *Int. J. Quantum Chem.* **23**, 1869-1889 (1983).

[159] Siegbahn, P. E. M. *Int. J. Quantum Chem*. **18**, 1229-1242 (1980).

[160] Werner, H. J. *ab initio Methods in Quantum Chemistry II*, K. P. Lawley, Ed.;*Advances in Chemical Physics*, I. Prigogine and S. A. Rice, Eds.; Vol. LXIX; J. Wiley & Sons Ltd.: Chichester, UK, **1987**, 1.

[161] Werner H. J. and Reinsch, E. A. *J. Chem. Phys.* **76**, 3144-3154 (1982).

[162] Roos, B. O., Fülscher, M. P., Malmqvist, P.-A., Merchán, M., Serrano-Andrés, L. Langhoff S. R., (Ed.), Kluwer, Dordrecht, **1995**, p. 357.

[163] Roos B. O. and Andersson, K. *Chem. Phys. Letters* **245**, 215-221 (1995).

[164] Roos, B. O., Andersson, K., Fülscher, M. P., Serrano-Andrés, L., Pierloot, K., Merchan, M. and V. Molina, *J. Mol. Stuct. (Theochem)* **388**, 257-276 (1996).

[165] Forsberg, N., and Malmqvist, P.-Å. *Chem. Phys. Letters* **274**, 196-204 (1997).

[166] Frisch, M. J., et al., **Gaussian** 2003, Revision B.04; Gaussian Inc, Pittsburgh PA.

[167] Andersson, K., et al., **MOLCAS** 2002**, Version 5.4**; University of Lund, Lund, Sweden.

[168] Fuelscher, M. P., et al., **MOLCAS** 2004**, Version 6.2**; University of Lund, Sweden.

[169] Malmqvist, P. Å. and Roos, B. O. *Chem. Phys. Lett.* **155**, 189-194 (1989).

[170] Blatz, P. E., Mohler, J. H. and Navagul, H. V. *Biochemistry* **11**, 848-855 (1972).

[171] Suzuki, H., Komatsu, T. and Kitajima, H. *J. Phys. Chem. Jpn*. **37**, 177-185 (1972).

[172] Honig, B., Greenberg, A. D., Dinur, U. and Ebrey, T. *Biochemistry*. **15**, 4593-4599 (1976).

[173] Schaffer, A. M., Waddell, W. H. and Becker, R. S. *J. Am. Chem. Soc*. **96**, 2063-2068 (1973).

[174] Pitt, G. A. J. *Exptl. Eye. Res*. 3, 316 (1964).

[175] Bridges, C. D. B. *Comp. Biochem*. **27**, 31 (1967).

[176] Abrahamson, E. W. and Ostroy, S. E. *Progr. Biophys*. **17**, 181 (1967)

[177] Ceasar, G. P. and Gray, G. B. *J. Am. Chem. Soc*. **91**, 191-193 (1969).

[178] Irving, C. S., Byers, G. W. and Leermakers, P. A, *J. Am. Chem. Soc*. **91**, 2141-2143 (1969)

[179] Houjou, H., Inoue, Y. and Sakurai, M. *J. Phys. Chem. B* **105**, 867-879 (2001).

[180] Ren; L., Martin, C. H., Wise, K. J., Gillespie, N. B., Luecke, H., Lanyi, J. K., Spudich, J. L. and Birge. R. R. *Biochemistry* **46**, 13906-13914 (2001).

[181] Hayashi, S., Tajkhorshid, E., Pebay-Peyroula, E., Royant, A., Landau, E. M., Navarro, J. and Schulten. K. *J. Phys. Chem. B* **105**, 10124-10131 (2001).

[182] Rajamani, R., and Gao. J. *J. Comp. Chem.* **23**, 96-105 (2002).

[183] Andruniów, T., Ferre, N. and Olivucci. M. *Proc. Natl. Acad. Sci. U.S.A.* **101**, 17908-17913 (2004).

[184] Fujimoto, K., Hasegawa, J., Hayashi, S., Kato, S. and Nakatsuji. H. *Chem. Phys. Lett.* **414**, 239-242 (2005).

[185] Andersen, L. H., Nielsen, I. B., Kristensen, M. B., Ghazaly, M. O. A., Haacke, S., Bronsted Nielsen, M. and Petersen. M. A. *J. Am. Chem. Soc.* **127**, 12347-12350 (2005).

[186] Nielsen, I. B., Lammich, L. and Andersen, L. H. *Phys. Rev. Lett.* **96**, 018304(1)-018304(4) (2006).

[187] Petersen. M. A., Nielsen, I. B., Kristensen, M. B., Kadziola, A., Lammich, L., Andersen, L. H. and Nielsen, M. B. *Org. Biomol. Chem.* **4**, 1546-1554 (2006).

[188] Terstegen, F. and Buss. V. *J. Mol. Struct. THEOCHEM.* **430**, 209-218 (1998).

[189] Waddell, W. H., Schaffer, A. M. and Becker, R. S, *J. Am. Chem. Soc*. **99**, 8456- 8460 (1977).

[190] Dähne, L., Grahn, W., Jones, P. G. and Chrapkowski, A. *Z. Kristallog*. **209**, 514–516. (1994).

[191] Buss, V., Schreiber, M. and Fülscher, M. P, *Angew. Chem. Int. Ed.* **40**, 3189–3190 (2001).

[192] Kulpe, S., Zedler, A., Dähne, S. and Nolte, K. D. J. *Prakt. Chem*. **315**, 865–872 (1973).

[193] Palmer, B., Jumper, B., Hagan, W., Baum, J. C. and Christensen, R. L. *J. Am. Chem. Soc.* **104**, 6907-6913 (1982).

[194] Christensen, R. L., Goyette, M., Gallagher, L., Duncan, J., DeCoster, B., Lugtenburg, J., Jansen, F. J. and van der hoef, I. *J. Phys. Chem. A* **103**, 2399-2407 (1999).

[195] Grossjean, M. F. and Tavan, P. *J. Phys. Chem*. **88**, 4884-4896 (1987).

[196] Nielsen, I. B., Petersen. M. A., Lammich, L., Nielsen, M. B. and Andersen, L. H. *J. Phys. Chem. B* **110**, 12592-12596 (2006).

[197] Serrano-Andres, L., Lindh, R., Roos, B. O. and Merchan, M, *J. Phys. Chem.* **97**, 9360-9368 (1993).

[198] Birge. R. R., Bennett, J. A., Pierce, B. M., Thomas, T. M. *J. Am. Chem. Soc.* **100***,* 1533-1539 (1978).

[199] Okada, T., Sugihara, M., Bondar, A. M., Elstner, M.; Entel, P., Buss, V. *J. Mol. Biol.* **342**, 571-583 (2004).

[200] Nakamichi, H. and Okada, T. *Angew. Chem. Int. Ed.* **45**, 4270-4273 (2006).

[201] Sugihara, M., Buss, V., Entel, P., Elstner, M. and Frauenheim. T. *Biochemistry* **41**, 15259-15266 (2002).

[202] Schreiber, M. and Buß, V *Int. J. Quantum Chem.* **95**, 882-888 (2003).

[203] Sugihara, M., Hufen, J. and Buss, V. *Biochemistry* **45**, 801-810 (2006).

[204] Mathies, R. A., Lugtenburg, J., in Stavenga, D. G., DeGrip, W. J. and Pugh Jr., E. N. Editors, Molecular *Mechanisms of Visual Transduction*. Elsevier, Amsterdam, **2000**, p.55

[205] Hufen, J., Sugihara, M. and Buss, V. *J. Phys. Chem. B* **108**, 20419-20426 (2004).

[206] Horiuchi, S., Tokunaga, F. and Yoshizawa, T. *Biochim. Biophys. Acta* **591**, 445-457 (1980)

[207] Creemers, A, F. L., Bovee-Geurts, P. H. M., DeGrip, W. J., Lugtenburg, J., and de Groot, H. H. M. *Biochemistry* **43**, 16011-16018 (2004).

[208] Burke, M. J., Pratt, D. C., Faulkner, T. R. and Moscowitz, A. *Exp. Eye Res.* **17**, 557- (1973).

[209] Reed, A. R., Weinstock, R. B. and Weinhold, F. *J. Chem. Phys.* **83**, 735-746 (1985).

[210] Mulliken, R. S. *J. Chem. Phys.* **23***,* 1833-1840 (1955).

[211] Mackerell, A. D. Jr., Wiorkiewicz-Juczera, J. and Karplus, M. *J. Am. Chem. Soc.* **117***,* 11946-11975 (1995).

[212] Han, M., Lin, S. W., Smith, S. O. and Sakmar, T. P. *J. Biol. Chem,* **271***,* 32330-32336 (1996).

[213] Nagata, T., Oura, T., Terakita, A., Kandori, H. and Schichida, Y. *J. Phys. Chem. A* **106***,* 1969-1975 (2002).

[214] Carravetta, M., Zhao, X., Johannessen, O. G., Lai, W. C., Verhoeven, M. A., Bovee-Geurths, P. H. M., Verdegem, P. J. E., Kiihne, S., Luthaman, H., de Groot, H. J. M.; deGrip, W. J., Lugtenburg, J., Levitt, M. H. *J. Am. Chem. Soc.* **126**, 3948-3953 (2004).

[215] Terakita, A., Yamashita, T. and Schichida, Y. *Proc. Natl. Acad. Sci. U.S.A.* **97***,* 14263-14267 (2000).

[216] Nathans, J. *Biochemistry* **29**, 937-942 (1990).

[217] Morais-Cabral, J. H., Kaufman, A. and Mackinnon, R. *Nature*, **414**, 37-42 (2001).

[218] Imai, T., Hiraoka, R., Kovalenko, A. and Hirata, F *J. Am. Chem. Soc.* **127**, 15334-15335 (2005).

[219] Furutani, Y., Shichida, Y. and Kandori, H. *Biochemistry*, **42**, 9619-9625 (2003).

[220] Matsumoto, H. and Yoshizawa, T. *Nature* **258**, 523-526 (1975).

[221] Buss, V., Sugihara, M., Entel, P. and Hafner, J. *Angew. Chem. Int. Ed,* **42***,* 3245-3247 (2003).

[222] Yan, E. C. Y., Kazmi, A. M., Ganim, Z., Hou, J. M., Pan, D., Chang, B. S. W., Sakmar, T. P. and Mathies, R. A. *Proc. Nat. Acad. Sci. U.S.A.* **100**, 9262-9267 (2003).

[223] Garczarek, F. and Gerwert, K. *Nature* **439**, 109-112 (2006).

[224] Haupts, U., Tittor, J. and Oesterhelt, D. *Annu. Rev. Biophys. Biomol. Struct.* **28**, 367-399 (1999).

[225] Muneda, N., Shibata, M., Demura, M. and Kandori, H. *J. Am. Chem. Soc.* **128**, 6294-6295 (2006).

[226] Hayashi, S. and Ohmine, I. *J. Phys. Chem. B* **104**, 10678-10691 (2004).

[227] Kandori, H. and Shichida, Y. *J. Am. Chem. Soc.* **122**, 11745-11746 (2000).

[228] Shibata, M., Muneda, N., Ihara, K., Sasaki, T., Demura, M., Kandori, H. *Chem. Phys. Lett.* **392**, 330-, (2004).

[229] Kusnetzow, A.; Dukkipati, A.; Babu, K. R.; Singh, D.; Vought, B. W.; Knox, B. E.; Birge, R. R. *Biochemistry* **2001**, *40*, 7832.

[230] Cooper, A. *Nature* **282**, 531-533 (1979).

[231] Warshel, A., Barboy, N. *J. Am. Chem. Soc*. **104**, 1469-1476 (1982).

[232] Birge, R. R., Einterz, C. M., Knapp, H. M., Murray, L. P. *Biophys. J*. **53**, 367-385 (1988).

[233] Bifone, A., de Groot. H. J. M., and Buda, F. *J. Phys. Chem. B* **101**, 2954-2958 (1997).

[234] Verdegem, P. J. E., Bovee-Geurts, P. H. M., de Grip. W. J., Lugtenburg, J. and de Groot. H. J. M. *Biochemistry* **38**, 11316-11324 (1998).

[235] Cooper, A. *FEBS Lett*. **100**, 382-384 (1979).

[236] Schick, G. A., Cooper, T. M., Holloway, R. A., Murray, L. P. and Birge, R. R, *Biochemistry* **26**, 2556-2562 (1987).

[237] Sekharan, S., Sugihara, M. and Buss, V. *Angew. Chem. Int. Ed.* **46**, 269-271 (2007).

[238] Schreiber, M., Sugihara, M., Okada, T. and Buss, V. *Angew. Chem. Int. Ed*. **45**, 4274-4277 (2006).

[239] Gascon, J. A. and Batista, V. S, *Biophys. J.* **87**, 2931-2941 (2004).

[240] Coto, P. B., Strambi, A., Ferre, N. and Olivucci, M. *Proc. Natl. Acad. Sci. U.S.A.* **103**, 17154-17159 (2006).

[241] Nakamichi, H. and Okada, T. *Proc. Natl. Acad. Sci. U.S.A.* **103**, 12729-12734 (2006).

[242] Salom, D., Lodowski, D. T., Stenkamp, R. E., Le Trong, I., Golczak, M., Beata, J., Harris, T., Ballesteros, J. A. and Palczewski, K. *Proc. Natl. Acad. Sci. U.S.A.* **103**, 16123-16128 (2006).

[243] Hunt, D. M., Fitzgibbon, J., Slobodyanyuk, S. J., Bowmaker, J. K. and Dulai, K. S. *Mol. Phlogenet. Evol.* **8**, 415-422 (1997).

[244] Salcedo, E., Huber, A., Henrich, S., Chadwell, L. V., Chou, W, H., Paulsen, R. and Britt, S. G. *J. Neuroscience* **19**, 10716-10726 (1999).

[245] Salcedo, E., Zheng, L., Phistry, M., Bagg, E. E. and Britt, S. G. *J. Neuroscience* **23**, 10873-10878 (2003).

Abbreviations and Symbols

Chapter-1 PREAMBLE

PSB11	protonated Schiff base of 11-*cis*-retinal
ROS	rod outer segment
GTP	guanosine triphosphate
cCMP	cyclic guanine monophosphate
M/LWS	mid and long wavelength sensitive
SWS	short wavelength sensitive
RH	rhodopsin family
GPCR	G protein-coupled receptor
TM	transmembrane
R	rhodopsin
bR	bacteriorhodopsin
hR	halorhodopsin
sRI	sensoryrhodopsin-I
sRII	sensoryrhodopsin-II
Lys (K)	lysine
Glu (E)	glutamate
Gln (Q)	glutamine
Asp (R)	asparate
Cys (C)	cysteine
DNA	deoxyribo nucleic acid
NMR	nuclear magnetic resonance
CD	circular dichroism
PDB	protein data bank
E	extracellular
I	intracellular
RR	resonance Raman
UV	ultraviolet
FTIR	Fourier-transform infra red
BSI	blue shifted intermediate
RX	phototransformed protein
GDP	guanosine diphosphate
SBH^+	protonated Schiff base
OS	opsin shift
CH_3OH	methanol

Chapter-2 THEORETICAL FRAMEWORK

QM	quantum mechanics
MM	molecular mechanics
SCRF	self-consistent reaction field
BO	Born-Oppenheimer
H_{elec}	electronic hamiltonian

Ψ_{elec}	electronic wave function
CSF	configuration state function
CI	configuration interaction
φ	basis function
χ	spin-orbital
$\{\phi\}$	configuration state function
$\hat{H}$	Hamiltonian operator
c_i	*i*-th orbital coefficient
E_{trial}	energy of a trial wave function
E_{exact}	exact ground state electronic energy
HF	Hartree-Fock
MO	molecular orbital
ξ	radial exponent of a primitive gaussian function
RHF	restricted Hartree-Fock
ROHF	restricted open-shell Hartree-Fock
UHF	unrestricted Hartree-Fock
BS-UHF	broken-spin unrestricted Hartree-Fock
HOMO	highest occupied molecular orbital
LUMO	lowest unoccupied molecular orbital
α	spin function $+\frac{1}{2}$
β	spin function $-\frac{1}{2}$
ω	spin coordinate
F_{ij}	Fock matrix with elements *i, j*
c	eigen vector matrix
S	overlap matrix
D	density matrix
E_{corr}	correlation energy
FCI	full configuration interaction
CIS	configuration interaction single
CID	configuration interaction double
MCSCF	multi-configuration self-consistent field
CASSCF	complete active space self-consistent field
MRCI	multi-reference configuration interaction
MPPT	Moeller-Plesset perturbation theory
$\hat{V}$	fluctuation operator
$\hat{F}$	Fock operator
MP2	Moeller-Plesset perturbation theory to second order
MP4	Moeller-Plesset perturbation theory to fourth order
SDTQ	single double triple quadruple
CASPT2	complete active space second-order perturbation
PES	potential energy surface
RAS	restricted active space

MRMP	multi-reference Moeller-Plesset
MBPT	many body perturbation theory
PT2D	diagonal part of the Fock matrix
PT2F	non-diagonal elements of the Fock matrix
LS	level shift
DFT	density functional theory
B	correlation functional of Becke
LYP	correlation functional of Lee, Yang and Parr
B3LYP	A hybrid generalised gradient approximation functional employing B exchange and LYP correlation
ANO	atomic natural orbital
CASSI	complete active space state interaction

Chapter-3 THEME

Å	angstrom
vac	vacuum
dist	distorted
ip	ion-pair
PSB9	protonated Schiff base of 9-*cis*-retinal
PSBT	protonated Schiff base of all-*trans*-retinal
SBN^+T	deprotonated Schiff base all-*trans*-retinal with proton charge moved to the next neighbouring heavy atom
SB11	deprotonated Schiff base of 11-*cis*-retinal
SB9	deprotonated Schiff base of 9-*cis*-retinal
SBT	deprotonated Schiff base of all-*trans*-retinal
C	carbon
N	nitrogen
O	oxygen
S	sulphur
f	oscillator strength
μ	dipole moment
deg	degrees
S_0	ground state
S_1	first excited state
S_2	second excited state
Ala (A)	alanine
Gly (G)	glycine
His (H)	histidine
Ile (I)	isoleucine
Leu (L)	leucine
Met (M)	methionine
Phe (P)	phenylalanine
Ser (S)	serine
Thr (T)	threonine
Tyr (Y)	tyrosine
Trp (W)	tryptophan
Wat2a	water2a

Wat2b	water2b
SCC-DFTB	self consistent charge density functional tight binding
5.PSB11	five double bond protonated Schiff base of 11-*cis*-retinal
5.PSBT	five double bond protonated Schiff base of all-*trans*-retinal
NPA	natural population analysis
MPA	Mulliken population analysis
CHARMM	chemistry at Harvard macromolecular mechanics
EII	extracellular loop II

Declaration

I declare that this thesis is my own work and has not been submitted in any form for another degree or diploma at any university or other institution of tertiary education. Information derived from the published or unpublished work of others has been acknowledged in the text and a list of references is given.

Sivakumar Sekharan 09-01-07